MainRoads
Connecting Queensland

Suspension testing of 3 heavy vehicles – methodology and preliminary frequency analysis

Report

Author: **Lloyd Davis**
Department of Main Roads

Co-Author: **Dr. Jonathan Bunker**
Queensland University of Technology

1st Edition

July 2008

ISBN 978 - 1 - 9207 - 1909 - 8

Prepared by	Lloyd Davis & Dr. Jon Bunker
Version no.	Mk III
Revision date	July 2008
Status	final draft
DMS ref. no.	890/00037
File/Doc no.	890/00037

File string: C:\masters\suspension frequencies report Mk III.doc

Corresponding author contact:

Lloyd Davis BEng(Elec) GDipl(Control) Cert(QMgt) CEng RPEQ
Fellow, Institution of Engineering & Technology
Principal Electrical Engineer
ITS & Electrical Technology
Planning Design and Operations Division
Main Roads
GPO Box 1412
Brisbane, Qld, 4001

P 61 (0) 7 3834 2226

M 61 (0) 417 620 582

E davis@student.qut.edu.au

Table of Contents

Table of Figures

Executive Summary

Three air-sprung heavy vehicles (HVs) were instrumented and tested on typical suburban and highway road sections at typical operational speeds. The vehicles used were a tri-axle semi-trailer towed with a prime mover, an interstate coach with 3 axles and a school bus with 2 axles. The air springs (air bags) of the axle/axle group of interest were configured such that they could be connected using either standard longitudinal air lines or an innovative suspension system comprising larger-than-standard longitudinal air lines. Data for dynamic forces on axles, wheels and chassis were gathered for the purposes of:

- analysis of the relative performance of the HVs for the two sizes of air lines;
- informing the QUT/Main Roads project *Heavy vehicle suspensions – testing and analysis*; and
- providing a reference source for future projects.

This reports sets down the methodology and preliminary results of the testing carried out. Accordingly, Fast-Fourier plots are provided to show indicative frequency spectra for HV axles, wheel forces and air springs during typical use. The results are documented in Appendices 3 to 5.

There appears to be little or no correlation between dynamic forces in the air springs and the wheel forces in the HVs tested. Axle-hop at frequencies between 10-15 Hz predominated for unsprung masses in the HV suspensions tested. Air-spring forces are present in the sub-1.0 Hz to approximately 2 Hz frequency range.

With the qualification that only one set of data from each test speed is presented herein, in general, the peaks in the frequency spectra of the body-bounce forces and wheel forces were reduced for the tests with the larger longitudinal air lines.

More research needs to be done on the load sharing mechanisms between axles on air-sprung HVs. In particular, how and whether improved load sharing can be effected and whether better load sharing between axles will reduce dynamic wheel and chassis forces. This last point, in particular, in relation to the varied dynamic measures used by the HV testing community to compare different suspension types.

1 Introduction

1.1 Background

The Queensland Department of Main Roads is becoming increasingly concerned that heavy vehicles (HVs) with air-sprung suspensions are not as sympathetic to roads as they might otherwise be. When air-sprung HVs were granted concessions to carry greater mass at the end of the 1990s, Australian road authorities knew that air-sprung HVs with industry-standard (or conventionally sized) air lines between air springs did not load share in the dynamic[1] sense. It was known at the time that concomitant increases in dynamic wheel loads from air-sprung HV suspensions as a result of ineffective dynamic load sharing had the potential to cause greater road damage than might otherwise be the case should air-sprung HVs incorporate more dynamic load equalisation into their design (OECD, 1992, 1998). That poor load sharing as defined by the load sharing coefficient (LSC) could contribute to increased road network damage was addressed (OECD, 1992) and estimated as shown in Table 1.

Type of damage	Δ increase in pavement damage (%) due to imperfect load sharing (LSC= 0.8)
Rutting	43 - 100
Fatigue	23 - 200

Table 1. Pavement damage increase for an LSC of 0.8

Noting that perfect load equalisation would give a LSC of 1.0 (Potter, Cebon, Cole, & Collop, 1996) LSC values (Sweatman, 1983) for steel suspensions were

[1] Wheel-loads loads were not spread as evenly and as quickly as they could have been during travel of air-sprung trucks over undulations.

documented in the range 0.791 to 0.957. Air suspensions were placed somewhere in the middle of this range with LSCs of 0.904 to 0.925. This was a decade before, and referenced in, the first OECD report (OECD, 1992). In fine, the effects of poor dynamic load equalisation were published and known at the time of granting air-sprung HVs concessions to carry greater mass at the end of the 1990s. With the clarity of hindsight, the disbenefits due to higher road network asset damage may not have been recognised as having the potential to discount the societal and economic benefits of higher HV payloads. Nonetheless, there is now a growing recognition of, (and therefore renewed research effort into) the phenomenon of imperfect dynamic load sharing within air-sprung HV suspension groups. This is not before time.

2 reports commissioned by the NTC (Estill & Associates Pty Ltd, 2000; Roaduser Systems Pty Ltd, 2002) have recommended, *inter alia*, evaluation of countermeasures which have corrected HV handling problems in air-suspended HVs. Some of the recommended tests were proposed to evaluate the effect of installing larger "pipes" or air lines so that "longitudinal air flow between axles is increased; this should improve the load-sharing capability of the suspension; in both cases where this was implemented, it was reported to fix the problem" (Roaduser Systems Pty Ltd, 2002). Further, as far back as 2000, the NTC had the recommendation put to it to "investigate and evaluate 'after market improvements' to air suspensions" from installation of "larger diameter pipes to supply and exhaust air flow to the bag quickly and hence improve the response time of the air bag. The modification also reduces the roll and has improved stability." (Estill & Associates Pty Ltd, 2000). Since then, the 2005 test programme funded by the Queensland Department of Main Roads (Davis, 2006), the 2007 test programme (Davis, 2007; Davis & Kel, 2007) and as documented herein comprise the only known published testing of HVs with larger longitudinal air lines since those recommendations were made.

Dynamic load sharing can be defined as the equalisation of the axle group load across all wheels/axles under typical travel conditions of a HV (that is, in the dynamic sense at typical travel speeds and operating conditions of that vehicle). Attempting to quantify this concept has resulted in a number of methods proposed

and documented (Sweatman, 1983), amongst which were the load sharing coefficient (LSC) and the dynamic load coefficient (DLC). Potter (1996) clarified various methods for quantitative derivation of measures to describe the ability of an axle group to distribute the total axle group load during travel. Despite this work, that of Mitchell & Gyenes (1989) and Gyenes (1994), more recently Potter at al (1997) and Fletcher (2002), there is no agreed testing procedure to define or measure dynamic load sharing at the local nor national level in Australia. Further, the Australian specification for RFS, VSB 11 (Australia Department of Transport and Regional Services, 2004c), nominates only that RFS suspensions must have static load sharing, to a defined value, "between axles in the axle group". Surprisingly, it does not define a formal methodology (Prem, Mai, & Brusza, 2006) to determine a static load sharing value; that detail has been left to a method suggested in a monograph (official status unknown) issued by Mr KC Wong of DoTaRS.

Previous work (Davis, 2006; Davis & Sack, 2004) has shown that RFS do not load share dynamically when in multi-axle groups. That testing, in Feb 2003 (Davis & Sack, 2004), was on a semi-trailer fitted with standard longitudinal air lines (6.5mm inside diameter, 9.5mm outside diameter). The results showed that the transfer of air between air springs on the test vehicle was in the order of 3 s. Simple logic yields that if the axle spacings on a HV are 1m apart at their closest (worst case), then at 100km/h (27.7 ms^{-1}) the reaction time for air to start to transfer between air springs as described above needs to be in the order of 1/28 s (0.036 s) for any reasonable dynamic load sharing to occur. This value may be relaxed to about 1/21 s (0.047 s) for axle spacings of 1.3m at 100km/h. Hence air transfer with time constants in the order of 3 s will not load share dynamically, causing more distress to the road network than the case where air-sprung HVs have a better ability to load-share than the current fleet. Recent work on tri-axle and quad-axle semi-trailers (Blanksby, George, Peters, Ritzinger, & Bruzsa, 2008) has confirmed that load sharing in air-sprung HVs with conventionally sized air lines does not occur in the dynamic sense, confirming the current concerns.

Quad-axle semi trailers are being introduced to Australia. If previously the inability of air suspensions to equalise (say) 22.5 t loads across tri-axle groups resulted in unequal loadings on one axle over another for that group, the emerging scenario will

be 27 t similarly imbalanced within a group of 4 axles. Arising from this, road authorities in Australia, officially or otherwise, are becoming increasingly concerned that HVs with air springs are not as sympathetic to the network asset as they might otherwise be.

3 heavy vehicles were used in a test programme to gather data on HV suspension dynamics. One objective was to determine if any changes to dynamic parameters (particularly in dynamic equalisation) would result from altering the size of the longitudinal (front-to-back) air lines between the air springs. The 3 HVs used for the testing were a tri-axle semi-trailer towed with a prime mover, an interstate coach with 3 axles and a school bus with 2 axles. Instrumentation consisting of strain gauges, accelerometers and air pressure transducers (APTs) was installed on the tri-axle group of the semi-trailer, the drive and tag axle of the coach and the drive axle of the school bus.

Before (standard longitudinal air lines) and after (the "Haire suspension system") testing was performed with the vehicles loaded to as close as practicable to full legal axle masses and driving them on typical, uneven roads at speeds from 40 km/h to 90 km/h. Quasi-static testing was performed on the instrumented axles to determine empirical values for damping ratio and body-bounce (Davis & Kel, 2007; Davis, Kel, & Sack, 2007).

The "Haire suspension system" is a proprietary suspension system which connects heavy vehicle air springs using larger-than-standard diameter air lines longitudinally as shown in Figure 1, Figure 3 & Figure 14. Note that, referring to Figure 1 (some detail has been removed for clarity): larger air lines (in black) run longitudinally and connect the air springs fore-and-aft. The transverse air line is left as standard for fitment of this system. Figure 14 shows the larger longitudinal air lines for the semi-trailer but the arrangement shown was typical for each air bag on axle/s of interest for this series of tests.

The manufacturer of the "Haire suspension system" has claimed that, by installation of this proprietary system, air-sprung heavy vehicle (HV) suspensions may be made "friendlier" than air-sprung HV suspensions possessing Australian industry-standard sized longitudinal air lines.

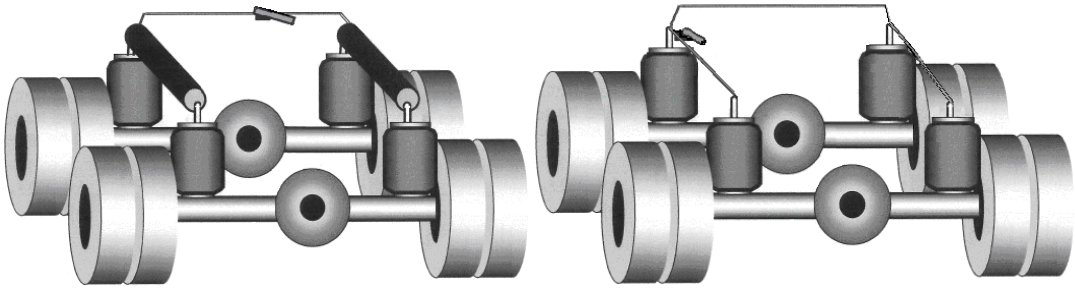

Figure 1. Schematic layout of the "Haire suspension system" (left) and standard air suspension system (right).

Further details may be found in Section 2.

Some preliminary results with respect to wheel forces from this test programme have been reported (Davis, 2007) as well as a preliminary parametric suspension analysis (Davis & Kel, 2007; Davis *et al.*, 2007).

1.2 Objectives

This report contributes to the project *Heavy vehicle suspensions – testing and analysis*.

In addition to other activities outlined for the project (Davis & Bunker, 2007) this report presents:

- ☞ a detailed record of the methodology used for gathering HV suspension data for that project; and
- ☞ indicative and typical results of fast Fourier transform (FFT) frequency-spectrum analysis as applied to the HV suspension data gathered.

Other publications have covered some of the methodology and material herein (Davis, 2005, 2006; Davis & Kel, 2007; Davis *et al.*, 2007; Davis & Sack, 2004, 2006). Being conference papers, these had, properly, space limitations.

This report provides a vehicle for detailing the methodology and results from the test programme mentioned briefly in Section 1.1 and detailed in Section 2 without the constraints on volume necessarily imposed by conference or journal papers. Nonetheless, it does not provide spectrum analysis results for every test but necessarily constrains the space used to documenting samples of indicative frequency spectra from the wheel-forces, air springs and axles from the test vehicles. This is, in part, to inform the project *Heavy vehicle suspensions – testing and analysis* by providing source material to:

- assist in the work of determining if larger longitudinal air lines on air-sprung HVs alter front-to-back interactions between air springs at operational speeds;
- inform analysis of any alterations to dynamic axle-to-body forces and wheel-force parameters by documentation of frequency spectra of these data; and
- contribute to research into HV suspensions by setting down reference data for broader application to future analysis by that project;

as well as contributing to research into HV suspensions by documenting reference data for future analysis by other researchers.

1.3 Scope

It is noted that, whilst VSB11 (Australia Department of Transport and Regional Services, 2004a) defines a limited scope for HV load sharing, it does not address transverse load sharing, only load sharing between axles. Accordingly, the unmodified transverse air lines of the "Haire suspension system" and lack of definition of load sharing between wheels on the same axle require this report to confine its scope to the effects of improving "front-to-back" air flow between axles.

The scope of this report is the frequency-domain analysis of the following data from the HV on-road testing with the HVs at full load:

- dynamic HV wheel-forces;

- accelerations at the HVs' hubs; and
- dynamic air spring forces as measured by air pressure transducers (APTs) in the air lines at the air springs.

Note that the methodology (but not the results) of the quasi-static, VSB 11-style testing are provided herein. Some results from those tests have been provided in other papers (Davis & Kel, 2007; Davis *et al.*, 2007) and further analysis of those data will be the subject of future reports.

1.4 Rationale

In the 1980s and 1990s a great effort in Europe went into in the research and testing of HV suspensions and their effects on bridges and pavements from the dynamic loading of air-sprung heavy vehicles (OECD, 1992, 1998). Within these programmes, Gillespie *et al.* (1993) noted that static loads were equalised in most HV multi-axle suspension configurations but that load sharing in the dynamic sense varied markedly between different suspension designs. Referring to the final report of the DIVINE project, p77 (OECD, 1998), authors' italics for emphasis:

"…large dynamic responses and multiple fatigue cycles were observed. These responses were up to *4.5 times the dynamic load allowance* specified in bridge design. Where axle hop was not induced, the dynamic response was much smaller. A probable explanation for this is the fact that the *very limited dynamic load sharing in air suspensions* allows the axles in a group to vibrate in phase at axle-hop frequencies. "Crosstalk" between conventional steel leaf suspensions limits this possibility…"

The final OECD report (1998), was used in Australia to support the argument that air-sprung heavy vehicles (HVs) should carry greater mass under the micro-economic reform popular at the time. That report acknowledged:

- these types of suspensions did not load share in the dynamic sense; and

- ☞ the nature of the design of air suspensions was such that they created greater dynamic loads than loads induced in conventional steel suspensions under similar circumstances.

Nonetheless, that report was used in Australia to justify the introduction of air-sprung HVs at HML loads. The implications of this decision with respect to allowing heavier HVs with greater axle loads (and, later, more axles) onto the road network with untested and undefined load sharing ability have been dealt with previously (Davis & Bunker, 2007).

The result was HVs carrying more mass in return for, amongst other requirements, having "road friendly" suspensions (RFS). The first "road friendly" suspensions were air-sprung and most still are, although some steel RFS have been certified in the recent past (Australia Department of Transport and Regional Services, 2004b).

Reassessment of the research into the dynamic forces imparted to road assets by air-sprung HVs has revealed that the original research showed very clearly that transfer of air within a HV axle group was not a feature of air suspensions (Simmons, 2005), particularly "front-to-back" sharing, that is; between consecutive axles. Subsequent review of that work has now confirmed that small longitudinal air lines do not allow quick movement of air between air springs on sequential HV axles (Davis, 2006; Davis & Sack, 2004). This reassessment has shown that the original research in the 1980s and 1990s indicated very clearly that transfer of air within a HV axle group was not a feature of air suspensions (Simmons, 2005). Mr. Simmons tested air suspended HVs with various longitudinal air pipe sizes between 8mm and 12mm outside diameter and co-authored reports in this field (Gyenes & Simmons, 1994; Simmons & Wood, 1990). He noted (2005) "these pipe sizes will not provide dynamic equalisation as there will not be sufficient transfer between displacers [air springs]..."

Karamihas and Gillespie put it more bluntly, p37 (Karamihas & Gillespie, 2004):

"Air spring suspensions do not possess a dynamic load sharing mechanism."

The inability of conventional air suspensions to load share dynamically in "front-to-back" equalisation mode (*i.e.*; between consecutive axles) and with a time constant

necessary for road travel was confirmed by Davis and Sack (2004). That work measured, *inter alia*, the air pressure in the high-pressure supply to the air springs of a quad-axle semi-trailer as it was driven over a 65mm step-down profile at 5km/h. The "base case" for that programme of work was on vehicles with standard longitudinal air lines of 6.5mm inside diameter and 9.5mm outside diameter.

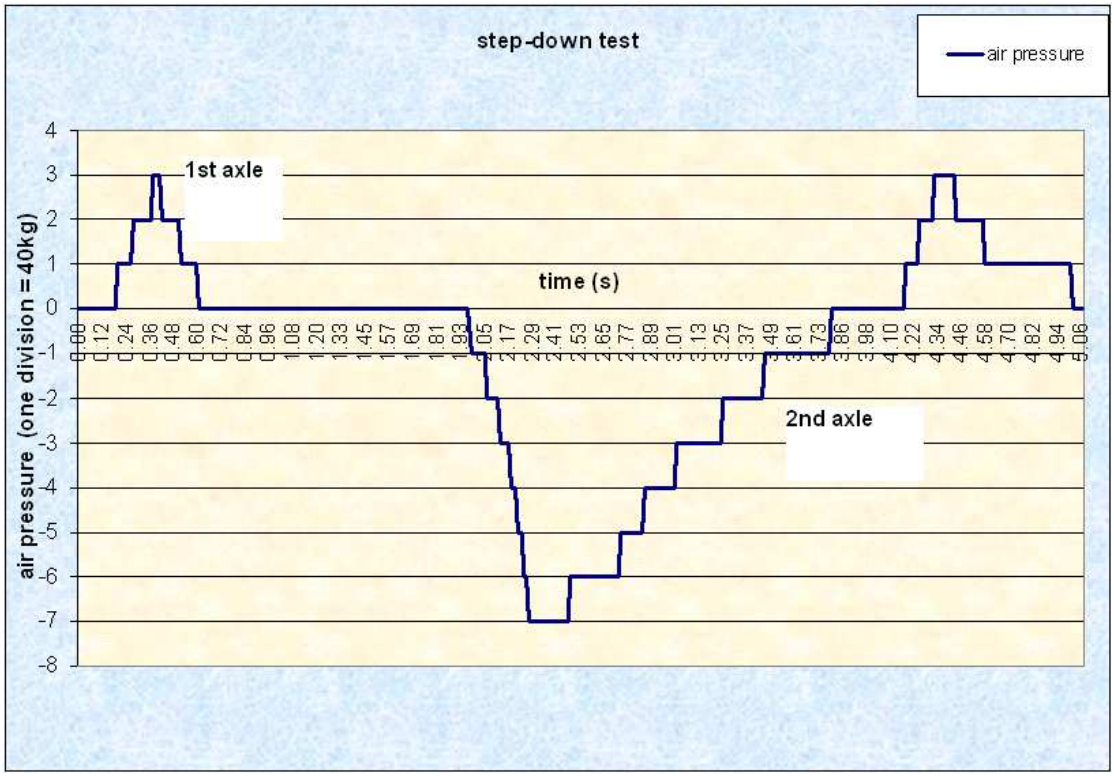

Figure 2. Equalisation of air pressure in the air springs of a quad-axle semi-trailer rolling over a 65mm step-down profile.

The equalisation of air pressure during that process is shown in Figure 2 (Davis & Sack, 2004), showing that equalisation during and after the 2nd axle passed over the step took approximately 3 s. Given that HV axles at highway travel speeds traverse the same point on the road surface separated by about 1/20 s, 3 s is too slow for any sort of effective and pragmatic dynamic load equalisation to occur. Given a 3 s time-constant for air transfer (Davis & Sack, 2004), HVs with conventionally-sized air lines are not having their air-spring pressures equalised within time-scales with similar orders of magnitude as the time-scales of wheel-force impacts between consecutive axles at highway speeds. This does not allow effective dynamic load equalisation between successive axles within an air-sprung multi-axle group during typical operation. This phenomenon creates the potential for unnecessarily high

pavement and suspension loads, with respect to the other axles in the group, when any given wheel encounters a bump. Confirmation of this effect has continued in recent work (Blanksby *et al.*, 2008).

Commercial applications of larger air lines in HV suspensions have been deployed on Australian roads. Innovative suspension systems from Kenworth and the "Haire suspension system" utilise larger-than-standard longitudinal air lines. The alterations to dynamic load sharing and dynamic wheel loads arising from changing the size of air-spring HV suspension air lines need to be investigated adequately.

Since the damage to road and bridge assets increases in an exponential relationship to load (Eisenmann, 1975), the data from the test HVs at full load as the worst case for damage will be used for the analysis and reported herein.

1.5 Organisation of this report

The body of this report for the project *Heavy vehicle suspensions – testing and analysis* is organised as follows:

Section 1, "Introduction" outlines a general summary of the issues surrounding the dynamic load equalisation for air-sprung HV suspensions and also sets out the scope and rationale for this report;

Section 2, "Experimental procedure" documents the methodology used to gather HV suspension data contributing to some of the project outcomes;

Section 3, "Equipment and instrumentation plus some rationale" specifies the instrumentation used for gathering the experimental data and includes a rationale for some of the details of the test programme;

Section 4, "Analysis" provides the background to the derivation of the forces measured in this test programme;

Section 5, "Results" introduces the appendices showing the results of the FFT plots for the dynamic forces at the air springs and wheels. Accelerometer data is also introduced as a reference for this project and future research;

Section 6, “Discussion” outlines where the research has found differences in the two test cases and proposes further avenues of endeavour, both for the project *Heavy vehicle suspensions – testing and analysis* and further post-graduate research that may prove useful; and

Section 7, “Conclusion” sums up the report with some conclusions drawn from the results and analysis sections.

2 Experimental procedure

3 HVs were used for the testing. They were a tri-axle semi-trailer towed with a prime mover, an interstate coach with 3 axles and a school bus with 2 axles. The axle/s of interest and therefore chosen to be instrumented for testing were the tri-axle group of the semi-trailer, the drive and tag axle of the coach and the drive axle of the school bus. All test vehicles had new shock absorbers fitted so that the body-bounce frequency was restored to manufacturer's specification. The air springs (air bags) of the axle/axle group of interest were configured such that they could be connected using either standard longitudinal air lines or an innovative suspension system comprising larger-than-standard longitudinal air lines denoted the "Haire suspension system". The drive axle of the coach and the drive axle of the school bus had a 4-spring configuration with a longitudinal beam attached slightly inboard of the hub on either side and with an air spring on each end of the beams. Figure 3 shows this arrangement for the test case of larger longitudinal air lines. This arrangement supported the chassis with 4 air springs in total for the drive axles of the two buses.

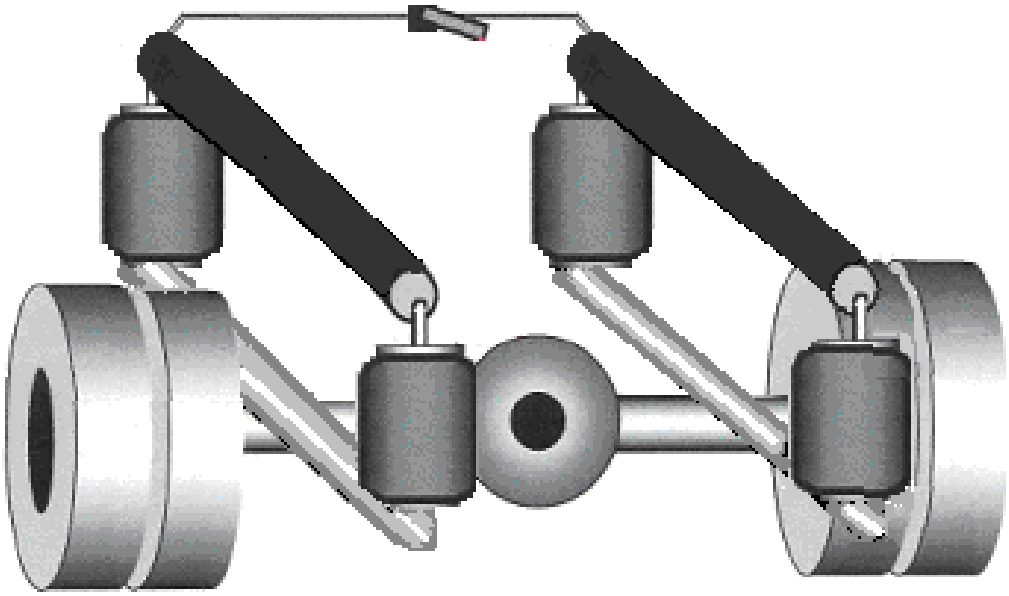

Figure 3. Schematic layout of the "Haire suspension system" as fitted to the school bus and the drive axle of the coach.

The drive axle of the school bus had no corresponding axle with which to "share" its air transfer. Further, whilst air transfer affecting forces between wheels on one axle is not within the scope of this report, "front-to-back" air transfer was altered for the bus during the tests and was analysed accordingly. The tag axle on the coach had an air spring mounted above it on either end. Photos of the test vehicles are shown in Figure 4 to Figure 7. The prime-mover's suspension was not tested in this programme.

Figure 4. Prime mover (top) used to tow the test trailer (bottom).

Figure 5. 3-axle coach used for testing.

Figure 6. 2-axle school bus used for testing.

Figure 7. Sacks of horse feed (yellow) used to achieve test loading on the buses.

3 Equipment and instrumentation plus some rationale

Strain gauges (one *per* hub, up to a maximum of 6 for the tri-axle trailer), were mounted on the neutral axis of each axle of interest between the spring and the hub (de Pont, 1999; Woodroofe, LeBlanc, & LePiane, 1986) as shown in Figure 8, Figure 9, Figure 11 & Figure 12. Shear loading at this point on the axle yielded the static wheel load plus any dynamic wheel load (less the inertial component of dynamic wheel forces due to the unsprung mass outboard of the strain gauges) on each wheel. Attachment was effected by using cyanoacrylate glue (Figure 8, Figure 9, Figure 11 & Figure 12). Figure 8 shows the tag axle arrangement with the bracket (in yellow) for mounting the accelerometer.

Strain gauges were mounted straddling the neutral axis of all axles onto which they were installed. Figure 12 shows the alignment of the strain gauge elements distributed either side of the neutral axis of the semi-trailer axle before the application of waterproofing foil. Strain gauges in final installed mode under waterproofing foil are shown in Figure 8, Figure 9 & Figure 11. Note also the removal of paint and polishing of the surface of the axle to get close contact when gluing the strain gauge to the metal of the axle in Figure 12. The same polishing process was carried out for attaching all the strain gauges but this is obscured by the waterproofing foil in the other photos.

Mounting on the neutral axis reduced, to as small as was practicable, any effect on the gauges due to bending moment as imparted to the axles by lateral forces on the wheels (de Pont, 1999). Previous work (Woodroofe *et al.*, 1986) mounted the strain gauge elements such that longitudinal separation along the neutral axis occurred. This resulted in the individual strain gauge elements measuring slightly different shear forces because one was mounted slightly further toward the wheel than the other on either side. This slight displacement in positioning compared with the ideal is unavoidable since the strain gauge elements cannot be installed (ideally) on top of each other. The installation for this testing took the same pragmatic view that there was no choice but to mount the gauge elements with some physical separation. Given the strain gauge array, the chevrons were mounted above and below the

neutral axis, an arrangement which resulted in as close to practicable to the ideal for measuring shear forces at that point on each axle whilst eliminating transverse wheel forces transmitted to the axle/s in the form of bending moment.

Figure 8. Accelerometer mounting for coach.

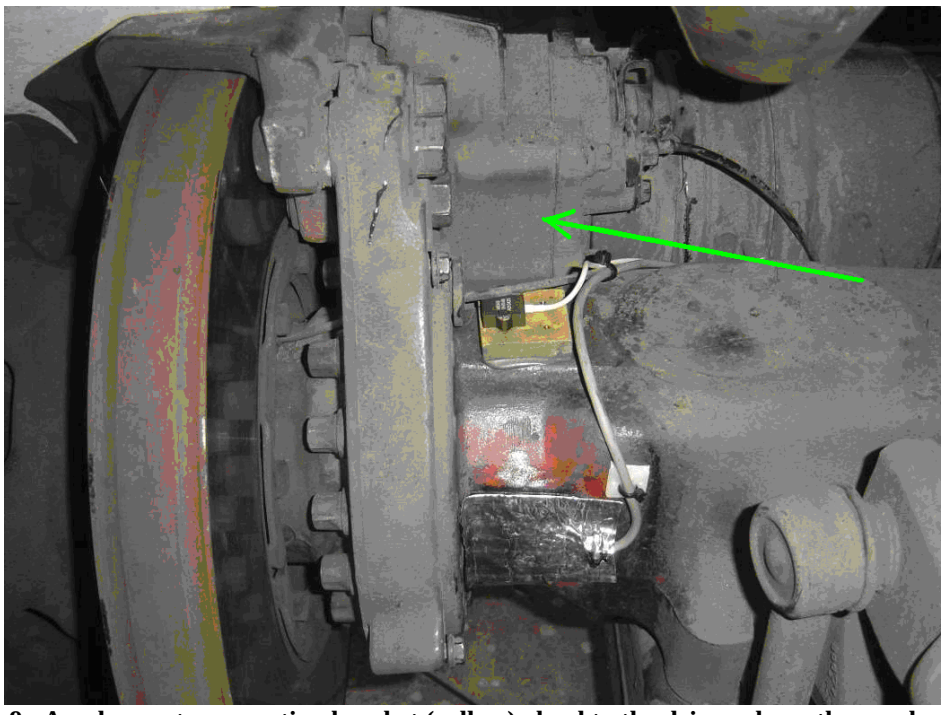

Figure 9. Accelerometer mounting bracket (yellow) glued to the drive axle on the coach and strain gauges (under foil).

Accelerometers (one *per* hub, up to a maximum of 6 for the tri-axle trailer), were mounted as closely as possible to each hub of the test vehicles' axle assemblies, in the case of the tag axle on the coach, or as close to the centreline of the inner wheel for the dual tyre assemblies as practicable. This was to measure vertical acceleration of the unsprung mass outboard of the strain gauges. The signals from these were used to derive the dynamic wheel forces due to the inertial effect of the unsprung mass of the axle and other attached masses (for example, brakes, wheels, hubs, and so on) outboard of the strain gauges (de Pont, 1999). Gluing, bolting or welding mounting brackets to the axles was used to attach the accelerometers as shown in Figure 8 to Figure 10 and Figure 13. Figure 9 & Figure 13 show accelerometer mounting brackets (yellow) glued to the drive axle of the coach and the bus, respectively. To get the mounting brackets or mounting blocks attached as close as possible to the hubs of the buses, portions of the brake assemblies needed to be dismantled. Figure 13 gives some indication of this detail and Figure 9 shows a particular example of this aspect of the test design. Figure 9 shows the coach drive axle with the disc brake cover removed and the position of the yellow accelerometer block mounted on the axle beneath the brake calliper/piston assembly (green arrow, Figure 9). The calliper/piston assembly was removed to allow access to the axle to get an accelerometer mounted at this location.

Figure 10. Accelerometer mounted on top of trailer axle.

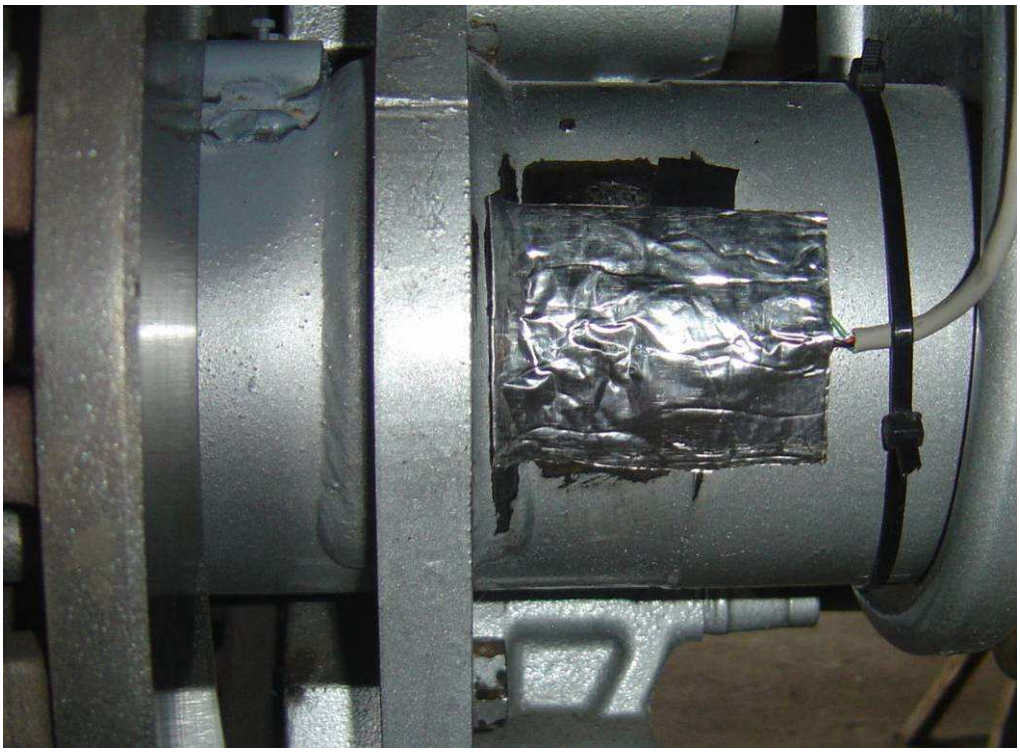

Figure 11. Strain gauge (under foil) on the side of the trailer axle.

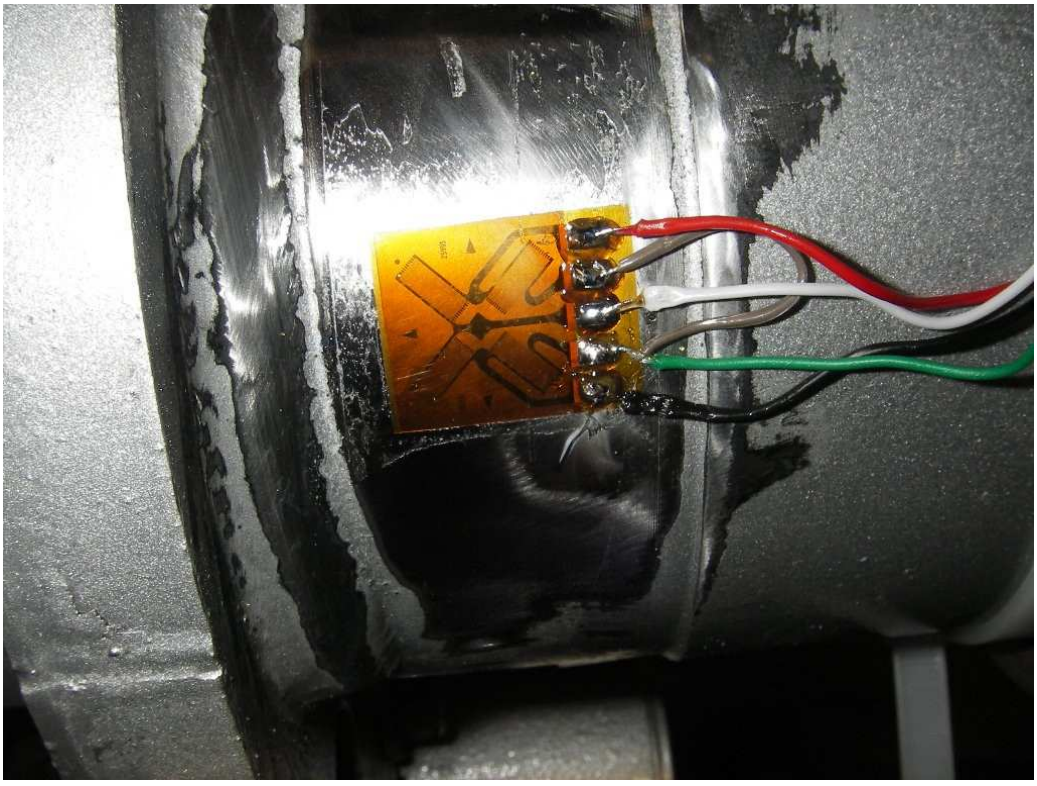

Figure 12. Strain gauge close-up.

Figure 13. Accelerometer mounted on top of school bus axle.

Air pressure transducers (APTs) were mounted in the air lines to the air springs as shown (Figure 15). They measured the air pressure in the air spring and therefore the static and dynamic forces between the axle-end of that spring the chassis.

An advanced version of the TRAMANCO p/l on-board CHEK-WAY® telemetry system was used to measure and record the dynamic signals from the outputs of the strain gauges and accelerometers. Figure 16 and Figure 17 show the CHEK-WAY® recording system for the semi-trailer and the coach respectively and Figure 18 shows the system management computers. Instrumentation trays (foreground and arrowed, Figure 16) were mounted between the semi-trailer rails. The coach instrumentation board was connected by having the rear seat removed and the cabling brought through the access hatch in the floor (bottom left of Figure 17). The school bus had a similar arrangement. The data were recorded in the memory of the CHEK-WAY® units (yellow boxes in Figure 16 & Figure 17). System management computers, Figure 18, were used to manage the data capture timing and post-test data downloads.

The CHEK-WAY® system is subject to Australian Patent number 200426997 and numerous international application numbers and patents which vary by country.

Figure 14. Large longitudinal air line (yellow).

Figure 15. Air pressure transducer (arrowed).

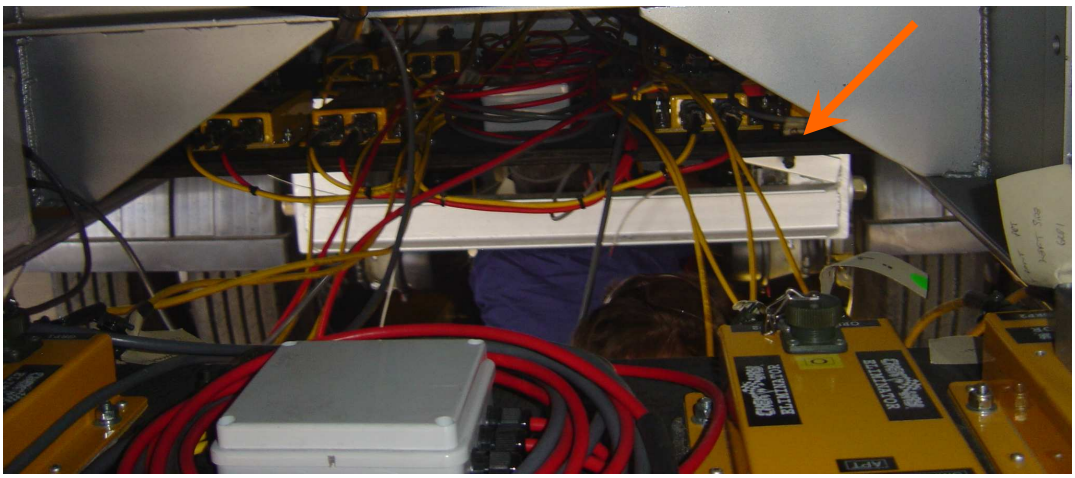

Figure 16. View underneath of semi-trailer, looking to rear.

Figure 17. Instrumentation tray for the coach.

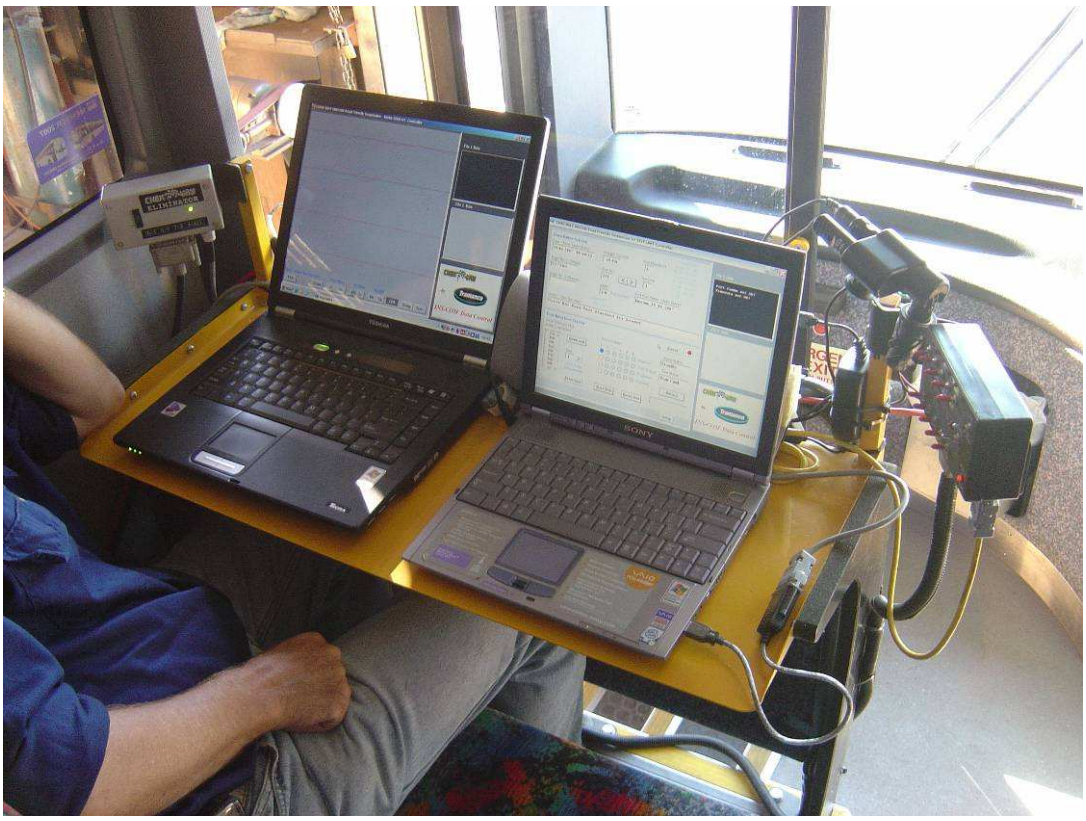

Figure 18. Computers used for data capture management.

3.1 Sampling frequency

The telemetry system sampling rate was 1 kHz giving a sample interval of 1.0 ms. Note that the natural frequency of a typical heavy vehicle axle is 10 - 15 Hz (Cebon, 1999) compared with a relatively low 2 - 3 Hz for sprung mass frequency (de Pont, 1999). Any attempt to measure relatively higher frequencies (such as axle-hop) using time-based recording will necessarily involve a greater sampling rate than when relatively lower frequencies (such as the body-bounce frequency) are to be determined (Houpis & Lamont, 1985). Since axle-hop was the highest frequency of interest for the analysis undertaken, the sampling frequency used by the CHEK-WAY® system was more than adequate to capture the test signal data since its signal sample rate was much greater than twice any axle-hop frequency. Accordingly, and to check the validity of the choice of sampling frequency, the Nyquist sampling criterion (Shannon's theorem) was met (Houpis & Lamont, 1985).

3.2 Calibrating the strain gauges and rationale for mounting

The hub-to-strain gauge distance is small compared to the wheel radius. If strain gauges were fitted to the top and/or the bottom of the axle, they would measure all forces present during testing (including those from lateral wheel forces) as bending moment. This mounting arrangement would then yield combined signals from the strain gauges; the vertical shear force component of which would be indistinguishable from lateral wheel forces, making analysis difficult. Accordingly, strain gauges to measure the shear component of the wheel forces were mounted on the neutral axis of each axle. This method reduced to negligible (as near as practicable) any effects on the strain gauges due to bending moment as imparted to the axles by lateral forces on the wheels (de Pont, 1997). Less complex sets of data were the result and these were more easily analysed because they did not include lateral wheel forces (de Pont, 1997).

The telemetry system and strain gauges were calibrated as follows:

- the static force being exerted by each wheel of the axle group under test on the test vehicle was measured as a static mass value *via* certified scales used by transport inspectors for roadside HV interception. This static mass value was recorded. This was done in conjunction with the calibration of the on-board telemetry system, for efficiency, after it was installed;
- the chassis of the test vehicle was jacked up so that the wheel force registered as close to zero as possible (+5/-0 kg) on the portable scales (Figure 30);
- the reading of the strain gauges under the resultant zero wheel force load was set at that point in the telemetry system as zero using set potentiometers;
- the corresponding strain gauge reading was recorded;
- the chassis was lowered to normal operating mode; and then

- ☞ the static reading of the strain gauges at that point yielded a signal which matched the calibrated wheel force via transport inspector scales less the axle/wheel mass outboard of the strain gauges for each corresponding wheel (as outlined in more detail in Appendix 2).

These readings then provided the offset and slope on the strain *vs*. load graph (Woodroofe *et al.*, 1986) for each axle-end of the axle/s of interest. More details and background theory behind this procedure as well as the complete set of these graphs may be seen in Appendix 2.

After the zero vertical force reading had been taken and the vehicle/s lowered, the test vehicle/s were driven to the loading site and loaded with test weights. This also allowed the suspension to neutralise any lateral or other residual forces in the springs, bushings or tyres before the tare and loaded values were recorded. This procedure was then repeated with the vehicle at full load for the axle group of interest. Where possible, logistical considerations allowing, the procedure was repeated at tare to provide another point on the load/strain reading graph.

The logistical considerations for loading the semi-trailer were minimal: a forklift and standard loads in bins; however, the loading and unloading of the horse feed to provide the test loads in the buses was time and resource intensive.

Due to equipment failure and subsequent re-calibration of a replacement telemetry unit measuring the strain gauges on the school bus, tare and no-load values were used for the strain gauge calibration graphs up to test 238; no-load and full load values were used in the strain gauge calibration graphs after test 238.

3.3 Procedural detail

The road tests comprised driving the HVs over a series of typical, uneven road sections and recording the data generated from each APT, accelerometer and each strain gauge. The sections of road varied in roughness from smooth with long undulations to rough with short undulations. The Brisbane road sections and speeds thereon were as follows:

Sherwood Rd, Rocklea – Westbound after the traffic signals at the Rocklea markets - 40 km/h and 60km/h;

Fairfield Rd, Rocklea and Fairfield – Northbound after the Hi-Trans depot - 60 km/h and 70 km/h;

Fairfield Rd, Fairfield – Northbound after the roundabout at Venner Rd - 60km/h;

Ipswich Mwy – Westbound under the Oxley Rd/Blunder Rd roundabout - 80 km/h and 90 km/h; and

Ipswich Mwy – N/Eastbound after the Progress Rd on-ramp - 80 km/h and 90 km/h.

The same section of road was not used for all speeds during these tests. This was for logistical, safety and consideration of other road-users. Nonetheless, different roads with different roughnesses at different speeds have been used previously and was not unusual for this type of testing (Woodroofe *et al.*, 1986). Further, the variety of surface roughnesses was not available over one section of road within the 10 s recording window of the telemetry system.

The test weights on the vehicles were tare and as close to maximum general access weight was on the rear axle/axle group under test. The vehicles were driven over the test road sections at a variety of speeds from 40 km/h to 90 km/h with the standard air lines connected at tare and at full load. The standard longitudinal air lines between the air springs were then disconnected and the “Haire suspension system” installed. The HVs were then driven over the same road sections *using the same*

wheel-paths at the same speeds as the previous tests at tare and full load. That the same wheel-paths were traversed has been detailed previously (Davis, 2007). At least two runs for each speed were made except for the case of the 70km/h where only one run *per* system was made due to logistical considerations and some localised equipment failure. Some 60km/h sections were traversed up to 5 times to and from the higher-speed test sections. The data for the 70km/h runs for the semi-trailer at tare were invalid due to transducer cables coming loose.

The dynamic signals from the APTs accelerometers and strain gauges on each axle-end of the rear axle/axle group of the HVs under test were recorded for 10 s for the two test cases (*i.e.* standard longitudinal air lines *vs*. the "Haire suspension system") and for the two load conditions (tare and loaded). This resulted in test data in the form of a 10 s time-series signal from each APT, each accelerometer and each strain gauge from each axle-end of interest on each test HV for the two test cases at the various test speeds and the two loading conditions.

The test vehicles were loaded to maximum legal loads and driven off an 80mm step to replicate the VSB11 step test (Australia Department of Transport and Regional Services, 2004c). This was done with standard-sized air lines and then with the "Haire suspension system" installed. For these VSB11-style step tests all wheels were rolled off a set of blocks simultaneously (Peters, 2003). The signals from the air pressure transducers on each air spring (Figure 15) were recorded using the on-board telemetry system during this test procedure. Figure 19 to Figure 21 shows the detail of these tests for the coach, for example. Chains (top left, Figure 19) attached to the chassis were used to drag the blocks once the wheels had moved off them so that the wheels were not fouled as they rolled subsequent to the step-down action.

Figure 19. Before: showing preparation for the step test on the coach.

Figure 20. During: the rear axle group of the coach ready for the step test.

Figure 21. After: the step test which was set up in Figure 20.

4 Analysis

4.1 APT data

The dynamic chassis-to-axle (body-bounce) forces were determined *via* the APT data for the two test cases (standard air lines *vs*. the "Haire suspension system") at the various test speeds for each test vehicle. This was in order to determine alterations to dynamic air-spring forces, if any, due to the fitment of the "Haire suspension system"; since the only alteration to each vehicle between tests was the size of the longitudinal air lines. This data is used in this report and will be used in future to inform the project *Heavy vehicle suspensions – testing and analysis*.

4.2 Dynamic wheel forces

From the work of previous researchers (Cebon, 1999; de Pont, 1997; LeBlanc, Woodroofe, & Papagiannakis, 1992; Whittemore, 1969; Woodroofe *et al.*, 1986), wheel-force may be derived from an instrumented HV axle as shown using the balance of forces (Figure 22) on a particular wheel. Again referring to Figure 22, the dynamic wheel-force, F_{wheel}, may be derived from an instrumented HV axle using the following equation:

$$F_{wheel} = F_{shear} + ma$$

Equation 1

Where:

a is the acceleration of the mass outboard of the strain gauge;

m is the mass outboard of the strain gauge;

F_{shear} is the shear force on the axle at the strain gauge; and

x is the distance from the strain gauge to the effective centroid of the wheel (Cebon, 1999; de Pont, 1997; LeBlanc *et al.*, 1992; Whittemore, 1969; Woodroofe *et al.*, 1986).

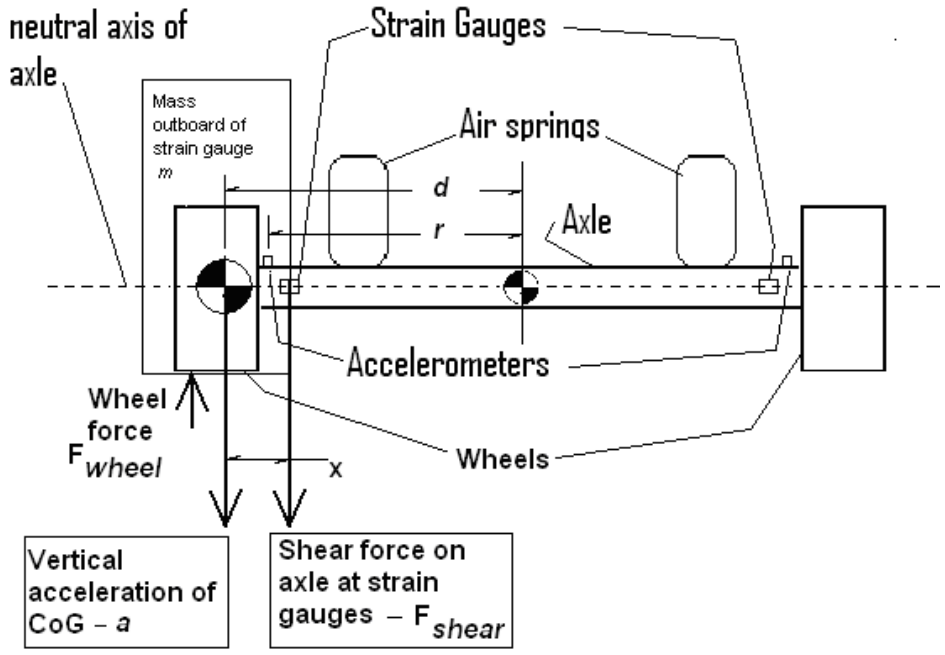

Figure 22. Showing variables used to derive dynamic tyre forces from instrumented HV axle.

Mounting the accelerometers as close as possible to the hubs of the wheels places them, in effect, at the CoG of the mass outboard of the strain gauges. Any small differences between the mounting point and the actual CoG may be neglected if:

- the roll angle is small; and
- the distance from the centre of the axle to the accelerometer approximates to that of the distance from the centre of the axle to the effective centroid of the mass outboard of the strain gauges;

i.e. when:

$d \simeq r$

and especially when:

$(d - r) << d$ (Cebon, 1999).

When comparing two different test cases with the same instrumented axle, the error due to $d \neq r$ will be present for both cases and will therefore cancel out (Woodrooffe & LeBlanc, 1987). Further, de Pont noted that large variations in the value of the mass outboard of the strain gauges do not contribute greatly to overall variations in the resultant wheel forces (de Pont, 1997).

F_{shear} was measured from the strain gauges on each axle-end after calibration (Section 3.2). The value of *m*, representing the unsprung masses outboard of the strain gauges, was determined. For the semi-trailer axle this was found from manufacturer's data (Giacomini, 2007) and weighing the wheels on transport inspector's scales. The bus and coach wheels were also weighed on the transport inspector's scales.

In order to determine the other unsprung masses of the coach and bus axles outboard of the strain gauges, a bent tag axle and a cracked drive axle housing were procured and cut through completely at the strain gauge mounting points. These portions of axle were then weighed on certified scales (Figure 23, Figure 25, Figure 26 & Figure 27). The tag axle was not identical to the one installed on the coach but it was similar enough to provide a valid mass for this portion of the unsprung mass value. Unfortunately, a drive axle half-shaft was not available for destruction but a sound spare was made available on loan. It was weighed and measured. Its mass outside the strain gauge mounting points could be calculated owing to the uniformity of its shape and by using a standard value for the density of steel (Figure 24). The resultant measurement was added to the measured masses of the wheel/s, the measured mass of the requisite portion of the axle housing and to the manufacturer's specified masses (Mack-Volvo, 2007) for the other components for the relevant axle/s. This process yielded the value for *m* (Table 3, p74) in Equation 1 that was applied to the derivation of wheel forces for each HV wheel under test, speed and test case. Signals representing a value of *a* from the accelerometers allowed completion of the equation for each axle-end of interest (de Pont, 1997).

The results of the analysis yielded dynamic wheel-force measures for the two test cases (standard air at full and tare loads. This data is used in this report and will be used in future in the project *Heavy vehicle suspensions – testing and analysis*.

Figure 23. Weighing the half-shaft.

Figure 24. Calculating the half-shaft mass outboard of the strain gauges.

Figure 25. Weighing the drive axle housing mass outboard of the strain gauges. This photo shows the bus axle portion.

Figure 26. Weighing the drive axle housing mass outboard of the strain gauges. This photo shows the coach axle portion.

Figure 27. Weighing the mass of the tag axle portion outboard of the strain gauges.

4.3 Summary of this section

In this section, the method and background theory used to derive wheel-force and axle-to-chassis (body-bounce) data from a test programme have been detailed. This and other data will be used in the project *Heavy vehicle suspensions – testing and analysis*.

5 Results

5.1 General

Appendices 3, 4 and 5 show FFT plots of indicative and representative (but not definitive) data from the APTs, wheel-forces and accelerometer signals at each test speed for the test vehicles for the two test cases. The only alteration to the test vehicles for any test speed was the size of the longitudinal air lines. Space limitations have restricted the provision of these plots to one *per* speed *per* test case *per* vehicle at full load. These data correspond to the data in the following sections for the same test speed and air line test case; *viz*, the FFT for (say) the wheel-forces at 40km/h used the wheel-force data recorded at the same time as the data used for the FFT on the air springs at that speed and test case. The data analysed are from the bus drive axle, the coach drive axle and the front axle of the tri-axle group of the semi-trailer. The recording did not always start at the same point on the test road segment, due to human triggering. Accordingly, the data were examined, time series by time series, and the data matched in time to the same position of the road segment as determined from observing the same impulse in the pair of data recordings. Start and finish times were then adjusted accordingly so that the same recording interval over the particular road segment was used for each matched pair of time-series data.

5.2 Air spring data

Appendix 3 shows FFT plots of APT signals recorded at each test speed. The data used for the FFT analysis are from the bus drive axle, the coach drive axle and the front axle of the tri-axle group of the semi-trailer.

5.3 Wheel-force data

Appendix 4 shows FFT plots of wheel-force data derived by using the accelerometer and strain gauge data and substituting for the variables *a* (from the accelerometers) and F_{shear} (from the strain gauges) into Equation 1. The constant value for *m* was taken from Table 3, p74 for each HV.

The FFT plots are for each test speed. The data analysed are from the bus drive axle, the coach drive axle and the front axle of the tri-axle group of the semi-trailer.

5.4 Accelerometer data

Appendix 5 contains FFTs of the left and right accelerometer signals from various tests. The data analysed are from the bus drive axle, the coach drive axle and the front axle of the tri-axle group of the semi-trailer.

6 Discussion

6.1 General

Vehicle suspensions, by design, are intended to equalise the wheels forces over the points of contact on uneven road surfaces and isolate the passengers and/or the vehicle body from the harshness and vibration of road surface irregularities. How well they do this is determined by the vehicle designer's specifications, the constraints imposed by the vehicle dynamics, the masses of its various components and the vehicle application. The outcome is a necessary compromise between cost, comfort, robustness and use.

Wheel-forces are the summation of dynamic forces originating from within and above the wheels of a vehicle. For the exercise described in this document, indicative (but not definitive) samples of wheel forces, acceleration signals at the hubs and the axle-to-body forces have had their frequency spectra described.

The dynamic loads at (say) air springs can be measured easily using air-pressure transducers, as shown, from the variation in pressures at the springs. This load will be different from the dynamic load at the wheels because the dynamic wheel loads comprise a component due to dynamic loadings from the springs and a component due to the unsprung mass of the axle, wheels, brakes, hubs, tyres, etc. This unsprung mass has its own inertia and will behave differently as it is more closely-coupled to the dynamics induced by irregularities from the road surface. That the unsprung mass dynamics are de-coupled from the chassis to the greatest extent also a design input directive.

6.2 FFT results

The FFT plots in Figure 91 to Figure 120 are provided here to show indicative spectra for HV axles during typical use. The dynamic characteristics of the accelerometers mounted on the axles at the hubs show that the frequencies in the range of approximately 10 - 15 Hz are predominant. The FFT plots, Figure 91 to Figure 120, show that this phenomenon, known as axle-hop (Cebon, 1999; de Pont, 1999) is predominant over most other frequencies with respect to signal strength. Of note, however, are some frequencies in the approximately 5 - 7 Hz range (Figure 93, Figure 112, Figure 113 & Figure 120). These smaller peaks in the frequency spectrum are probably attributable to wheel-hop or hub eccentricity (Cebon, 1999). When comparing the two test cases of air-line size in speed-for-speed FFT comparisons, there does not appear to be marked differences in the peak magnitudes of the frequencies from the accelerometer signals.

The FFT plots for the air-spring data (Figure 31 to Figure 60) show the body-bounce (de Pont, 1999) frequencies in the approximate range 0.8 - 2 Hz. Given that the standard for "road-friendly" suspensions in Australia, VSB 11 (Australia Department of Transport and Regional Services, 2004a) specifies 2.0 Hz as the upper limit for the fundamental body-bounce frequency, this is not surprising. Further, when comparing the test cases of two sizes of air line at each speed, the greatest magnitude of any frequency in the derived FFT spectra appears to be lower for the larger air line case over the standard sized air lines. This is somewhat noticeable for the two cases with the bus as the test HV but the coach and the semi-trailer FFTs show this quite markedly, particularly for the higher speeds. Of note is an anomaly in this hypothesis when comparing Figure 44 *vs.* Figure 59. The reductions in magnitudes of forces at the body-bounce frequencies may start to explain the anecdotal evidence of the efficacy of larger-than-standard air lines from the perspective of driver perception (Estill & Associates Pty Ltd, 2000; Roaduser Systems Pty Ltd, 2002). Both of these points will be the subject of further investigations.

A design choice may be made to isolate or de-couple axle vibration from the chassis by interposing a system of air springs with resonance at lower frequencies than the axles. If so, this should be evident in the results for the frequency spectra of the air

springs (Figure 31 to Figure 60). The air spring suspensions can be seen to be effective in reducing the transmission frequency of road imperfections into the chassis by an order of magnitude: effectively de-coupling axle-hop from passenger perception. Referring to the input parameters for suspension design, this indicates a successful design execution.

HV wheel forces are the primary concern of road authorities with respect to the road network asset. The FFT plots of the wheel forces for the test HVs are shown in Figure 61 to Figure 90. As discussed in detail in Appendix 2 and 4.2, dynamic HV wheel forces are a transmission to the road surface of combined dynamic body-to-chassis forces and dynamic axle forces. Wheel-force is a determining factor in the formulae (Davis & Bunker, 2007) for the dynamic measures of road stress factor (RSF), dynamic load coefficient (DLC) and peak dynamic wheel force (PDWF).

For the wheel forces in all of the vehicles tested:

- the body-bounce spectra predominated at the lower speeds;
- the frequency of greatest magnitude in the wheel-force FFT spectra shifted toward the wheel-hop end of the spectrum with increased test speed: at higher speeds, axle-hop dominated as the contributor of greater magnitude in the wheel-force spectra;
- the axle-hop force component in the wheel-force spectra sometimes was slightly greater than the body-bounce force at higher speeds and with standard suspension; and
- at its largest magnitudes (for higher speeds) the axle-hop force component in the wheel-force spectra was approximate to, or slightly greater than, the magnitude of the body-bounce.

When comparing the two test cases for the bus standard suspension (Figure 61 to Figure 65) *vs.* modified suspension (Figure 76 to Figure 80):

- there was no pattern one way or the other to the changes in wheel-force magnitudes when comparing the two test cases across the test speeds either overall or when comparing LHS with LHS, RHS with RHS;

- a mixed result in the changes in the dynamic measures of DLC, PDWF and RFS when comparing the two test cases for the bus has been reported previously (Davis, 2007). The lack of clear pattern in the peak magnitudes in the spectra for dynamic wheel-forces in the bus standard suspension (Figure 61 to Figure 65) *vs.* modified suspension (Figure 76 to Figure 80) bear out previous results (Davis, 2007); and

- this phenomenon may be linked to the fact that there was no other axle on the bus with which the drive axle could "share" its wheel loads and thus reduce them.

When comparing the two sizes of air line as test cases on the coach:

- the greatest magnitudes in the wheel-force FFT spectra (Figure 66 to Figure 70 and Figure 81 to Figure 85) were for the standard air lines;

- The LHS wheel forces peak magnitudes were greater (except for one instance) than the RHS peaks;

- whilst the bus FFT results were indeterminate with respect to changes in wheel-force peak magnitudes, the coach FFTs show a distinct difference in, and reduction of, the peaks for the two test cases; particularly at higher speeds.

The FFTs yielding wheel-force spectra for the semi-trailer show, for the case of the larger longitudinal air lines *vs.* the standard sized air lines:

- a mixed response when the greatest magnitude wheel-forces are examined;

- the body-bounce contribution to the wheel-force was always lower at all speeds for the modified suspension case; and

- uneven reductions in the magnitude when comparing left-hand to right-hand sides (e.g. Figure 72 *vs.* Figure 87).

The lowering of the fundamental wheel-force frequency by the fitment of larger longitudinal air lines would complement the reductions in magnitude of body-bounce forces noted above at the air springs. This would also inform further

investigations into anecdotal evidence (Estill & Associates Pty Ltd, 2000; Roaduser Systems Pty Ltd, 2002) regarding driver perception of ride and handling quality when larger-than-standard air lines were fitted. If reduction in axle-hop arose uniformly from this modification, the HV's wheels would be more likely stay in contact with the pavement during braking. Further (given the deliberate isolation of the chassis from the axles), harsh, high-frequency vibrations would not be as readily transmitted to the chassis and cabin were this modification implemented.

Woodrooffe (1996) compared the contribution of both axle hop forces and body-bounce forces to HV wheel forces on tandem suspensions. He noted, for shock absorbers in good condition, that the axle-hop contribution to wheel-force was up to 6 times greater than the body-bounce component. This was at the resonant frequencies of axle and chassis on a test-bed simulator. We see from the test results herein for the test vehicles (fitted with new shock absorbers), the wheel-force contribution from axle-hop only ever approximates to the magnitude of the body bounce component. It did not attain an order of magnitude 6 times greater.

All of these points will be the subject of further investigations, noting that the FFTs provided here are for a sample of a much larger data set.

6.3 Theoretical exercise using empirical data

The QUT/Main Roads project *Heavy vehicle suspensions – testing and analysis* continues to consider the mechanism of load sharing between axles on air-sprung HVs. In preparation for this, the simplified diagram of one side of a HV with air suspension in Figure 28 may assist.

The following is a simple theoretical exploration of dynamic load sharing but incorporating some of the empirical results documented in this report. Both the wheels, axles, etc. in Figure 28 are assumed to be of equal mass.

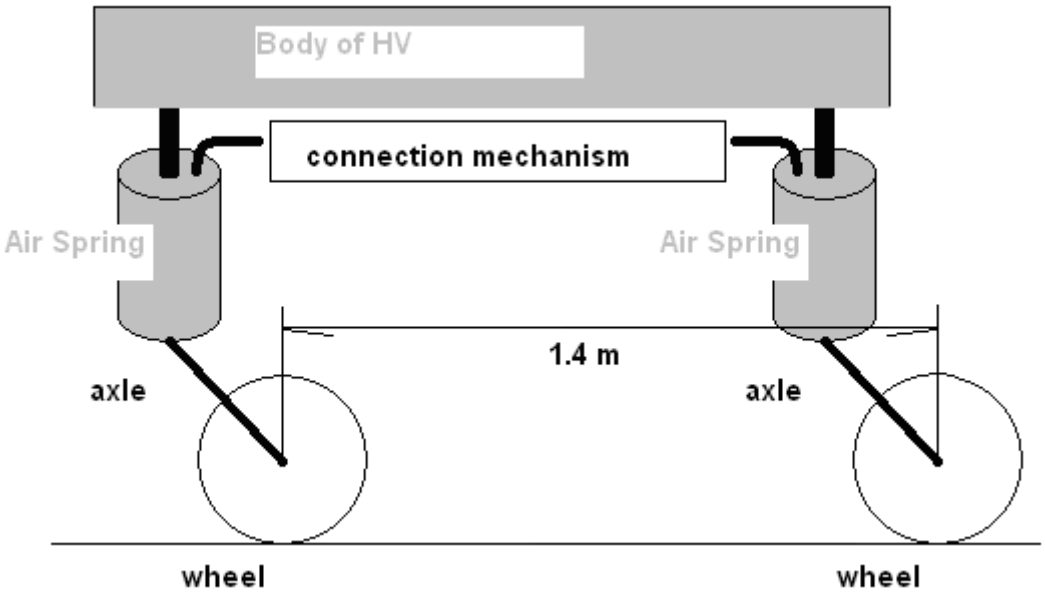

Figure 28. Simplified diagram of multi-axle HV air suspension.

Considering Figure 28: for a connection mechanism in the form of industry-standard longitudinal air lines (order of magnitude: 10mm diameter), then the axles may be considered to be independent of each other, resulting in no load sharing when one or the other wheel encounters a bump (Blanksby *et al.*, 2008; Davis & Sack, 2004). This assumption also means that, should the non-uniformity be large enough that tyre elasticity was not able to accommodate it; one wheel could be lifted of the ground momentarily. Between that scenario and flat pavement (with equal loads on all wheels) is a continuum of possibilities for differing degrees of load sharing between the two wheels in Figure 28.

Now consider a connection mechanism in Figure 28 where air is transferred effortlessly from one air spring to its sequential rear neighbour. The speed of travel would mean that the subsequent wheel would then meet the same bump encountered by the first wheel in a time inversely proportional to the speed of travel.

The time delay between successive wheels travelling over a bump encountered by one side of the HV for the example in Figure 28 can be denoted:

$$t = d / v$$

Equation 2

where:

v = speed in ms^{-1};

d = distance in m; and

t = time in s.

The time between axles encountering the same bump can be denoted the time constant of the system. Where a time constant is present, its inverse is the fundamental (or resonant) frequency of the system.

The diagram in Figure 28 shows the axle spacing at 1.4m. This was the axle spacing for the semi-trailer and the coach used for the testing described above.

Perfect dynamic load sharing would result in equalisation across all wheels of the load from the chassis and unsprung mass as the HV travelled; even when the wheels encountered bumps in the road surface. Now consider the modes of vibration in the axles and the body, as documented in this report, transmitted to the wheels as wheel forces. The axle-hop frequency would be in the range 10 - 15 Hz and would tend to predominate (or at least increase in contribution to wheel-forces) as the speed increased. A bump encountered by the leading wheel would start axle-hop that would then transmit a series of pneumatic pulses to its rear neighbour. If the suspension dampers were working properly, the shock absorbers would damp out this vibration but not before the second air spring received a series of pressure pulses of the same frequency at which its own axle is predisposed to hop. Assume that the frequency of the resonant system thus created would be at the axle-hop frequency. Shortly the rear wheel would encounter the bump experienced by its leading neighbour. The time between these events for 1.4 m axle spacing is dependent on travel speed (Equation 1) and is shown in Table 2.

speed (km/h)	elapsed time between axles (ms)	Frequency (Hz)
40	0.126	8
60	0.084	12
70	0.072	14
80	0.063	16
90	0.056	18

Table 2. Relationship between different speeds and the elapsed time between wheels at 1.4 m spacing.

Assuming an idealised transfer of air from one air spring to its rear neighbour, Table 2 shows that speeds between 60 km/h and 70 km/h result in a resonant frequency in the system of between 12 and 14 Hz. These are coincident with the axle-hop frequencies in the range of 10-15 Hz as reported in the FFTs for wheel-force and hub accelerometers in the Appendices.

6.4 Future work and rationale for some preliminary work to date

From the preliminary analysis in Section 6.3 it is postulated that an imperfect transfer of air between air springs by the use of (say) some constriction device, such as a smaller pipe, to join the connection mechanism to the air springs would be advantageous in that it would damp out pneumatic excitation of resonant frequencies in such air spring systems. This will be the subject of further investigations. Maximum transfer of air from one air spring to its associated rear air spring could be seen to be an ideal situation for load equalisation. However, the practicality of the phenomenon of axle-hop requires that some imperfection needs to be introduced into the transfer mechanism to reduce the possibility of standing waves in the air spring

connector exciting sympathetic oscillations in neighbouring air springs. This line of reasoning may explain some anomalous results in the work on larger longitudinal air lines in this report and other work to date (Davis, 2006, 2007; Davis & Kel, 2007; Davis & Queensland Department of Main Roads, 2006a, 2006b).

The different measures used to compare and determine the quality of one suspension type *vs*. another has been addressed in part previously (Davis & Bunker, 2007). From the results reported here, the alteration of dynamic forces due to design changes may not necessarily improve one particular dynamic measure but may alter another significantly, depending on which one is chosen. This will be the subject of further investigations.

The assumption of equal masses (therefore equal inertias) of the wheels and axles in Figure 28 would change for the case of the coach; the tag axle being lighter. Detailed analysis has not been performed here but it postulated that the axle-hop frequency of the tag axle would be higher than that of the drive axle. If so, then the improved flow of air from the larger air lines between the drive and tag axle on the coach may have resulted in the resonant frequencies of the two axles complementing, rather than competing with, each other for frequency spectrum space when compared with the results of the semi-trailer with its equal mass axles and wheels. It is postulated that, with further research to be done, this may explain the consistent improvements in wheel force frequency spectrum peak magnitudes for the larger air line case on the coach when compared to the varied semi-trailer results in Appendix 4. Further, if there were no second or subsequent wheel and air spring in Figure 28, this would mean that the axle forces would result in compression and rarefaction of the air in the air spring and any connecting reservoirs such as a blanked-off connection mechanism. This would result in a softening of the shock from dynamic forces on the axle due to the ability to compress more air in the increased effective volume of air in the air springs and associated blanked-off connection mechanism. This type of device has been used in HVs to soften suspensions, particularly in passenger buses; it is called a “ping tank” The influence of the larger air lines acting as a “ping tank” for the case of the school bus used in the testing will be the subject of further investigations.

In general, the magnitudes of the left hand side body-bounce, axle hop and wheel forces are greater than are those on the right hand side. It is postulated here, with further research to be done, that this is due to two factors:

- potholes on the left hand side predominating over right-hand side potholes in frequency of occurrence and magnitude; and
- the left hand camber of the road shifts the centre of mass of the body to the left during typical vehicle operation.

Further work needs to be done in the area of how well the forces at the axle and other unsprung suspension components are correlated with air spring forces. From the preliminary results outlined here, there appears to be no or little correlation. Axle inertia combined with suspension damping acting to de-couple the pavement frequencies from the chassis is postulated. An alternate method for postulating on this phenomenon in system terms would be that the suspension is acting as a low-pass filter, isolating high-frequency road irregularities from the chassis. This is postulated as a result of the suspension design meeting one of its criteria in that the range of frequencies measured for the unsprung masses below the axle are not the same as the resonant body bounce frequencies, effectively isolating the chassis as much as is possible (and therefore the payload and/or the passengers) from the harshness and vibration due to pavement irregularities.

Upon analysis of the data from the various instruments on the test vehicles, it became apparent that, for some speeds and road sections the minima and maxima were different due to the different surface roughnesses present on the test sections of road. Some of the results published elsewhere (Davis, 2006, 2007; Davis & Kel, 2007) or submitted for review at the time of writing have dealt with that issue. One method for approaching this is to perform “matched-pair” testing. The data are paired with the data for the same run over the same section of road at the same speed for the two test cases. A t-test with unequal variances to determine the differences between the means of the two sample populations was then appropriate. The unequal variances resulted from the differences in the speeds and the differences in road segment characteristics. Nonetheless, the pairs of tests with and without the suspension modifications were able to be compared statistically in this way (Chieh,

2008). In summary, changes from one test condition to another may be determined for validity provided that each data pair in the set of data has only one change, in this case the size of the longitudinal air lines.

A t-test has been performed, the results of which will be published in another forum, to determine statistical significance of positive changes to the various dynamic measures for the two cases of longitudinal air line size. A heteroscedastic test option was chosen since the data from the two test cases had unequal variances (Kariya & Kurata, 2004). A one-tailed test was used (StatPac Inc, 2007) since:

- previous work (Davis, 2007) and the background analysis (to be published in future) of the dynamic measures from the APTs indicated that the larger longitudinal air lines generally improved dynamic measures; and
- the other tail would inform the case where performance was improved beyond the confidence limit (Hamburg, 1983).

7 Conclusion

This reports sets down the methodology and preliminary results of testing carried out to gather data for the QUT/Main Roads project *Heavy vehicle suspensions – testing and analysis*. The results as documented in Appendices 3 to 5 should provide useful source data for that project and other projects once that project concludes.

Some preliminary conclusions may be drawn at this stage:

- there appears to be little or no correlation between dynamic forces in the air springs and the wheel forces in the HVs tested;
- axle-hop at frequencies between 10 - 15 Hz predominated for unsprung masses in the HV suspensions tested;
- air-spring forces are present in the sub-1.0 Hz to approximately 2 Hz frequency range; and
- for the data samples analysed and presented in this report larger air lines alter HV wheel forces somewhat and body-bounce reasonably consistently.

More research needs to be done on these points and will from part of the work in the QUT/Main Roads project *Heavy vehicle suspensions – testing and analysis*. Further, more work is required on the load sharing mechanisms between axles on air-sprung HVs. In particular, how and whether improved load sharing can be effected and whether better load sharing between axles will reduce dynamic wheel and chassis forces. This last point, in particular, in relation to the varied dynamic measures used by the HV industry to compare different suspension types.

8 Acknowledgements

The authors would like to thank:

- the people at Tramanco for technical assistance in cutting up the axle/s, installing and removing the HV telemetry system and the transducers and test equipment;
- the people at Volvo (in various Australian States) for technical assistance, supply of the axle mass data, lending the testing team a half shaft, supplying a cracked drive axle housing so that we could destroy it for the greater good and their in-kind support and much patience rectifying the buses after we took the brakes apart to install the accelerometers;
- the Queensland Transport Darra depot transport inspectors who lent us the scales at a moment's notice;
- the RTA of NSW who contributed funding when we ended up with more test vehicles than our original budget allowed for;
- the people at Mylon Motorways for technical assistance, supply of drivers and the loan of the buses; and
- the people from Haire Truck and Bus for drivers, finding the unserviceable tag axle for the testing team to destroy, the loan of the semi-trailer/prime mover and for technical assistance.

Appendix 1. Definitions, Abbreviations & Glossary

Terms, abbreviations and acronyms	**Meaning**
APT	Air pressure transducer. A device for emitting an electrical signal as a proportional surrogate of input air pressure.
Axle hop	Vertical displacement of the wheels (and axle), indicating dynamic behaviour of the axle and resulting in more or less tyre force onto the road. Usually manifests in the frequency range 10 – 15Hz.
Body bounce	Movement of the sprung mass of a truck as measured between the axles and the chassis. Results in HV body dynamic forces being transmitted to the road via the axles & wheels. Usually manifests in the frequency range 1 – 4Hz.
CoG	Centre of gravity. The point at which a body's mass may be said be concentrated for purposes of determining forces on that body.
DIVINE	Dynamic Interaction between heavy Vehicles and INfrastructurE.
DoTaRS	Department of Transport and Regional Services. An Australian Government department.
Δ	Greek letter "delta" – denoting increment.

Dynamic load coefficient (DLC)	Coefficient of variation of dynamic tyre force. It is obtained by calculating the ratio of the root-mean-square (RMS) of the dynamic wheel forces (std. dev. of F_{mean}) divided by the static wheel-force, *i.e.* the coefficient of variation of the total wheel load: $DLC = \sigma / F_{mean}$ Where: σ = the standard deviation of wheel-force; and F_{mean} = the mean wheel-force. A perfect suspension would have a DLC of 0. The range in reality is somewhere between 0 and 0.4 (Mitchell & Gyenes, 1989).
FFT	Fast Fourier transform. A method whereby the Fourier transform is found using discretisation and conversion into a frequency spectrum.
Fourier transform	A method whereby the relative magnitudes of the frequency components of a time-series signal are converted to, and displayed as, a frequency series. If the integrable function is h(t), then the Fourier transform is: $\phi(\omega) = \int_{-\infty}^{+\infty} h(t) e^{-i\omega t} dt$ Where: ϕ is the Fourier series; ω is the frequency in radians/s; and $i = \sqrt{-1}$ (Jacob & Dolcemascolo, 1998).
HML	Higher mass limits. Under the HML schemes in Australia, heavy vehicles are allowed to carry more mass (payload) in return for their

	suspension configuration being "road friendly". See VSB 11.
HV	Heavy vehicle.
Hz	Hertz. Unit of vibration denoting cycles *per* second.

LSC	Load sharing coefficient – a measure of how well a suspension group equalises the total axle group load, averaged during a test. This is a value that shows how well the average forces of a multi-axle group are distributed over each tyre and/or wheel in that group. $LSC = \frac{F_{mean}(i)}{F_{stat\ (nom)}}$ Where: $F_{stat\ (nom)}$ = Nominal static tyre force = $\frac{F_{group\ (total)}}{n}$ $F_{group\ (total)}$ = Total axle group force; F_{mean} (i) = the mean force on tyre/wheel i ; and n = number of tyres in the group (Potter *et al.*, 1996).
OECD	Organisation for Economic Co-operation and Development
QUT	Queensland University of Technology
RFS	"Road-friendly" suspension. A HV suspension conforming to certain limits of performance parameters defined by VSB 11. (Australia Department of Transport and Regional Services, 2004a)
VSB 11	Vehicle Standards Bulletin 11. A document issued by DoTaRS that defines the performance parameters of "road-friendly" HV suspensions.

Appendix 2. Strain gauge calibration and unsprung mass data

The following Appendix details the values of the unsprung masses, the strain gauge calibration graphs and their derivation. The strain gauge calibration graphs include the correlation of strain gauge readings to wheel forces for no load and/or tare and/or full load readings for the various test vehicles.

As shown in Equation 1, the total dynamic wheel force F_{wheel} has two terms F_{shear} and ma.

The unsprung mass m outboard of the strain gauges contributes the m coefficient of a in the ma term of Equation 1. In order to determine the value of m in Equation 1, the unsprung mass outboard of the strain gauges was found as outlined in Section 4.2 and documented in Table 3, p74. Accordingly, the contribution to the total wheel force values of the mass m when subjected to the hub acceleration a was derived during the data analysis phase by multiplying the value of m by the measured value of a in Equation 1.

In order to determine a dynamic value of F_{shear} in Equation 1, the relationship between the strain gauge reading and the dynamic forces in the axle resulting from dynamic wheel-forces needed to be determined. As detailed in Section 3.2, the strain gauges were calibrated (Woodroofe *et al.*, 1986). This process will be reviewed in greater detail here.

When static weighing using the scales under each wheel of interest was performed, the static value of F_{wheel} measured on the scales contained two force components:

- A force component inboard of the strain gauge and acting through the spring. This component was due to the chassis and suspension components, etc. transmitted via the axle to the wheel; and
- a force component due to gravity acting on the unsprung mass outboard of the strain gauge.

The first force component was found via the strain gauge readings and their relationship with the wheel force registering as a mass on the scales. However, this wheel force was not totally aligned with the strain gauge readings since the static value of F_{wheel} measured on the scales contained two components: static F_{shear} and static ma. Further, the strain gauges measured deflection proportional only to the forces inboard of their mounting point. We needed to find the force component due to m. This was done as follows, with theoretical commentary included and referring to Figure 22:

- ☞ for the case of the chassis of the test vehicle jacked up until the wheel of interest was registering zero (+5/-0 kg) force on the calibrated scale under it, the static shear force measured at the strain gauge was not zero, even though the scales under the wheel registered zero mass (also described in Section 3.2);

- ☞ with the static wheel-force registering zero, the axle was experiencing a slightly negative shear force due to m at this point; *i.e.* as the unsprung mass of the wheel/hub of interest was in equilibrium and registering zero wheel force at the scales, the strain gauges were registering a shear force across the axle equivalent to a negative value of m at that point;

- ☞ in this condition, the strain gauge reading (corresponding to F_{shear} at that point) was recorded as the static but negative value analogous to m (as documented in Table 3) for that hub/axle stub;

- ☞ these negative values can be seen as the negative y-axis offsets in the plots of static wheel force *vs*. strain gauge readings in Table 4 to Table 6.

The value of m is documented in Table 3, p74; the a for the static reading was acceleration due to gravity, 9.81 ms^{-1}. Finding the value of unsprung mass outboard of the strain gauges forms the first (lowest) point on the static wheel force *vs*. strain gauge graphs (Table 4, Table 5 and Table 6) provided later in this Appendix. Hence, for the purposes of the wheel-force *vs*. strain gauge graphs, the negative value of m became the lowest point on the graph for each wheel of interest; *i.e.* when plotting the relationship between the strain gauge readings *vs*. known static mass

values, the lowest point was the static mass of each wheel/hub outboard of the strain gauge.

Tare load and/or full load was applied to the test vehicles. The strain gauge readings corresponding to these known (via the scales) wheel-force values were recorded for no-load, tare and/or full load. Additional points were then added to the graphs in Table 4, Table 5 and Table 6. Again, these were found by measuring the static wheel forces with the calibrated scale under each wheel of interest.

After the zero vertical force reading had been taken and the vehicle/s lowered, the test vehicle/s were driven to the loading site and loaded with test weights. This also allowed the suspension to neutralise any lateral or other residual forces in the springs, bushings or tyres before the tare and loaded values were recorded.

For each point in the graphs in Table 4, Table 5 and Table 6 the static wheel-force scale reading (corresponding to the strain gauge reading for that load point) had the value of *m* subtracted from it. This was because of the inequality between the strain gauge reading and the wheel-force values as outlined above; *i.e.* the strain gauge was only measuring F_{shear}, not F_{wheel}.

Using the linear regression lines of these graphs, direct mapping (or correlation) of dynamic signals recorded from the strain gauges during the testing could then be performed. Each dynamic strain gauge value recorded was then correlated directly to a wheel-force value extrapolated from the corresponding linear regression formula that defined the relationship between wheel-force (calibrated scale readings) *vs*. strain gauge readings for the particular wheel of interest. This then provided the dynamic values for F_{shear} in Equation 1. Adding this term to the derived term *ma* in Equation 1 produced dynamic F_{wheel} data for each wheel of interest.

For some tests on the bus, either the full load reading or the tare reading was not available for logistical reasons and equipment failure necessitating re-calibration after replacement data recorder/excitation units had been installed. Daily checks on the quiescent outputs of the strain gauges showed slight variations due to vehicle supply voltage fluctuations. The strain gauge digital count values were noted and the calibration graph equations for that series of tests were adjusted accordingly. Telemetry equipment failure after tests 197 and 238 necessitated recalibration of the

replacement system. The calibration graph for recordings after test 238 used a different calibration graph since the bus could not be unloaded and re-loaded to determine the tare values for the replacement measurement system. This detail is as noted in the titles in Table 5.

The school bus had its strain gauges mounted slightly more inboard on its drive axle than for those positions on the coach drive axle. This resulted in a slightly greater drive axle unsprung mass outboard of the strain gauges on the school bus compared with the coach.

As noted above, one of the steps in calibrating the strain gauges was to jack up the chassis of the test vehicle so that the wheel force registered as close to zero as possible (+5/-0 kg) on the portable scales. Figure 29 shows the method of jacking the chassis so that the wheels could have the scales placed under them. Figure 30 shows the detail of setting the wheel-force to equilibrium for the purposes of setting the recording equipment.

Figure 29. Jacking the test vehicle so that the static wheel-force could be set to zero.

Figure 30. Gradually reducing the wheel force as the chassis is jacked up: top panel, almost there; bottom panel, no wheel force.

Axle mass data

Unsprung axle/wheel mass outboard of strain gauge

	Coach drive axle/wheels	Coach tag axle/wheels	School bus axle/wheels	Semi-trailer axle/wheels
Hub, brakes, bearings, nuts etc	192.3 kg (Mack-Volvo, 2007)	140.2 kg (Mack-Volvo, 2007)	187.3 kg (Mack-Volvo, 2007)	149.4 kg (Giacomini, 2007)
Wheels	166 kg (measured on TI scales)	83 kg (measured on TI scales)	180 kg (measured on TI scales)	180 kg (measured on TI scales)
Housing/axle portion	30.8 kg (Figure 26)	5.2 kg (Figure 27)	32.8 kg (Figure 25)	7.1 kg (Giacomini, 2007)
Half shaft	10.7 kg (Figure 23 & Figure 24)	n/a	11.4 kg (Figure 23 & Figure 24)	n/a
Total	399.8 kg	228.35 kg	411.5 kg	336.5 kg

Table 3. Unsprung mass outboard of the strain gauges for the test vehicles.

Static wheel force *vs*. strain readings: coach

Table 4. Static wheel force *vs*. strain readings: coach

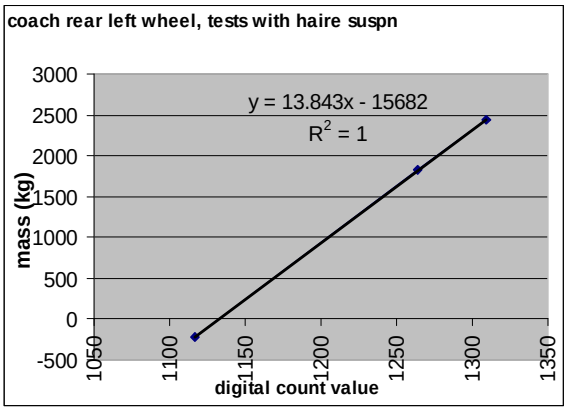

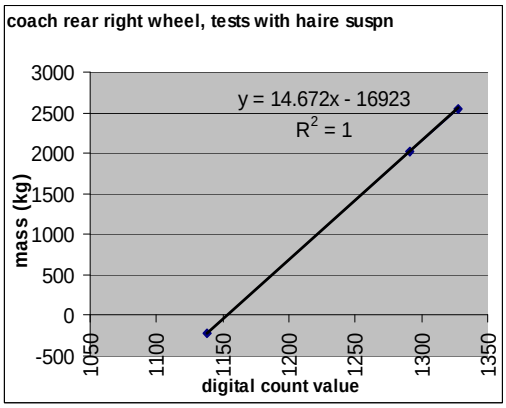

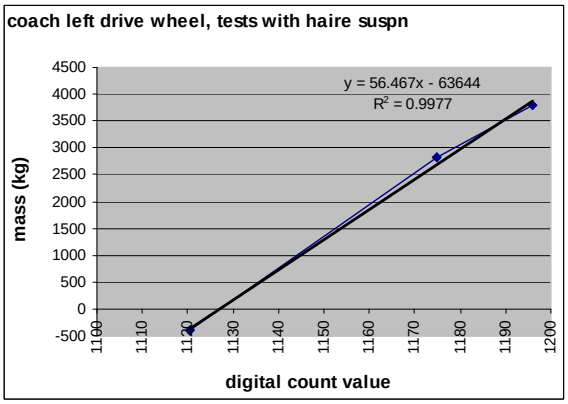

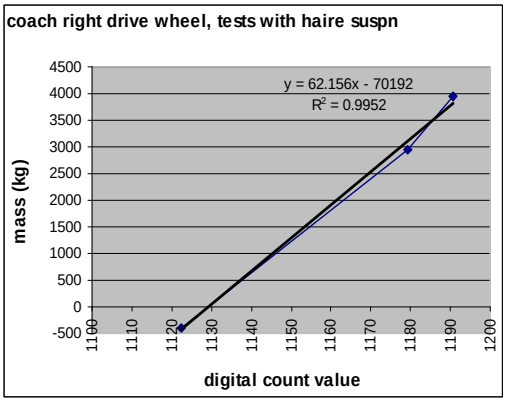

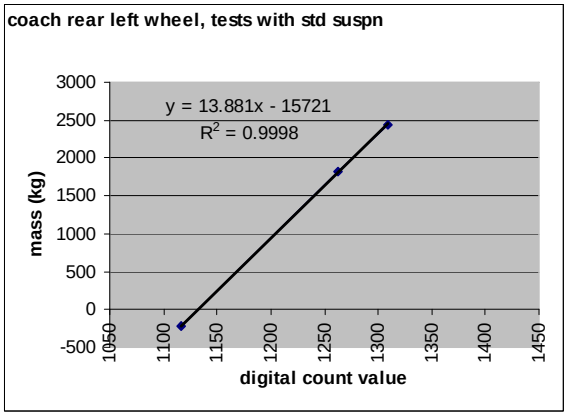

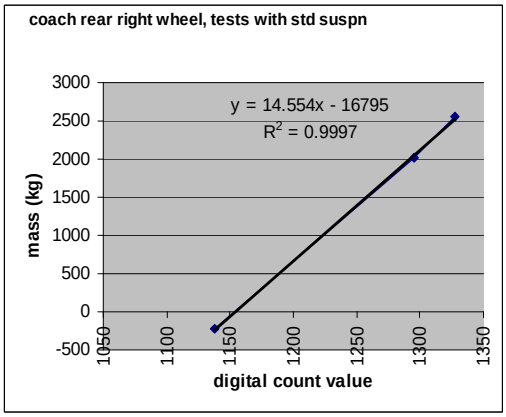

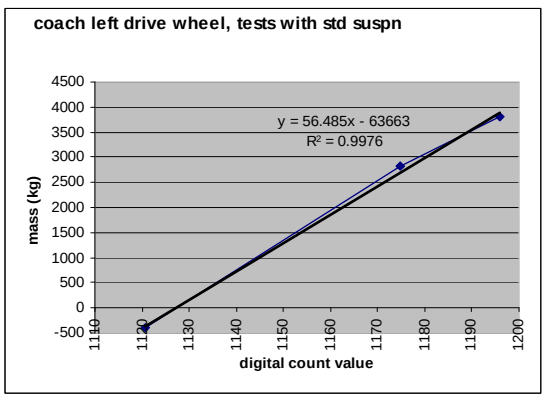

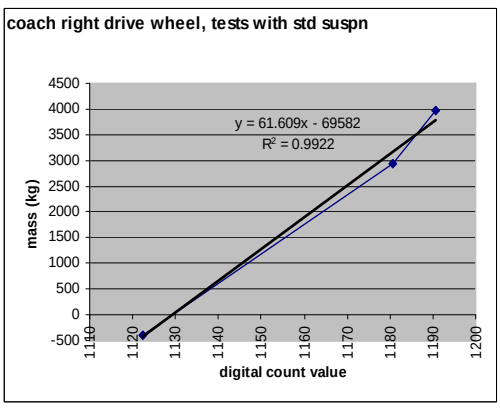

Static wheel force *vs*. strain readings: School bus

Table 5. Static wheel force *vs*. strain readings: bus

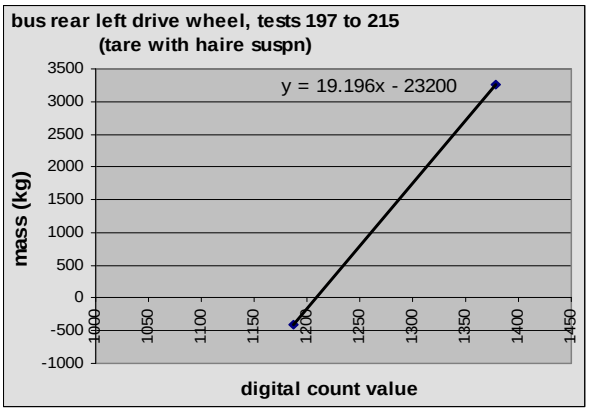

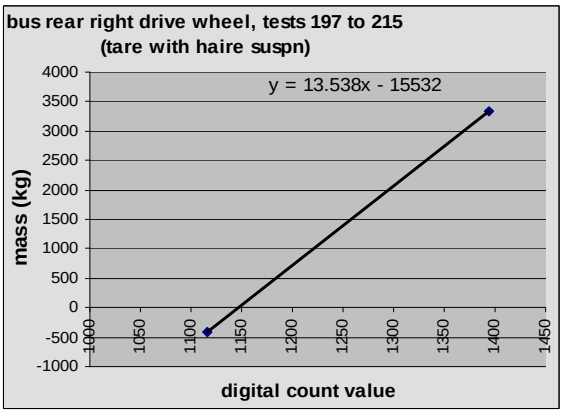

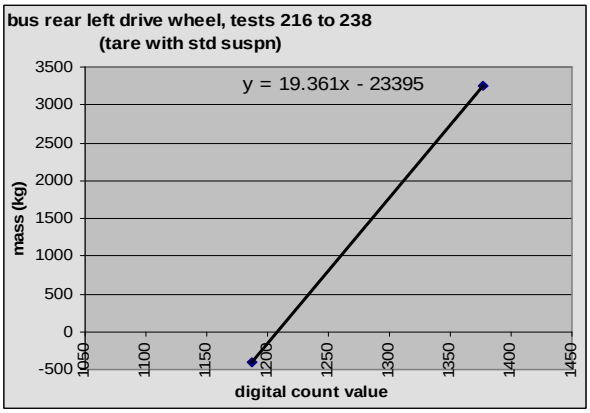

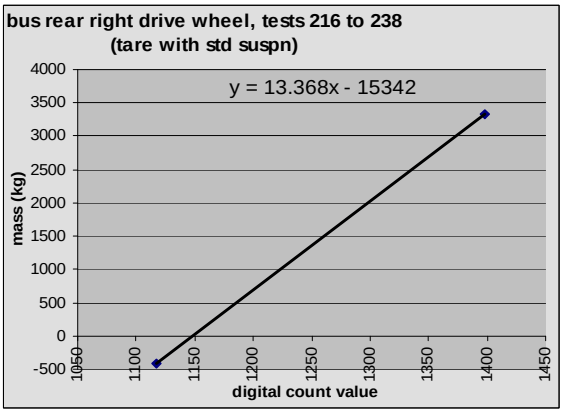

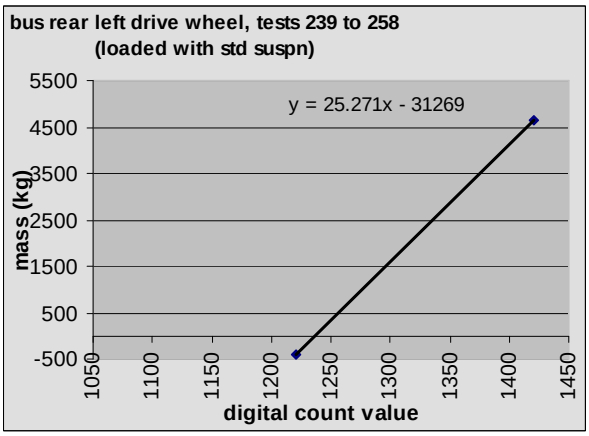

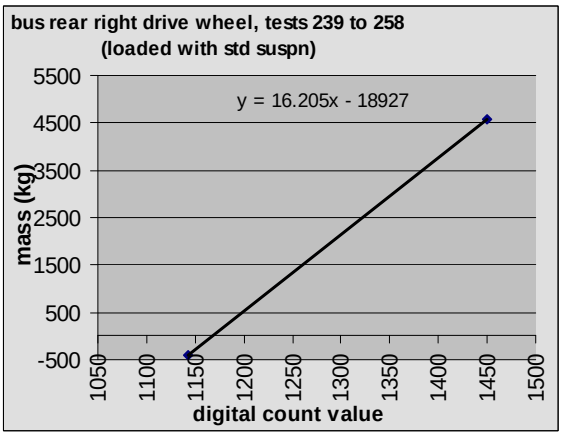

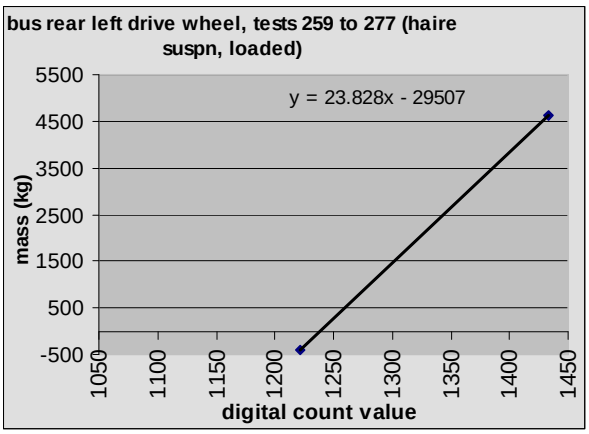
bus rear left drive wheel, tests 259 to 277 (haire suspn, loaded)
y = 23.828x - 29507
mass (kg)
5500
4500
3500
2500
1500
500
-500
1050
1100
1150
1200
1250
1300
1350
1400
1450
digital count value

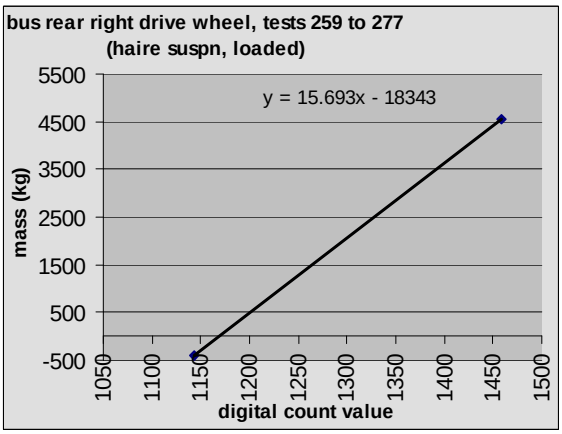
bus rear right drive wheel, tests 259 to 277 (haire suspn, loaded)
y = 15.693x - 18343
mass (kg)
5500
4500
3500
2500
1500
500
-500
1050
1100
1150
1200
1250
1300
1350
1400
1450
1500
digital count value

Static wheel force *vs*. strain readings: semi-trailer

Table 6. Static wheel force *vs*. strain readings: semi-trailer

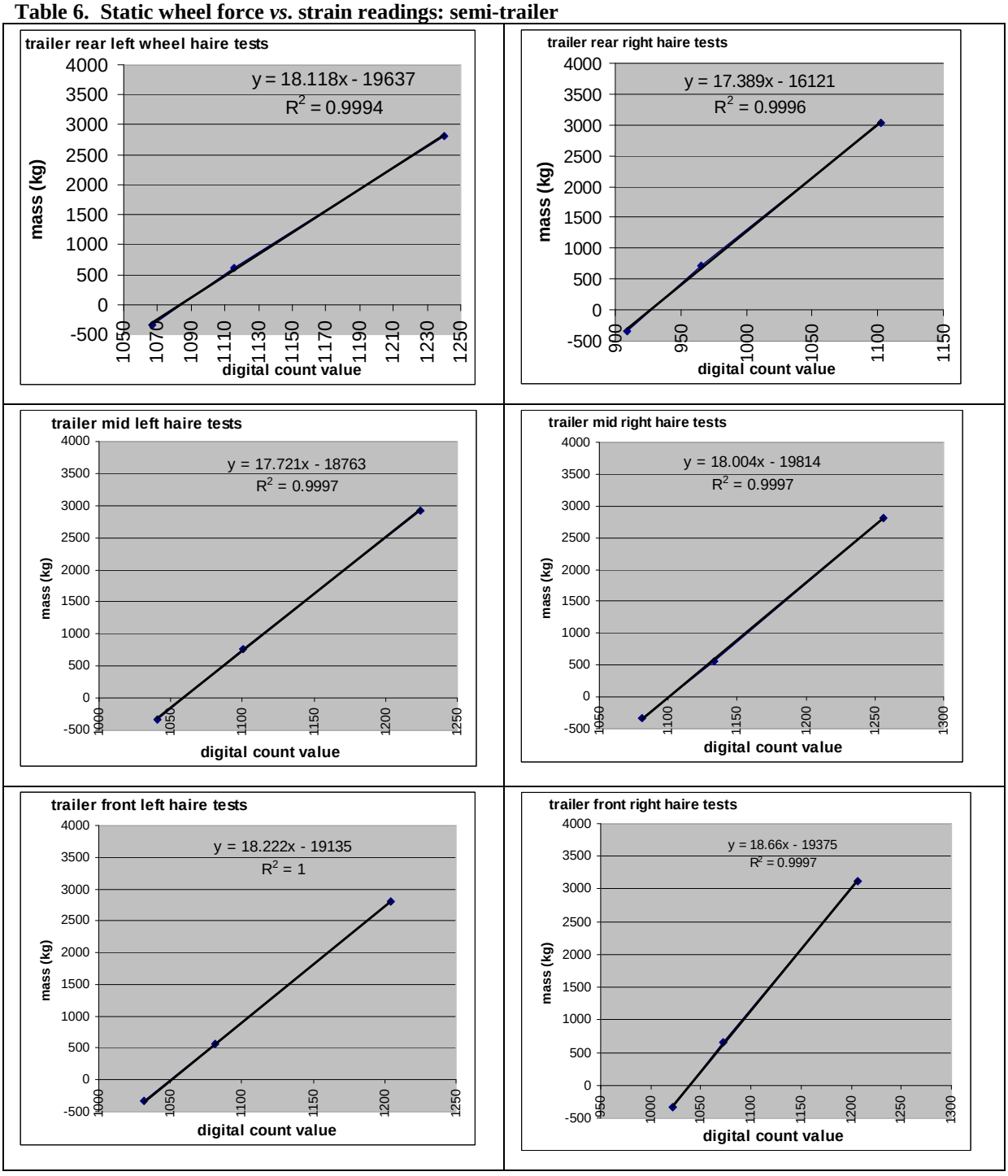

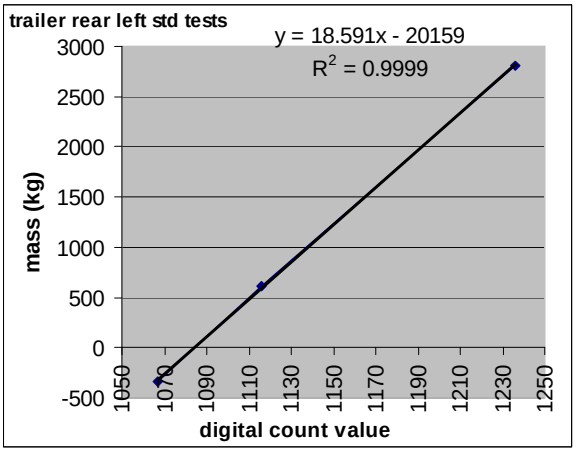
trailer rear left std tests
y = 18.591x - 20159
R2 = 0.9999
mass (kg)
digital count value

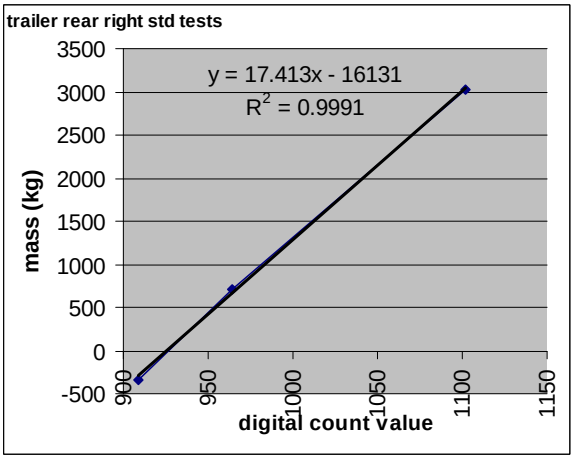
trailer rear right std tests
y = 17.413x - 16131
R2 = 0.9991
mass (kg)
digital count value

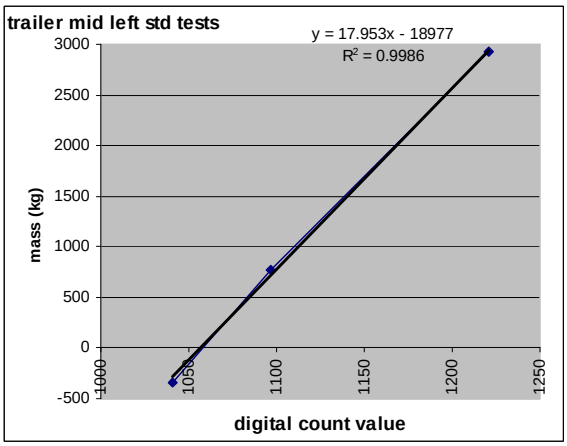
trailer mid left std tests
y = 17.953x - 18977
R2 = 0.9986
mass (kg)
digital count value

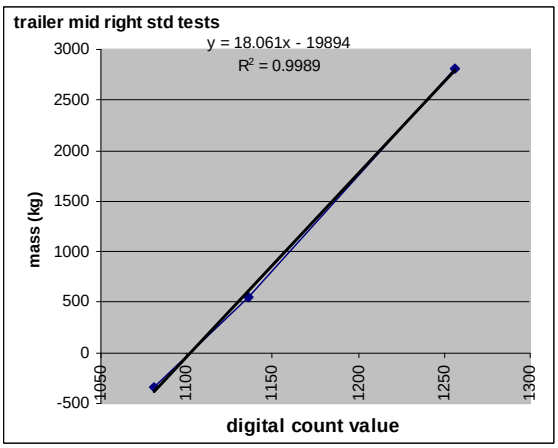
trailer mid right std tests
y = 18.061x - 19894
R2 = 0.9989
mass (kg)
digital count value

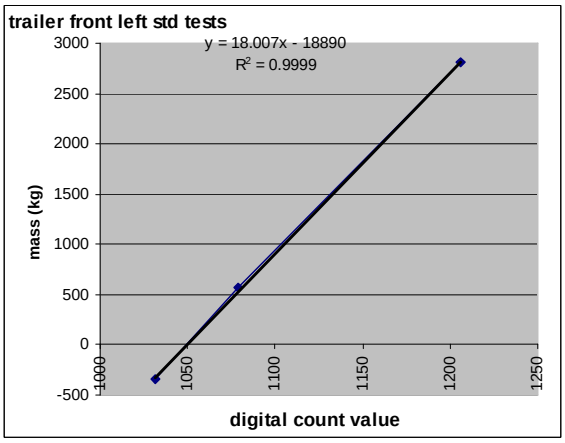
trailer front left std tests
y = 18.007x - 18890
R2 = 0.9999
mass (kg)
digital count value

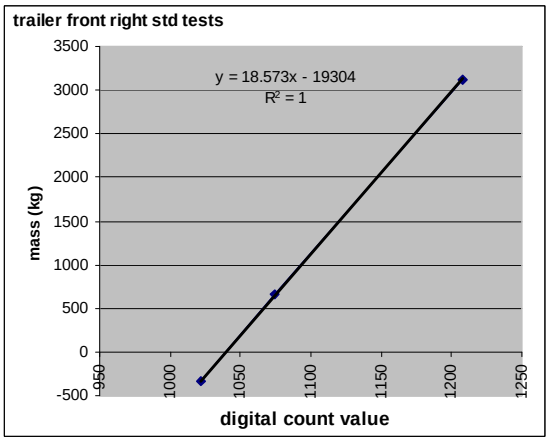
trailer front right std tests
y = 18.573x - 19304
R2 = 1
mass (kg)
digital count value

Appendix 3. Fast Fourier plots – air spring signals

Standard suspension

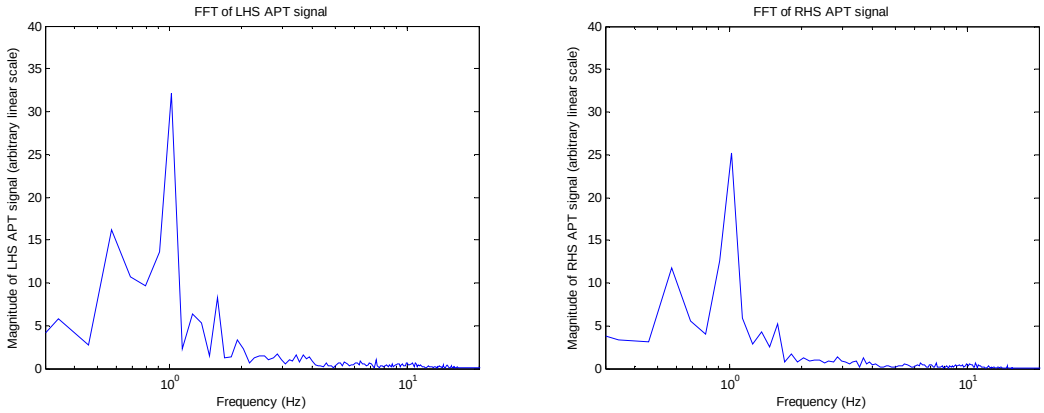

Figure 31. FFT of air spring signals - std suspension, bus loaded, 40km/h, test 235

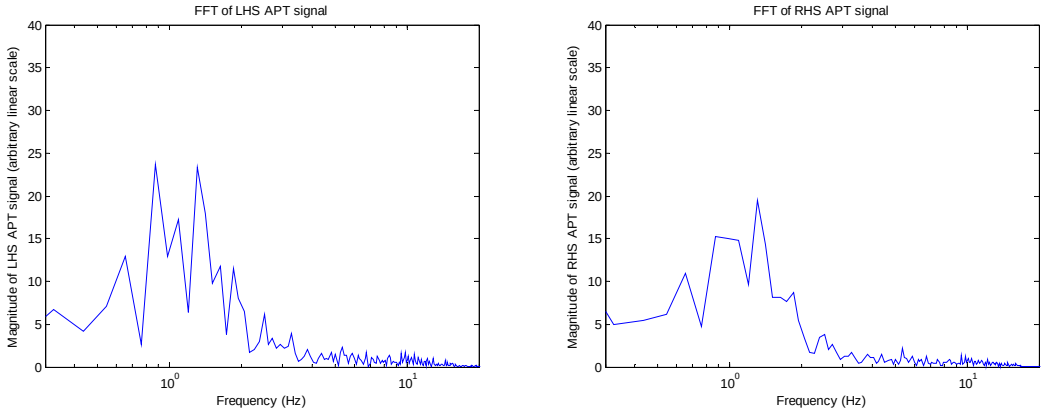

Figure 32. FFT of air spring signals - std suspension, bus loaded, 60km/h, test 254

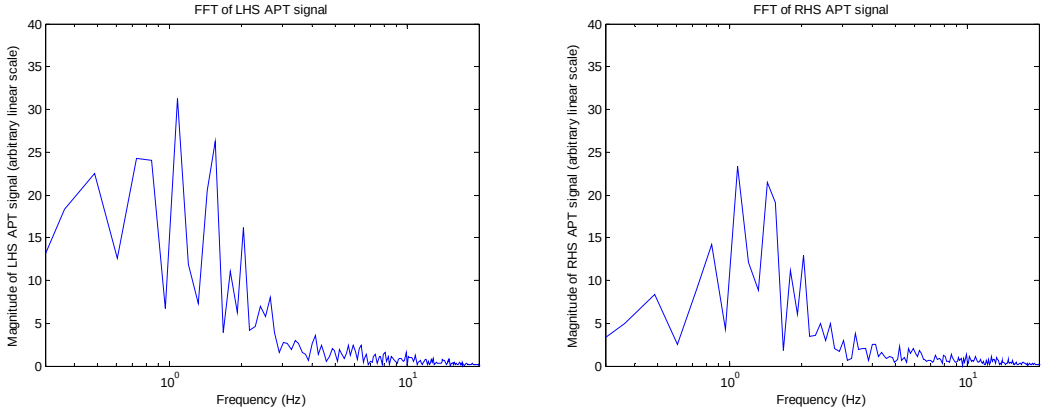

Figure 33. FFT of air spring signals - std suspension, bus loaded, 70km/h, test 253

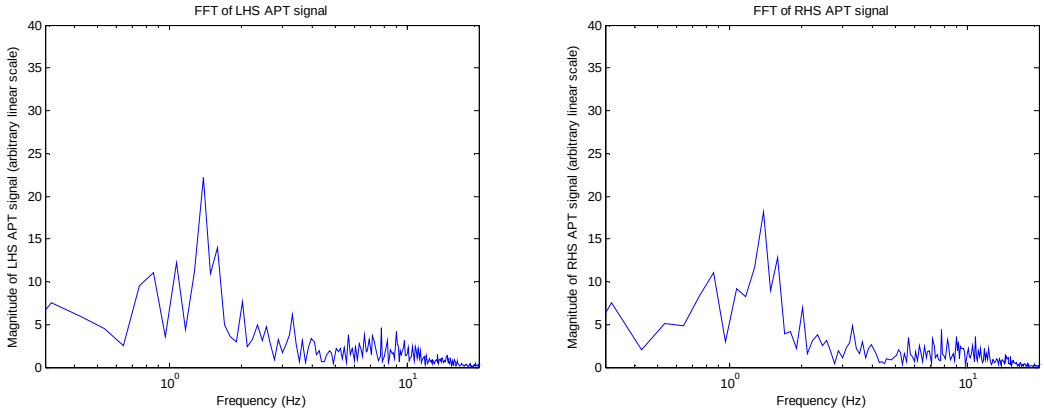

Figure 34. FFT of air spring signals - std suspension, bus loaded, 80km/h, test 247

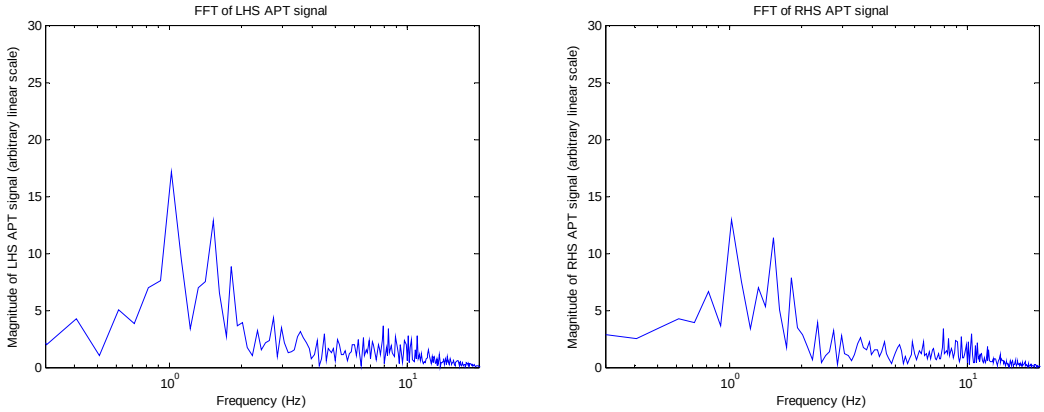

Figure 35. FFT of air spring signals - std suspension, bus loaded, 90km/h, test 245

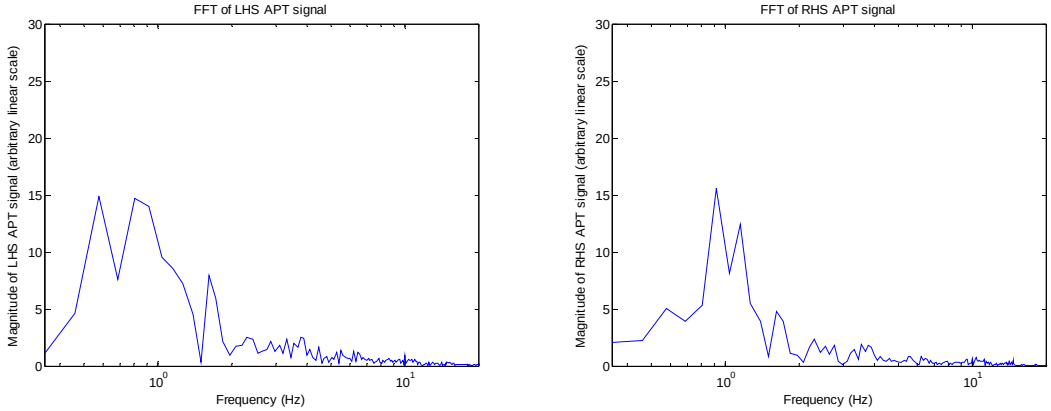

Figure 36. FFT of air spring signals - std suspension, coach loaded, 40km/h, test 54

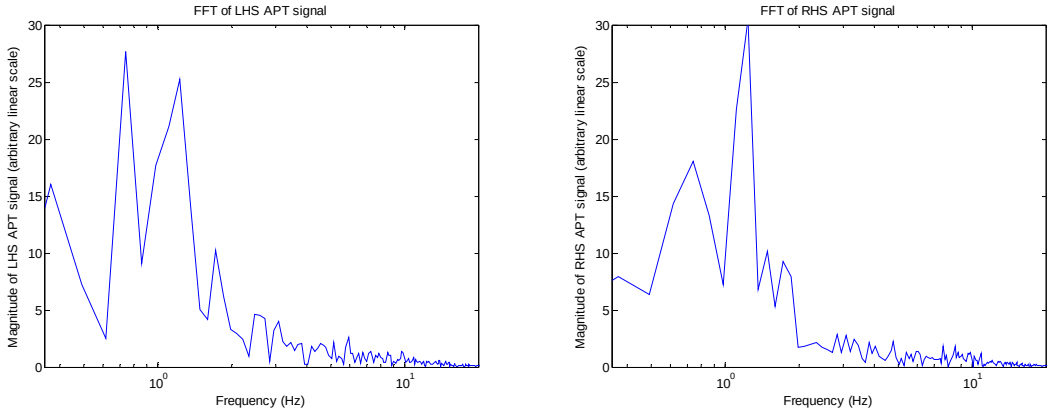

5

Figure 37. FFT of air spring signals - std suspension, coach loaded, 60km/h, test 56

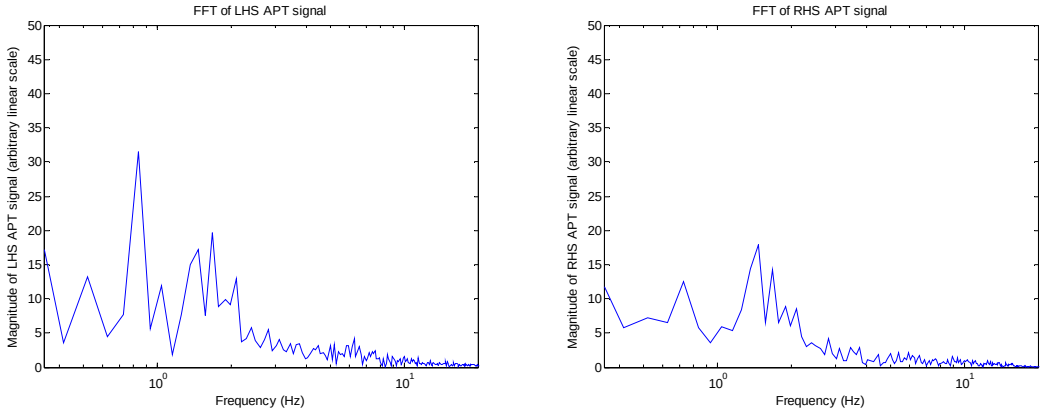

Figure 38. FFT of air spring signals - std suspension, coach loaded, 70km/h, test 61

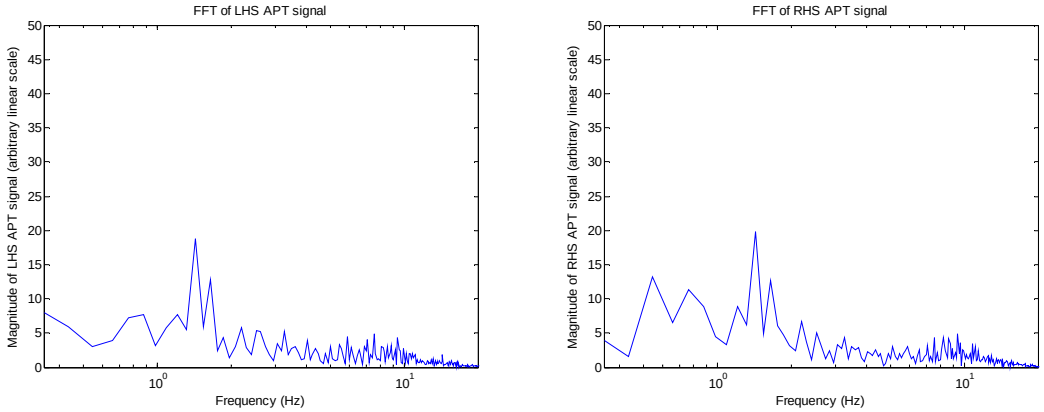

Figure 39. FFT of air spring signals - std suspension, coach loaded, 80km/h, test 43

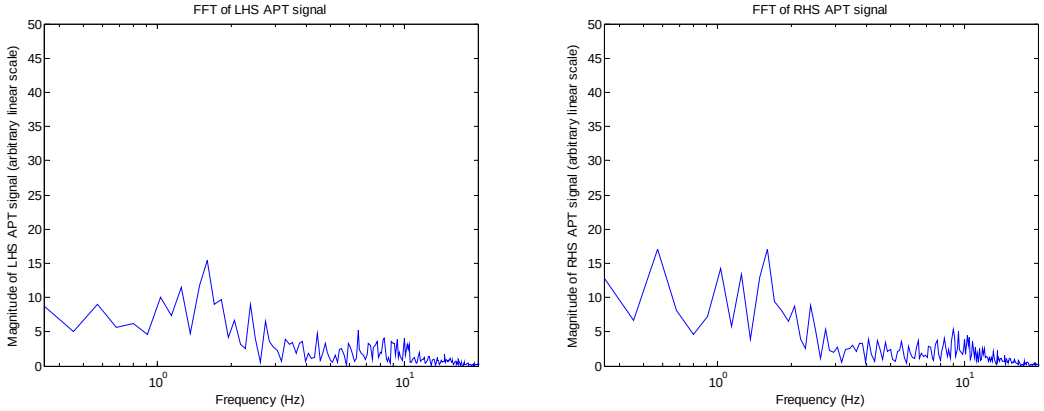

Figure 40. FFT of air spring signals - std suspension, coach loaded, 90km/h, test 46

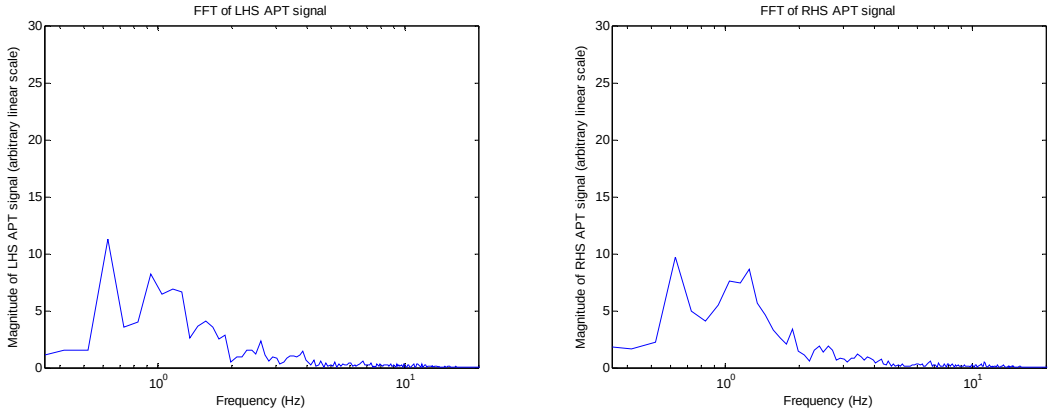

Figure 41. FFT of air spring signals - std suspension, semi-trailer loaded, 40km/h, test 132

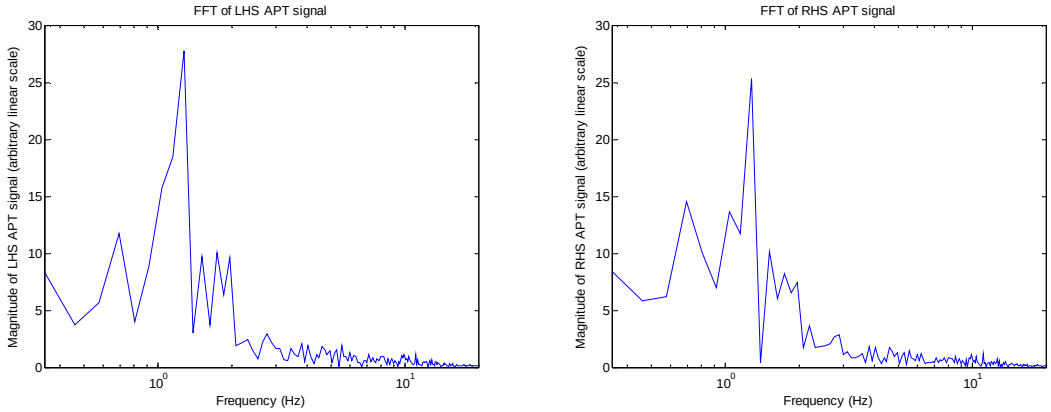

Figure 42. FFT of air spring signals - std suspension, semi-trailer loaded, 60km/h, test 134

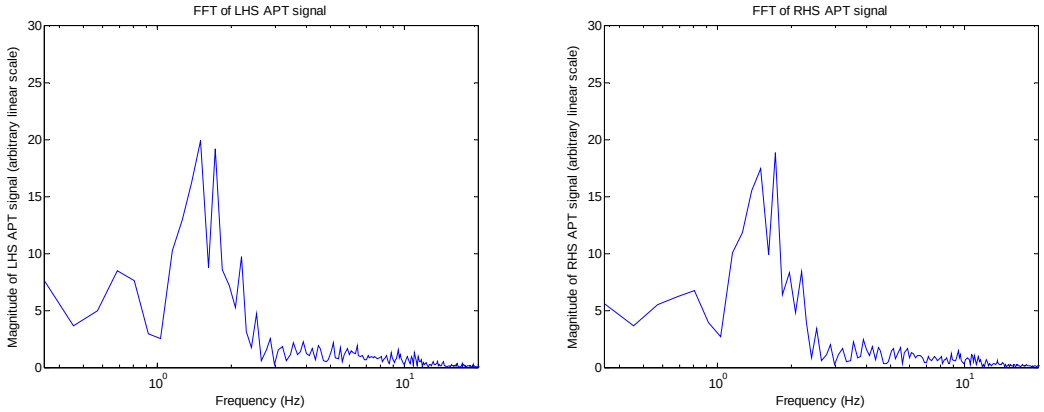

Figure 43. FFT of air spring signals - std suspension, semi-trailer loaded, 70km/h, test 143

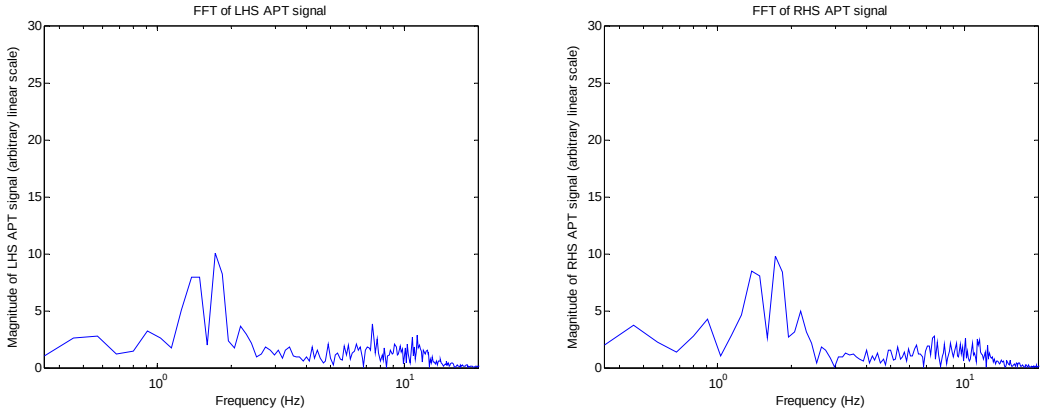

Figure 44. FFT of air spring signals - std suspension, semi-trailer loaded, 80km/h, test 136

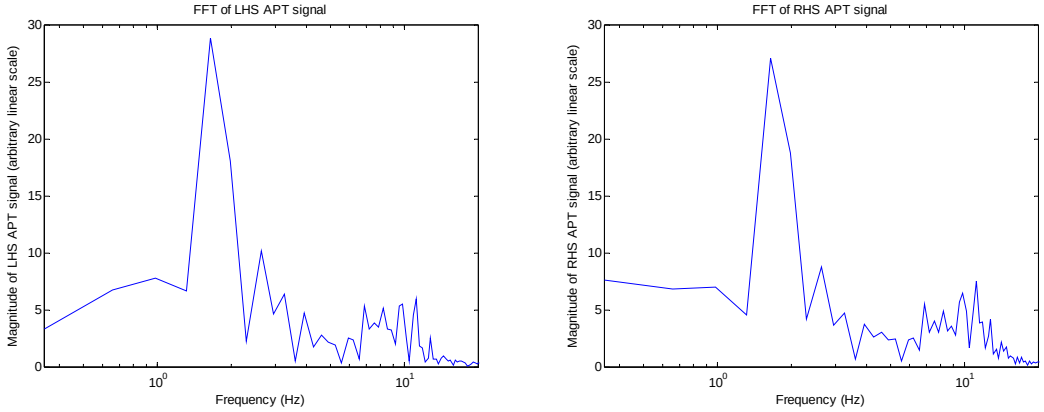

Figure 45. FFT of air spring signals - std suspension, semi-trailer loaded, 90km/h, test 138

Suspension with large longitudinal air lines

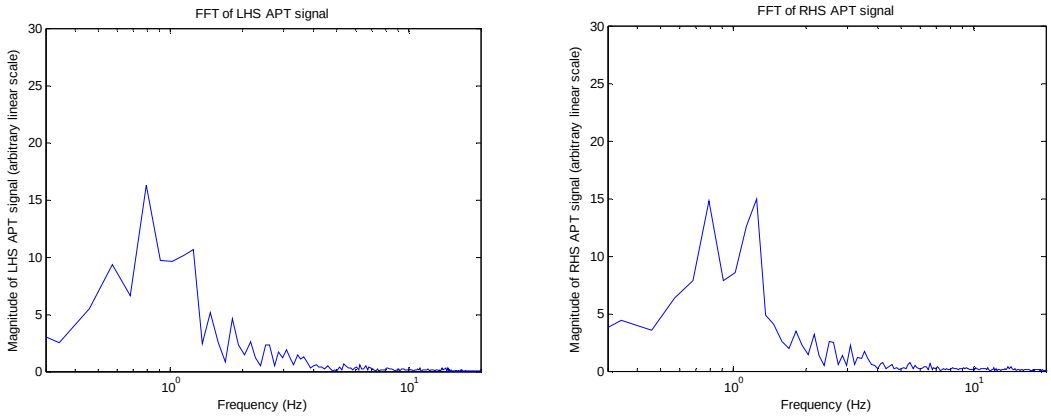

Figure 46. FFT of air spring signals - modified suspension, bus loaded, 40km/h, test 259

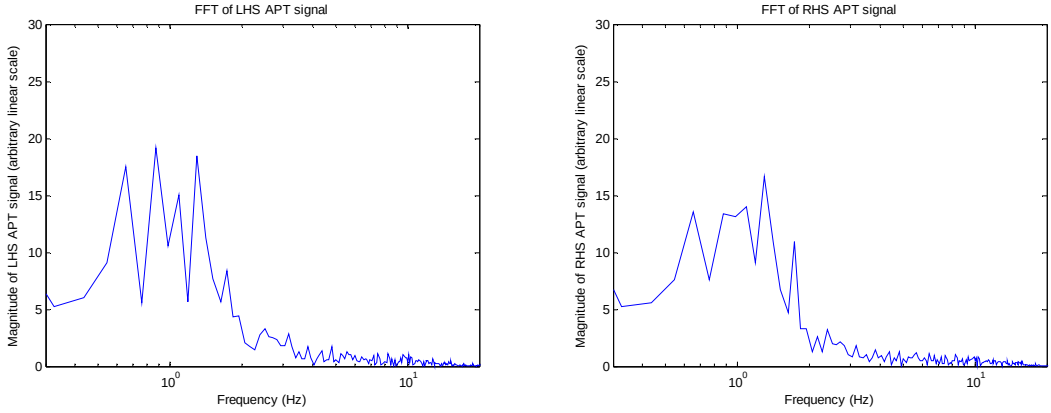

Figure 47. FFT of air spring signals - modified suspension, bus loaded, 60km/h, test 273

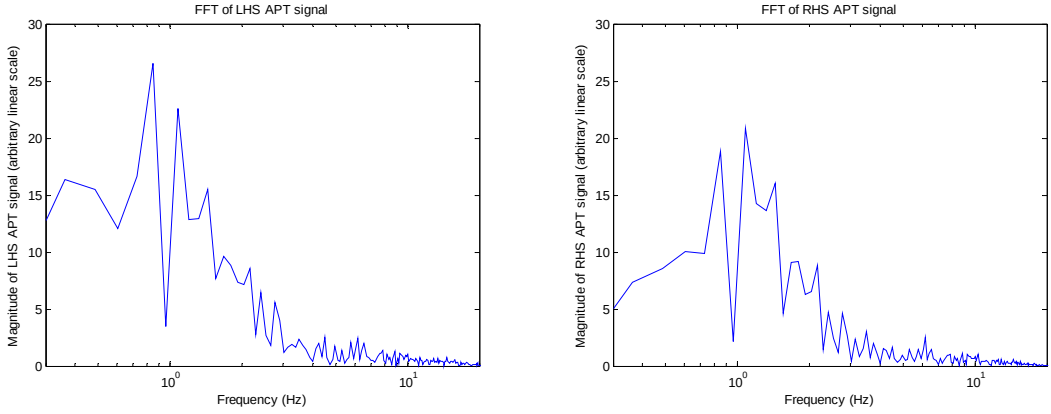

Figure 48. FFT of air spring signals - modified suspension, bus loaded, 70km/h, test 272

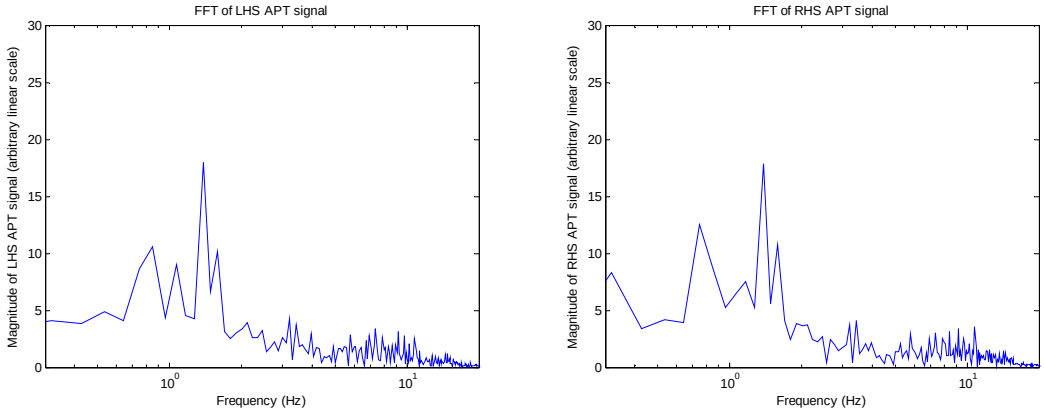

Figure 49. FFT of air spring signals - modified suspension, bus loaded, 80km/h, test 269

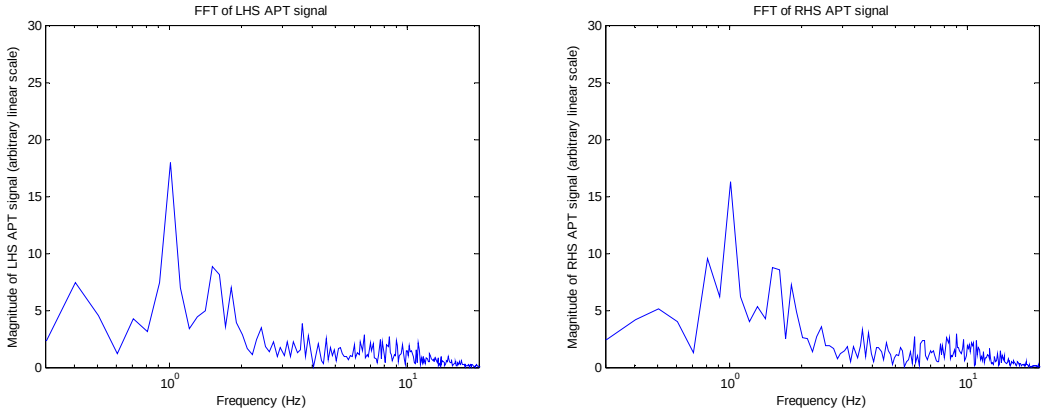

Figure 50. FFT of air spring signals - modified suspension, bus loaded, 90km/h, test 267

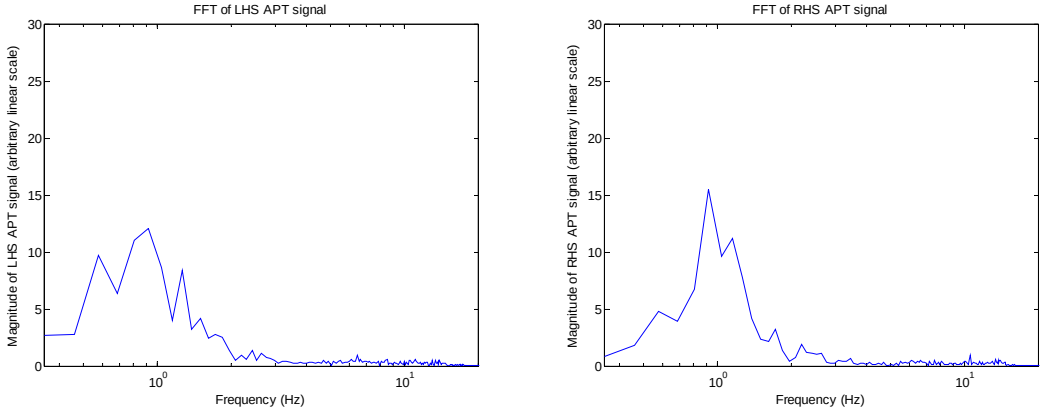

Figure 51. FFT of air spring signals - modified suspension, coach loaded, 40km/h, test 64

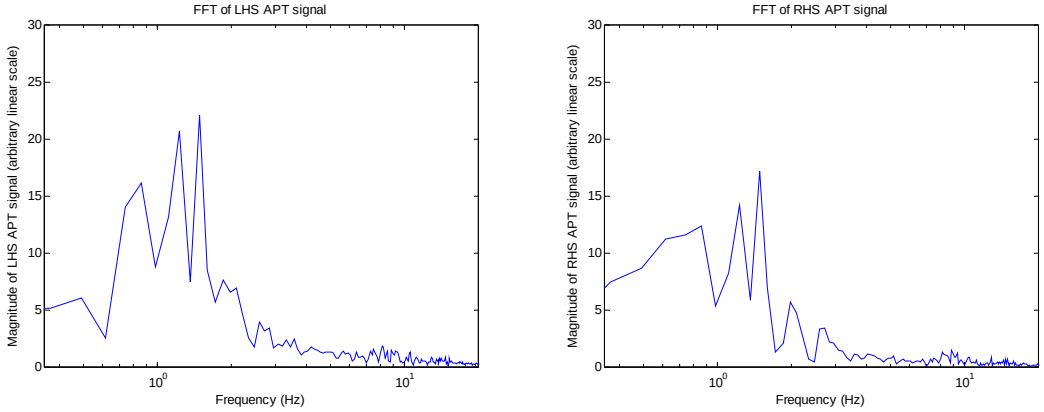

Figure 52. FFT of air spring signals - modified suspension, coach loaded, 60km/h, test 66

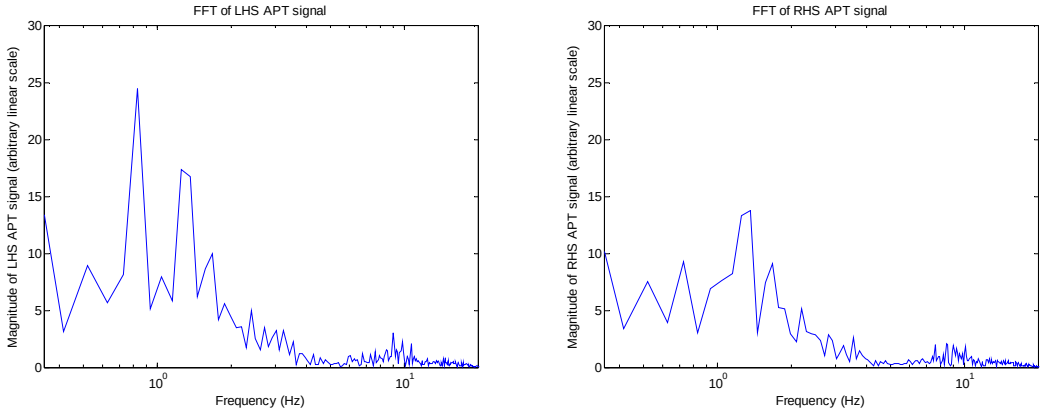

Figure 53. FFT of air spring signals - modified suspension, coach loaded, 70km/h, test 75

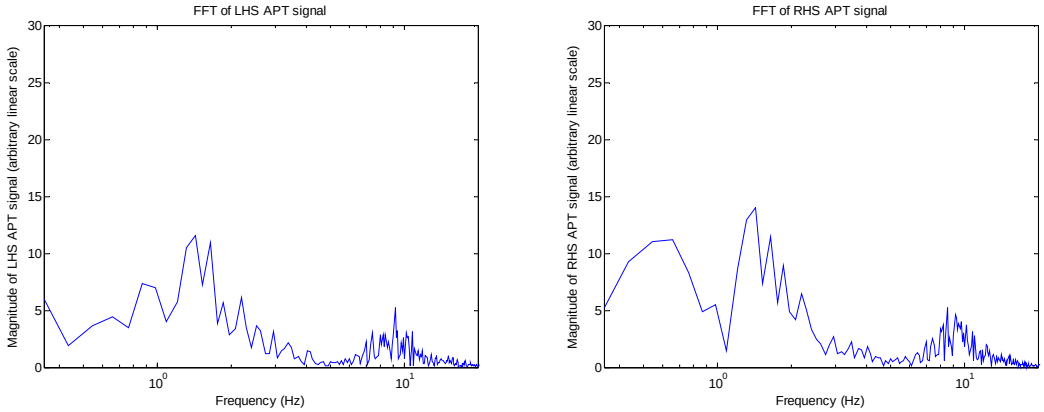

Figure 54. FFT of air spring signals - modified suspension, coach loaded, 80km/h, test 78

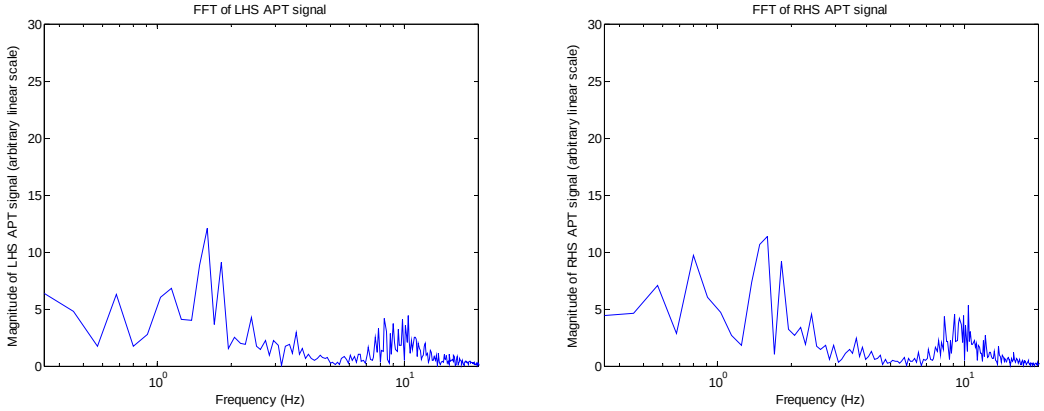

Figure 55. FFT of air spring signals - modified suspension, coach loaded, 90km/h, test 80

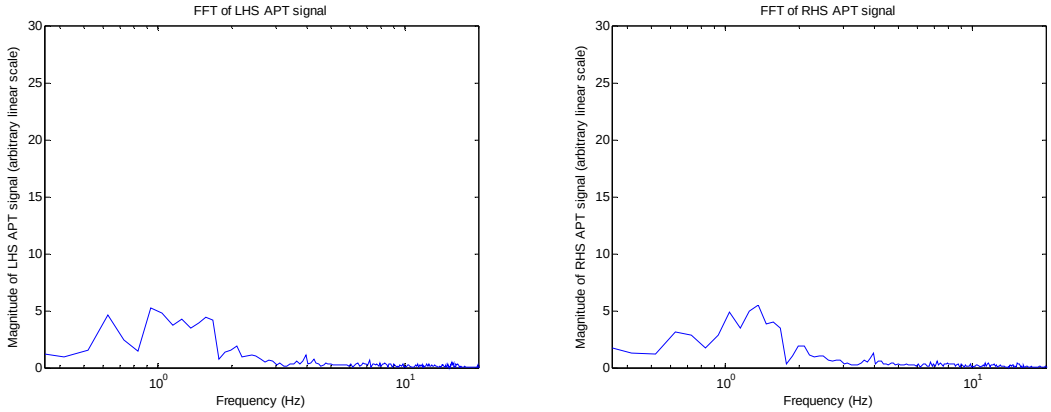

Figure 56. FFT of air spring signals - modified suspension, semi-trailer loaded, 40km/h, test 146

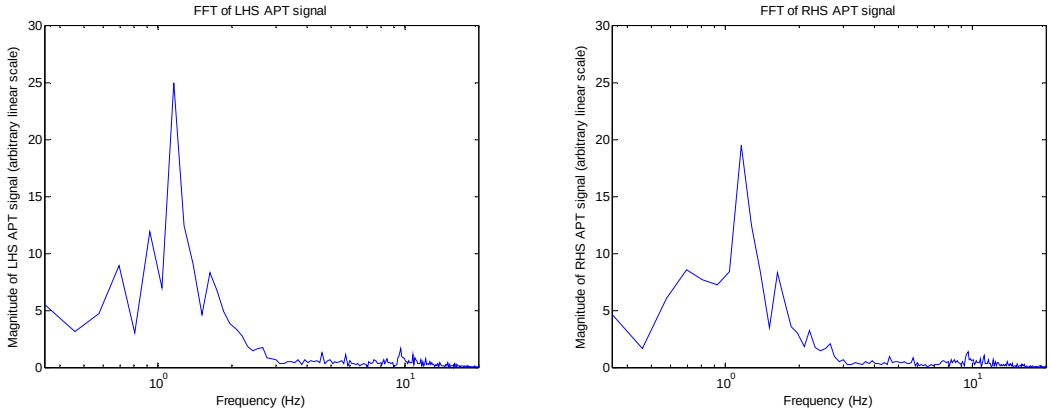

Figure 57. FFT of air spring signals - modified suspension, semi-trailer loaded, 60km/h, test 148

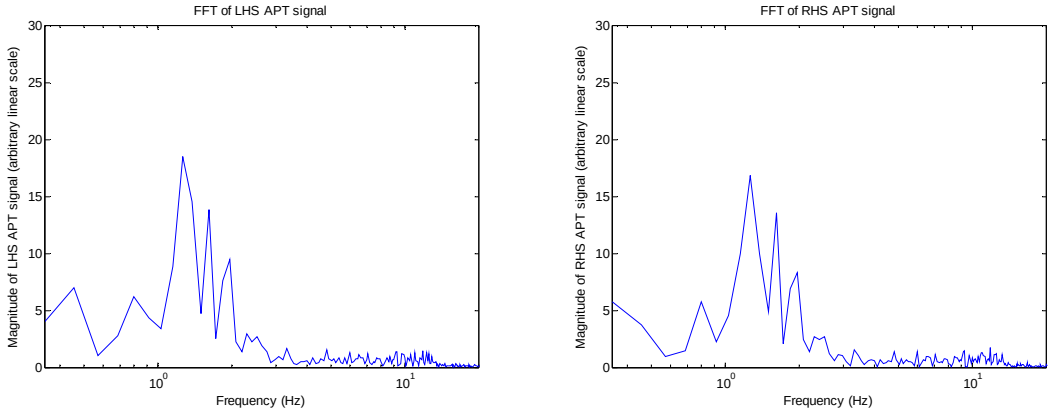

Figure 58. FFT of air spring signals - modified suspension, semi-trailer loaded, 70km/h, test 153

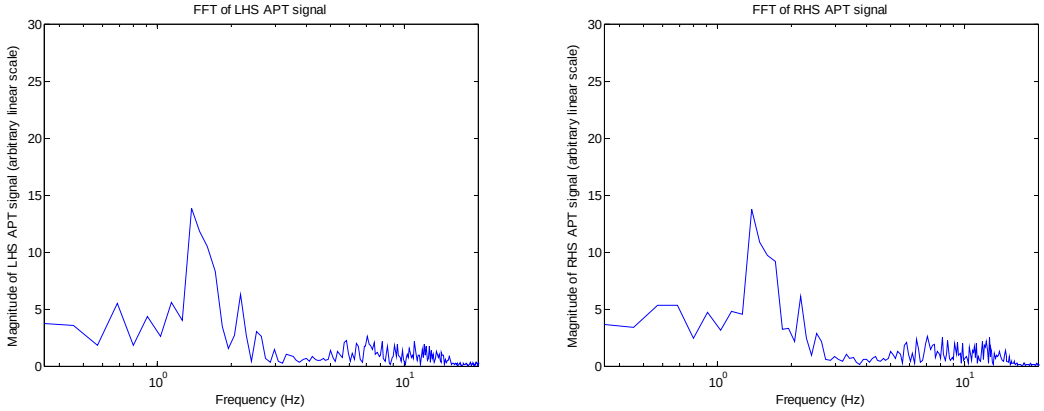

Figure 59. FFT of air spring signals - modified suspension, semi-trailer loaded, 80km/h, test 97

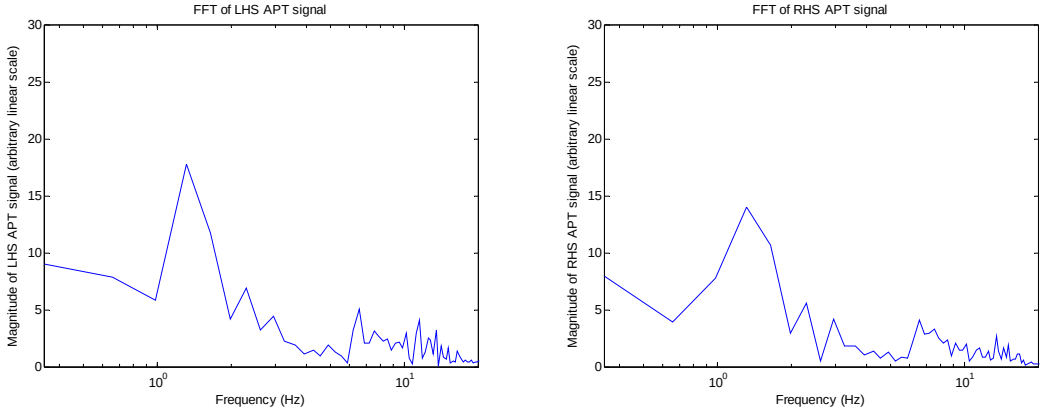

Figure 60. FFT of air spring signals - modified suspension, semi-trailer loaded, 90km/h, test 99

Appendix 4. Fast Fourier plots - wheel-force data

Standard suspension

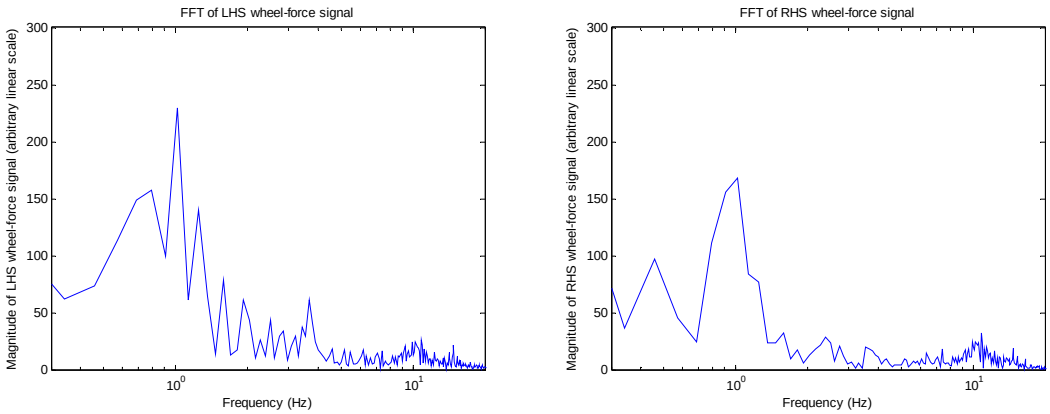

Figure 61. FFT of wheel forces - std suspension, bus loaded, 40km/h, test 235

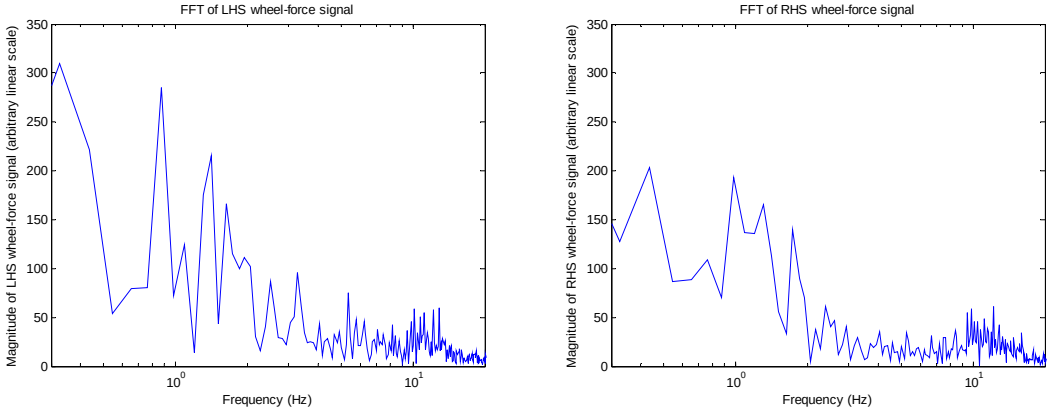

Figure 62. FFT of wheel forces - std suspension, bus loaded, 60km/h, test 254

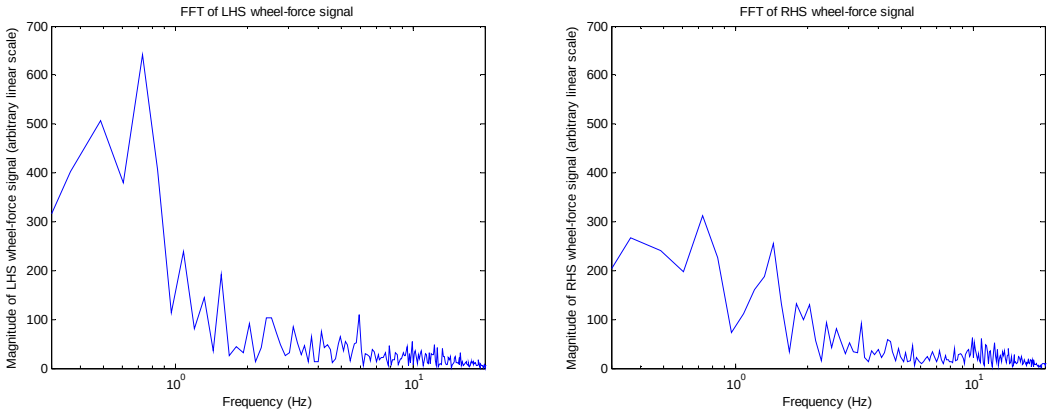

Figure 63. FFT of wheel forces - std suspension, bus loaded, 70km/h, test 253

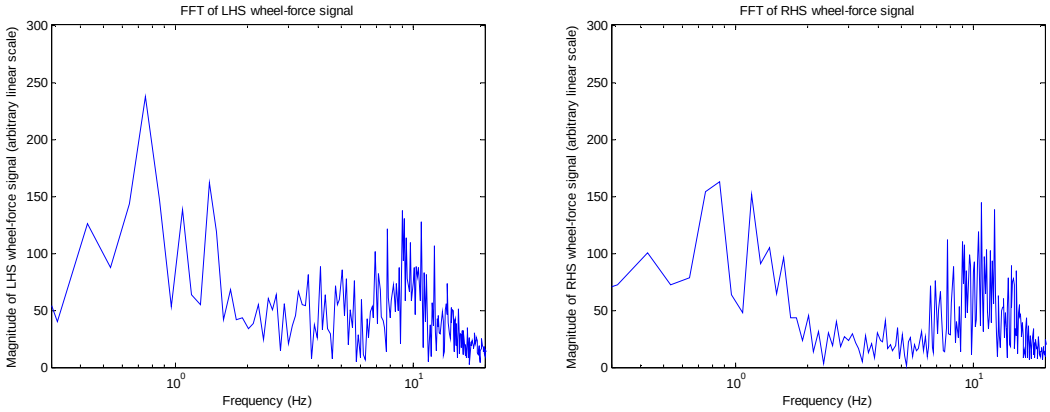

Figure 64. FFT of wheel forces - std suspension, bus loaded, 80km/h, test 247

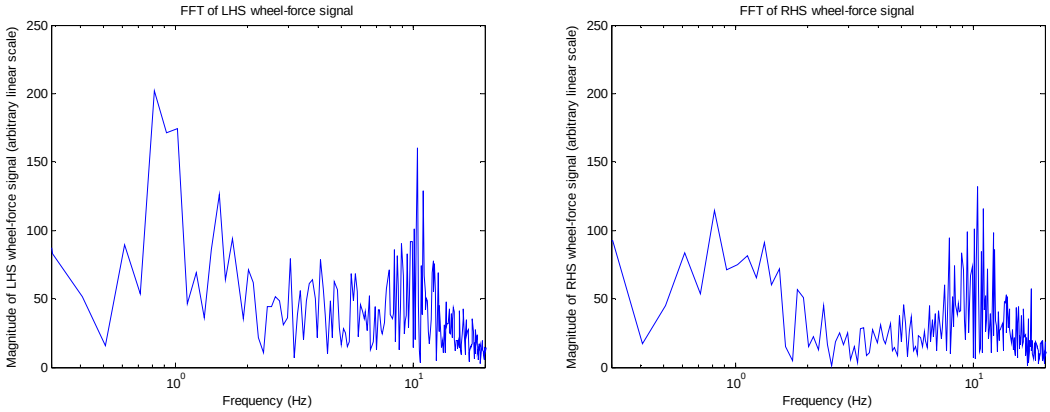

Figure 65. FFT of wheel forces - std suspension, bus loaded, 90km/h, test 245

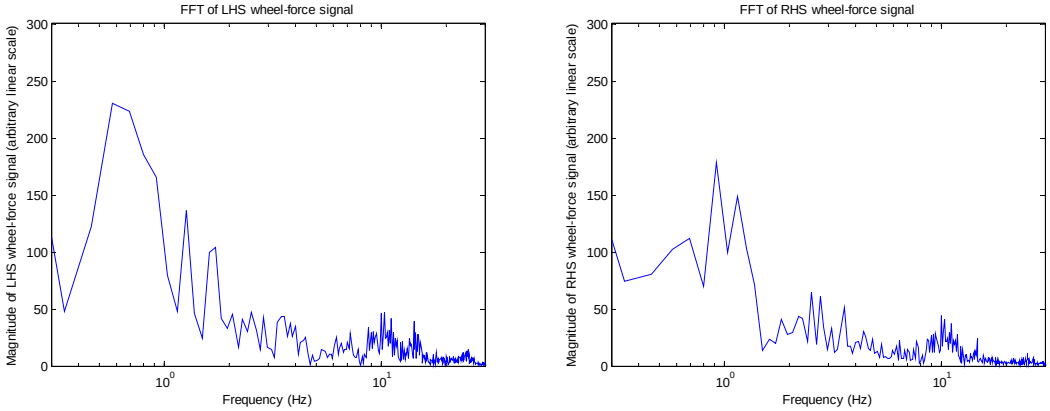

Figure 66. FFT of wheel forces - std suspension, coach loaded, 40km/h, test 54

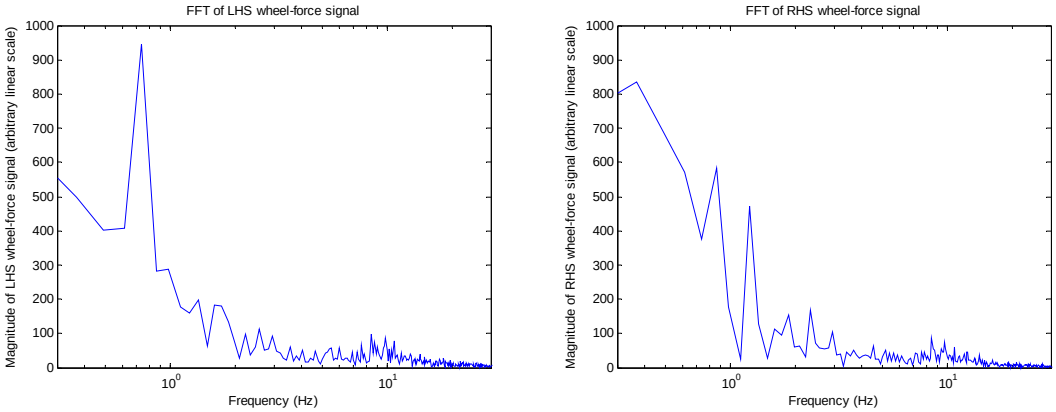

Figure 67. FFT of wheel forces - std suspension, coach loaded, 60km/h, test 56

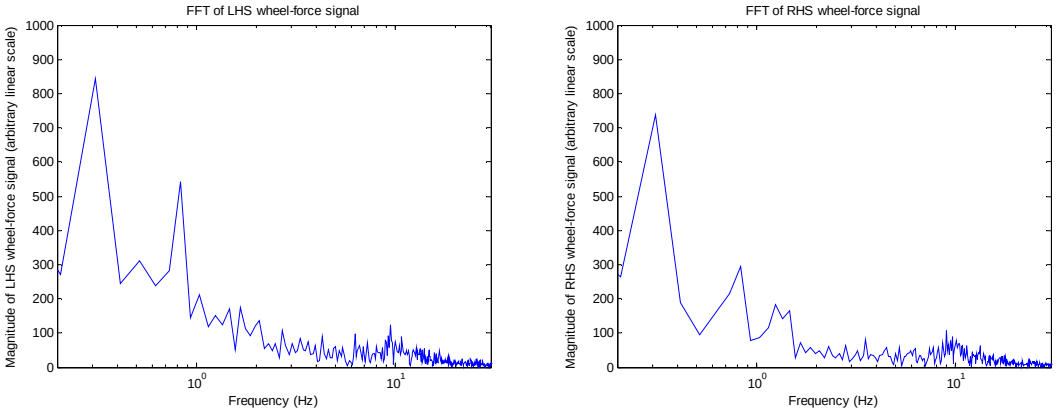

Figure 68. FFT of wheel forces - std suspension, coach loaded, 70km/h, test 61

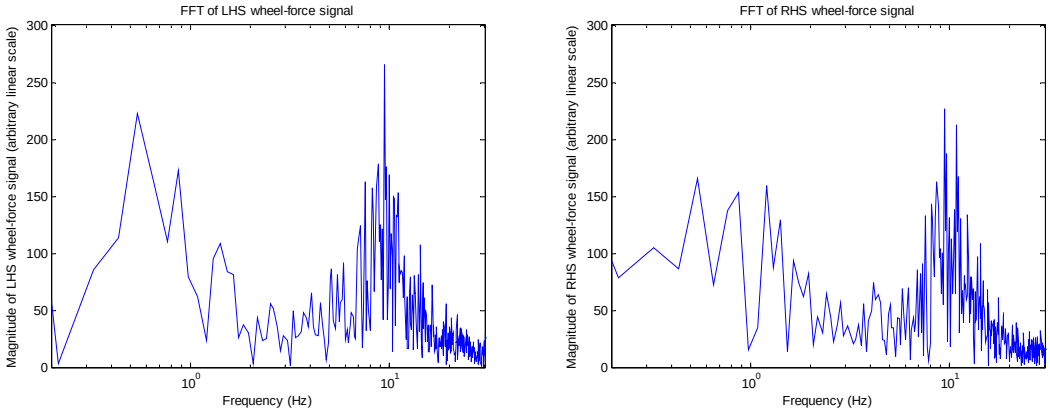

Figure 69. FFT of wheel forces - std suspension, coach loaded, 80km/h, test 43

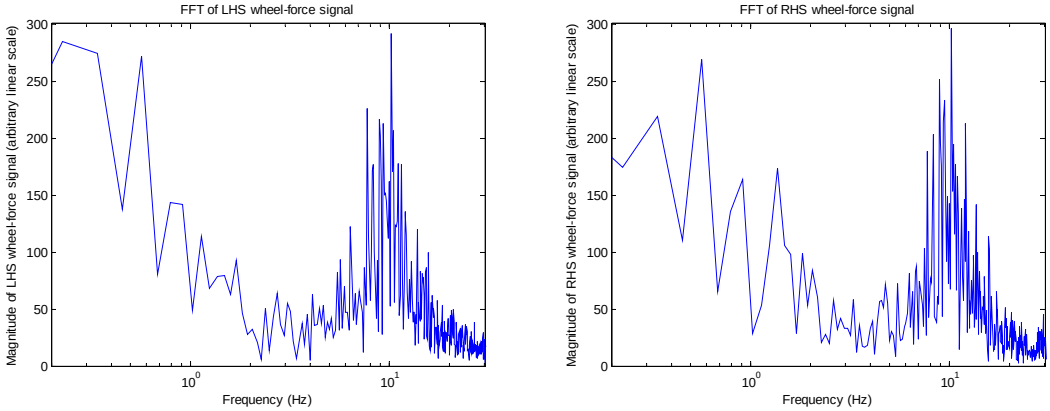

Figure 70. FFT of wheel forces - std suspension, coach loaded, 90km/h, test 46

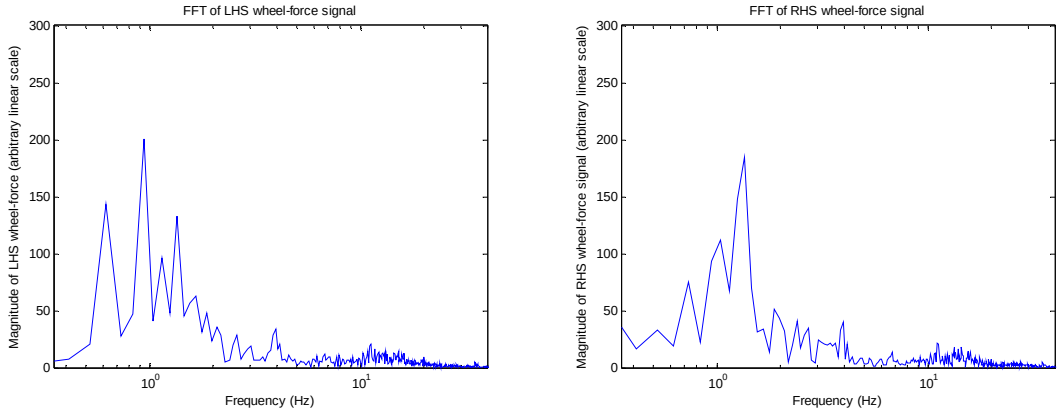

Figure 71. FFT of wheel forces - std suspension, semi-trailer loaded, 40km/h, test 132

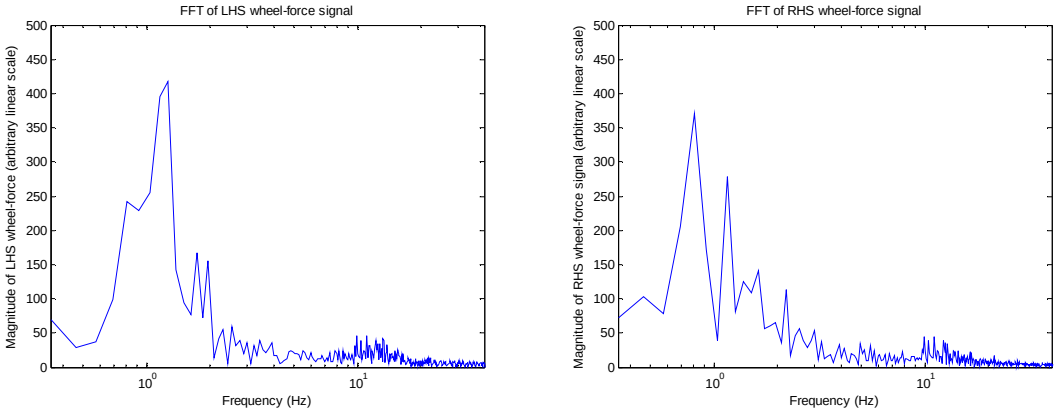

Figure 72. FFT of wheel forces - std suspension, semi-trailer loaded, 60km/h, test 134

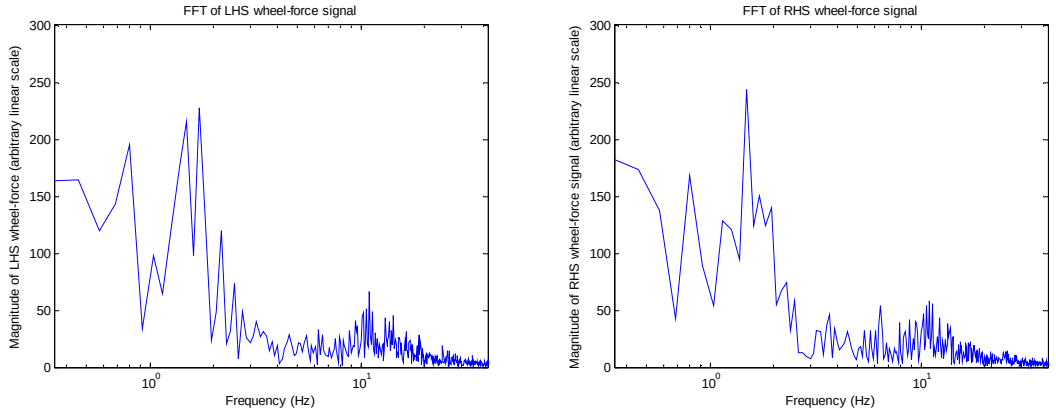

Figure 73. FFT of wheel forces - std suspension, semi-trailer loaded, 70km/h, test 143

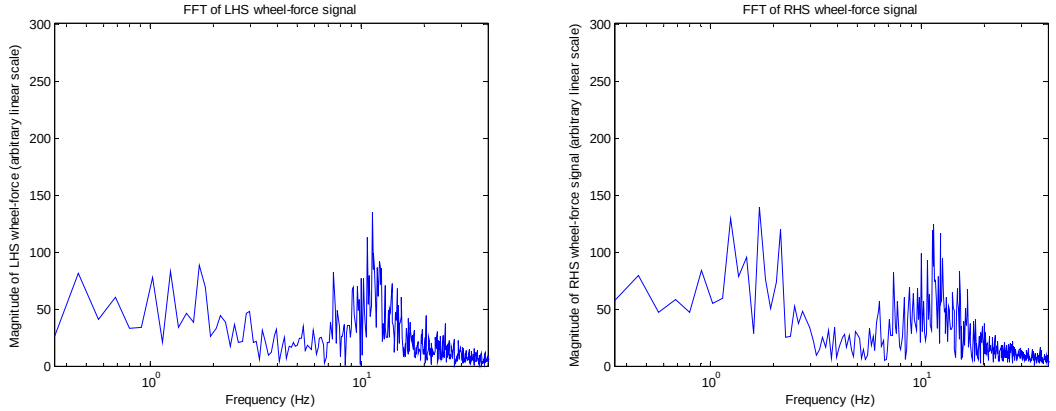

Figure 74. FFT of wheel forces - std suspension, semi-trailer loaded, 80km/h, test 136

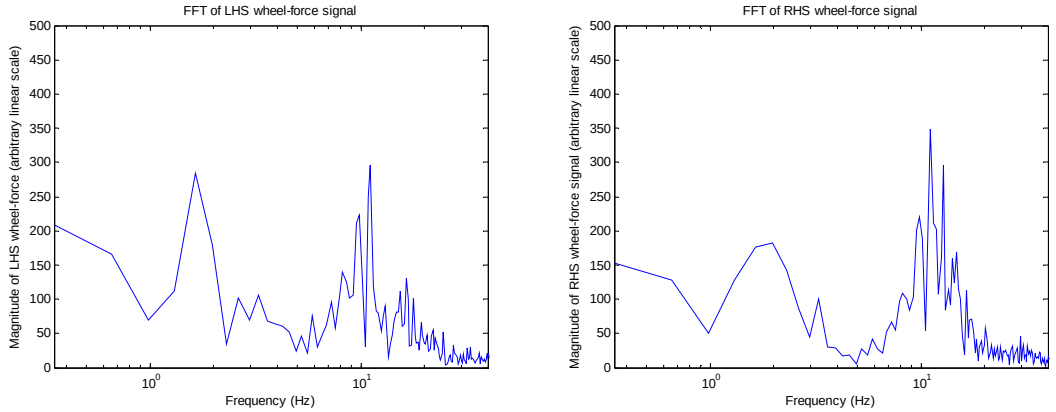

Figure 75. FFT of wheel forces - std suspension, semi-trailer loaded, 90km/h, test 138

Suspension with large longitudinal air lines

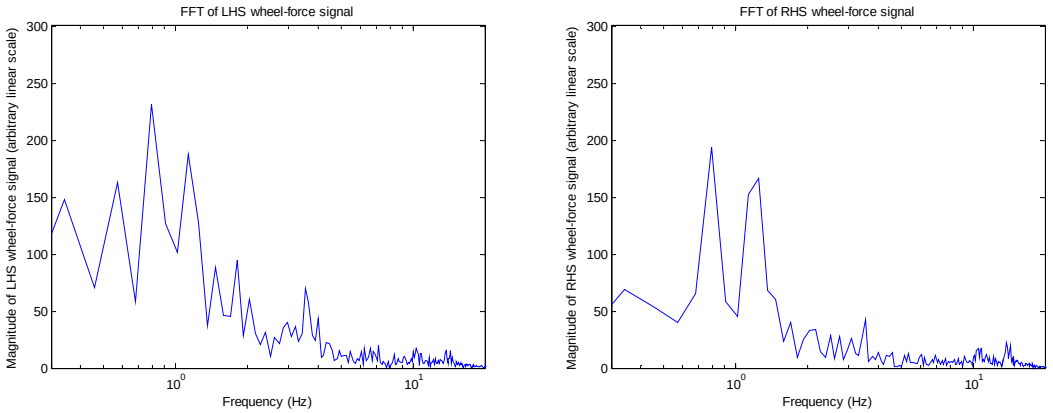

Figure 76. FFT of wheel forces - modified suspension, bus loaded, 40km/h, test 259

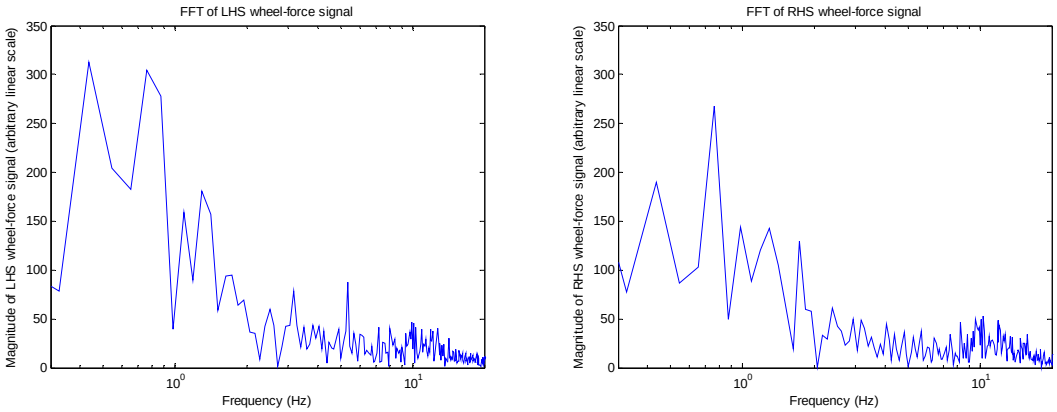

Figure 77. FFT of wheel forces - modified suspension, bus loaded, 60km/h, test 273

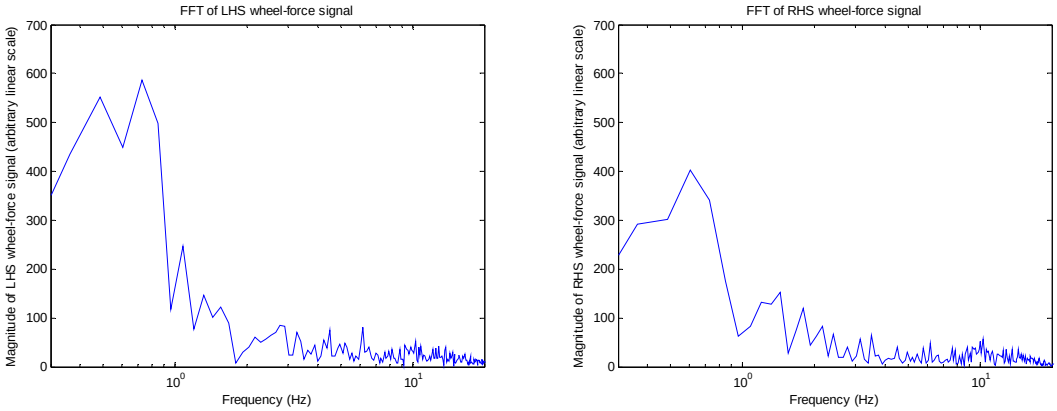

Figure 78. FFT of wheel forces - modified suspension, bus loaded, 70km/h, test 272

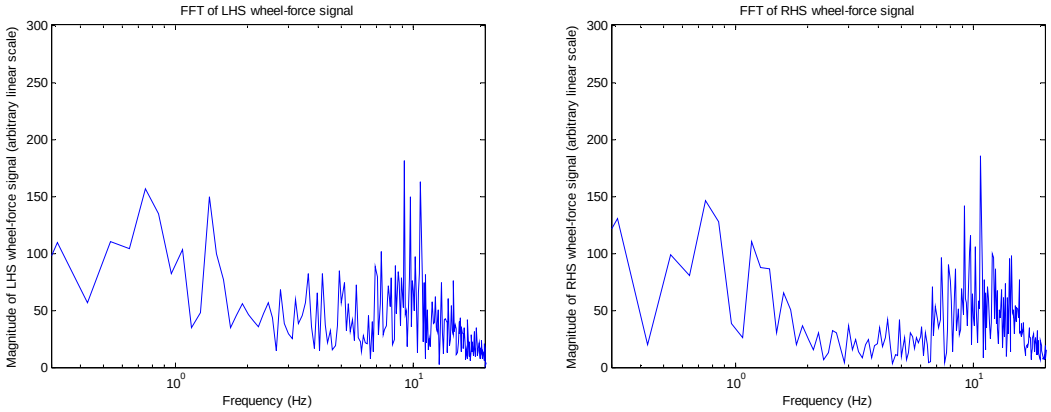

Figure 79. FFT of wheel forces - modified suspension, bus loaded, 80km/h, test 269

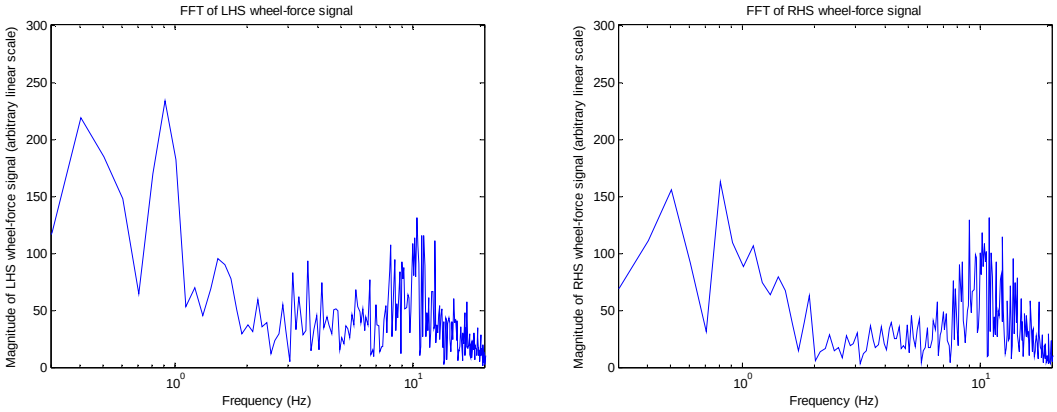

Figure 80. FFT of wheel forces - modified suspension, bus loaded, 90km/h, test 267

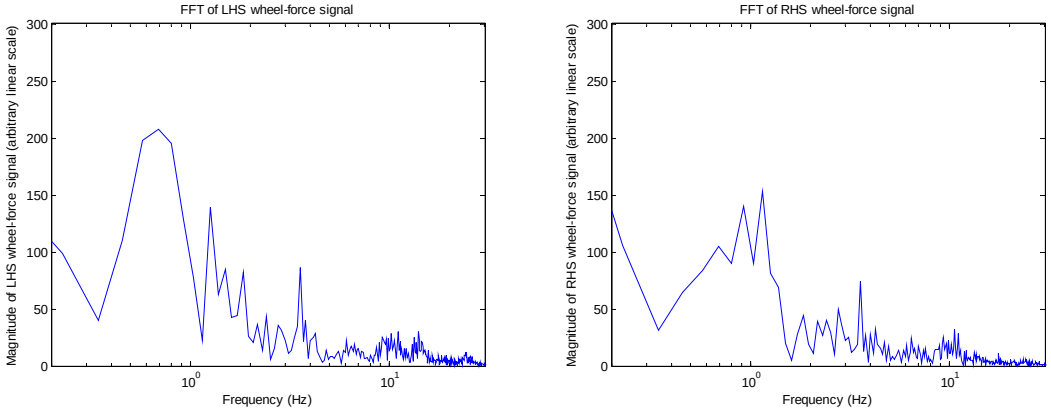

Figure 81. FFT of wheel forces - modified suspension, coach loaded, 40km/h, test 64

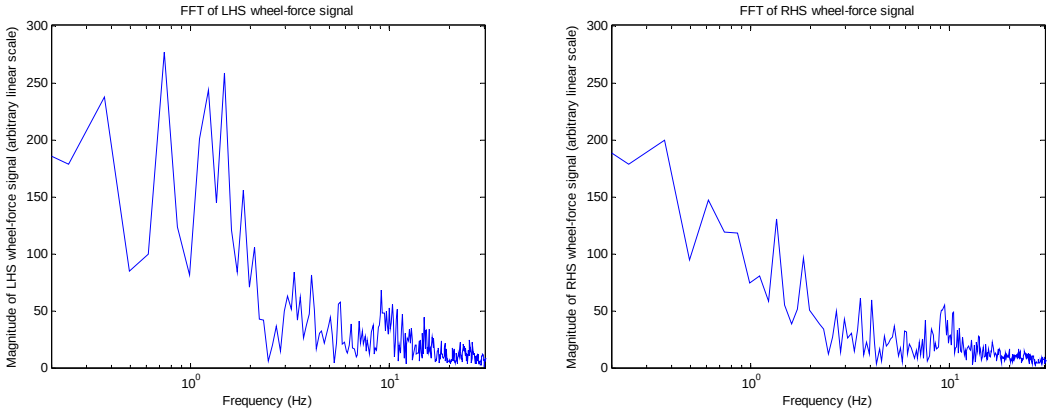

Figure 82. FFT of wheel forces - modified suspension, coach loaded, 60km/h, test 66

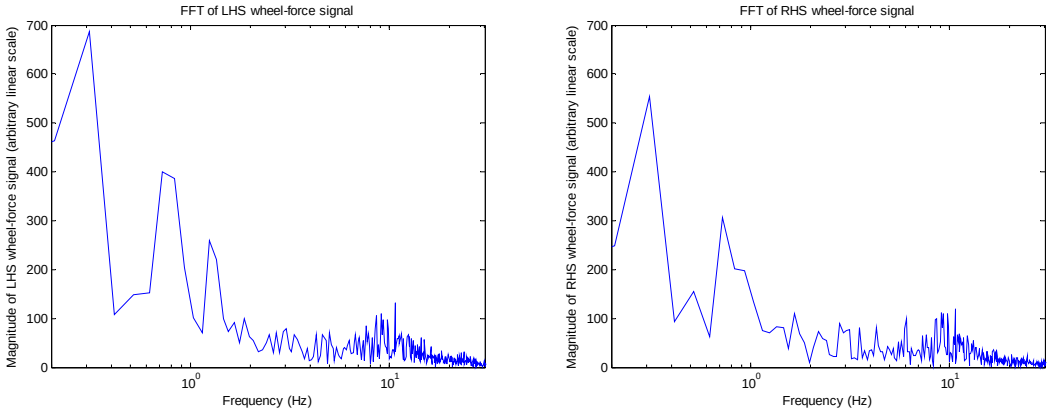

Figure 83. FFT of wheel forces - modified suspension, coach loaded, 70km/h, test 75

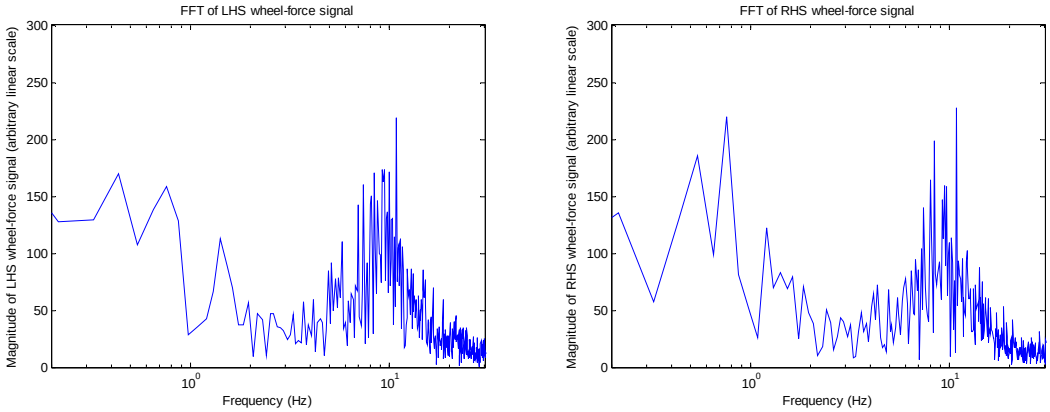

Figure 84. FFT of wheel forces - modified suspension, coach loaded, 80km/h, test 78

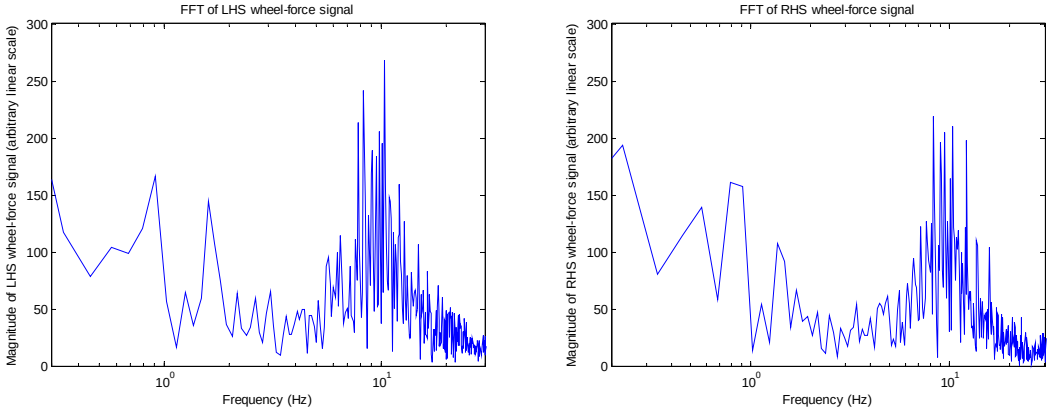

Figure 85. FFT of wheel forces - modified suspension, coach loaded, 90km/h, test 80

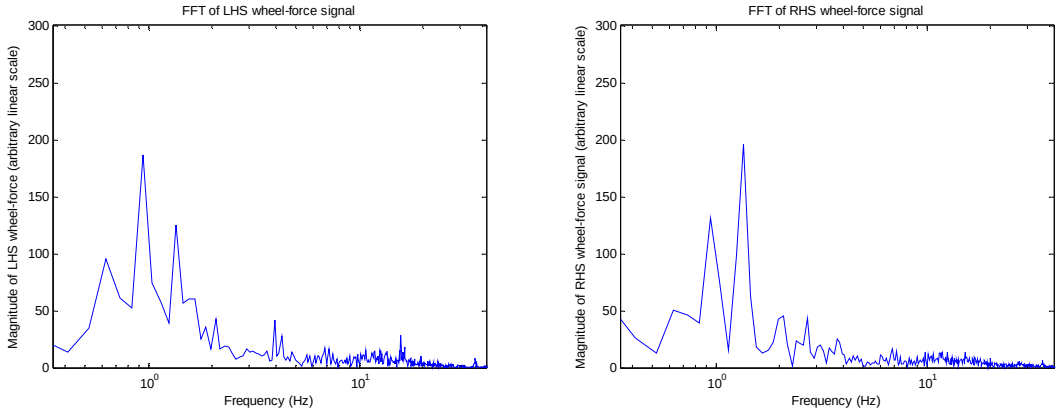

Figure 86. FFT of wheel forces - modified suspension, semi-trailer loaded, 40km/h, test 146

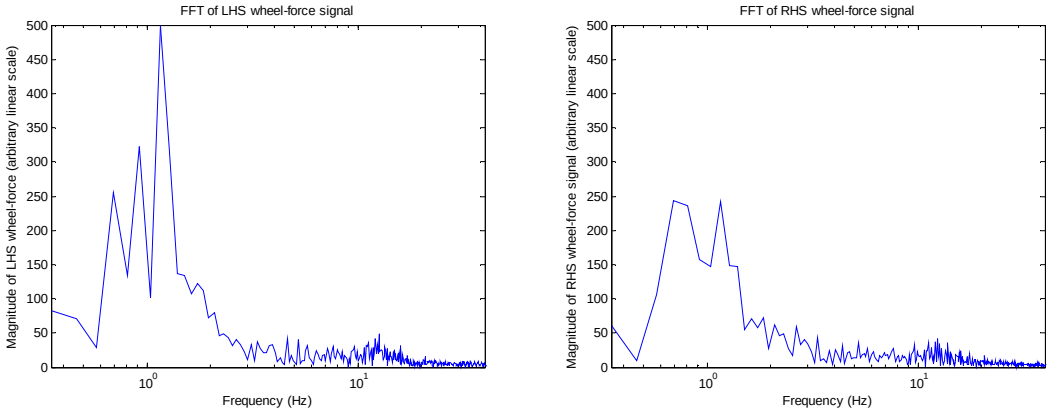

Figure 87. FFT of wheel forces - modified suspension, semi-trailer loaded, 60km/h, test 148

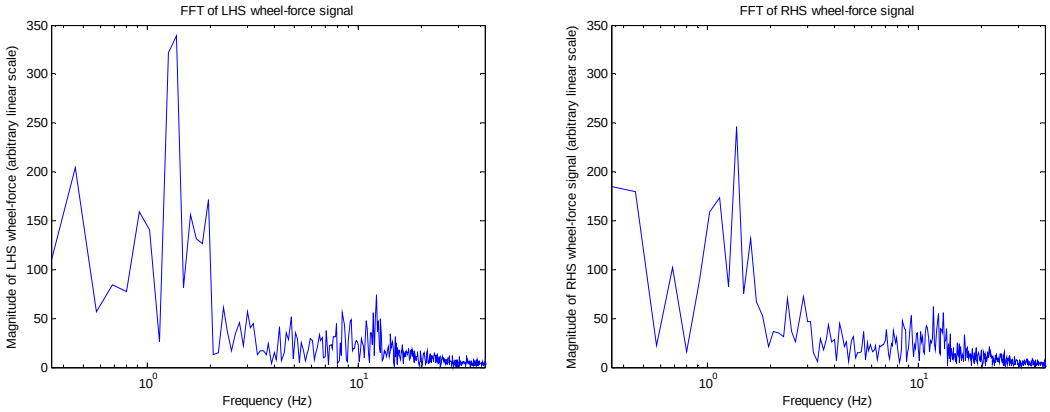

Figure 88. FFT of wheel forces - modified suspension, semi-trailer loaded, 70km/h, test 153

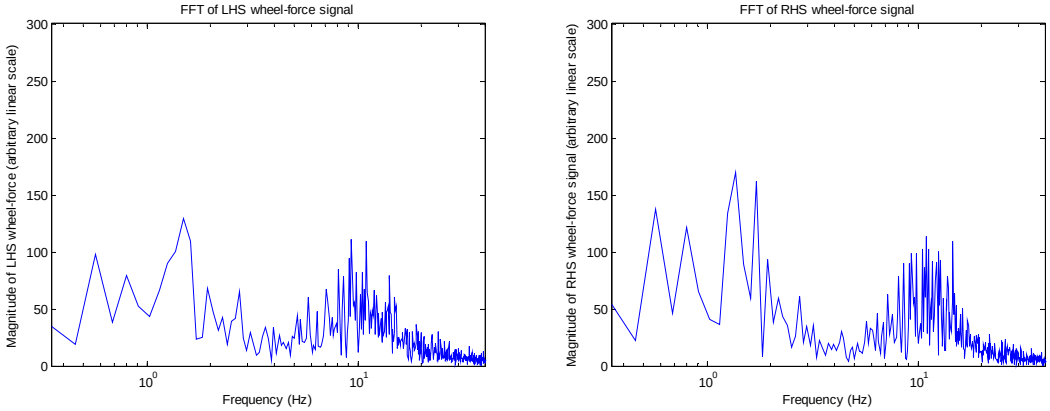

Figure 89. FFT of wheel forces - modified suspension, semi-trailer loaded, 80km/h, test 97

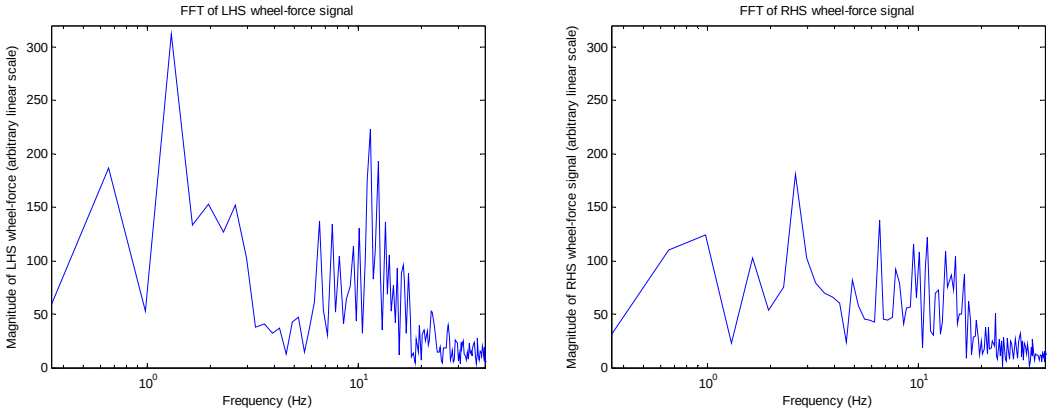

Figure 90. FFT of wheel forces - modified suspension, semi-trailer loaded, 90km/h, test 99

Appendix 5. Fast Fourier plots - accelerometer data

Standard suspension

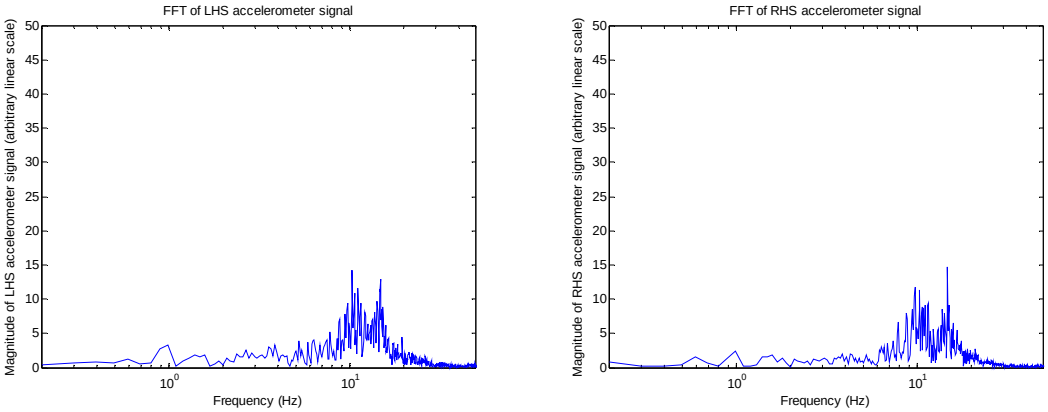

Figure 91. FFT of accelerometers - std suspension, bus loaded, 40km/h, test 235

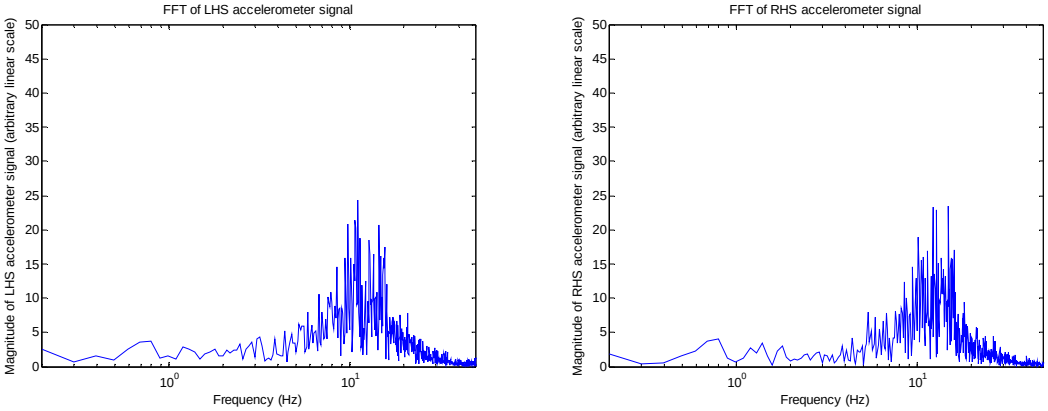

Figure 92. FFT of accelerometers - std suspension, bus loaded, 60km/h, test 254

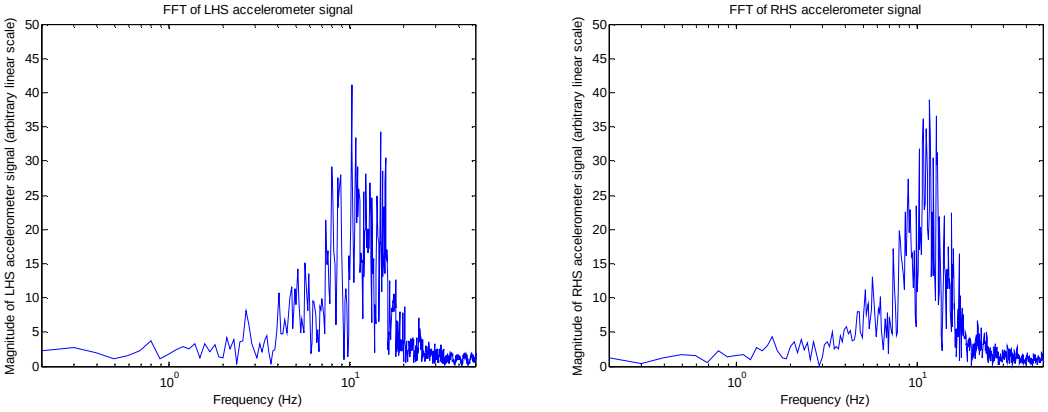

Figure 93. FFT of accelerometers - std suspension, bus loaded, 70km/h, test 253

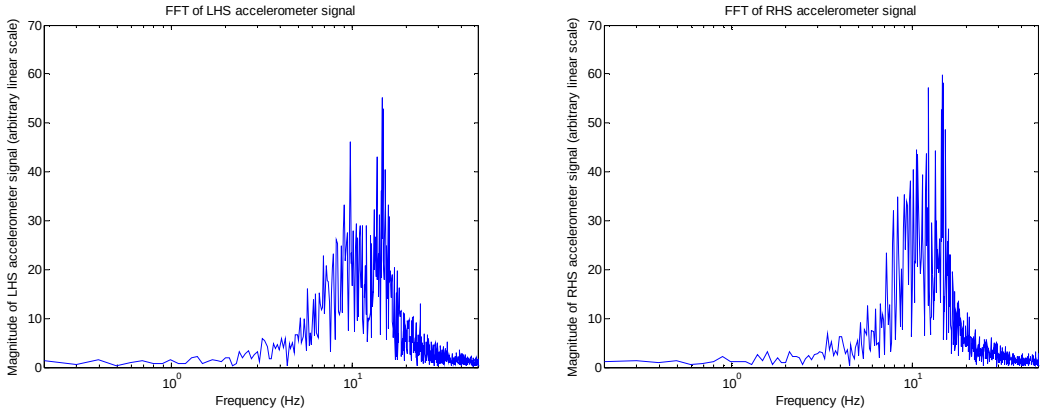

Figure 94. FFT of accelerometers - std suspension, bus loaded, 80km/h, test 247

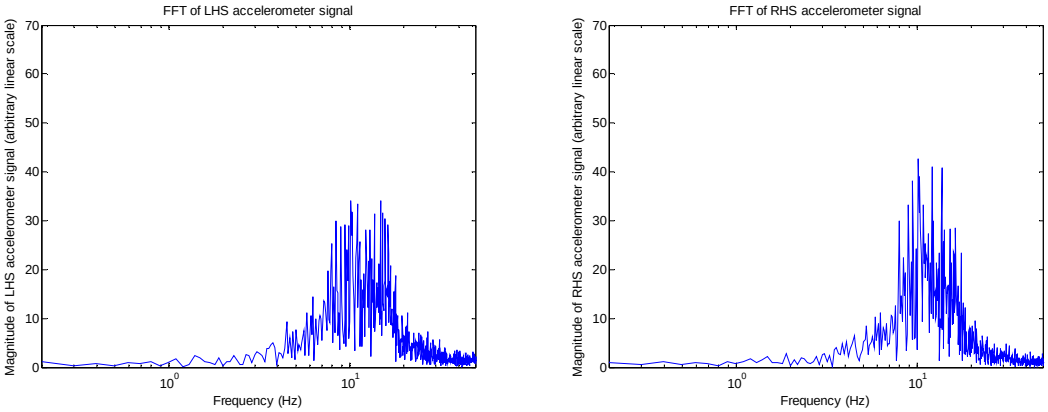

Figure 95. FFT of accelerometers - std suspension, bus loaded, 90km/h, test 245

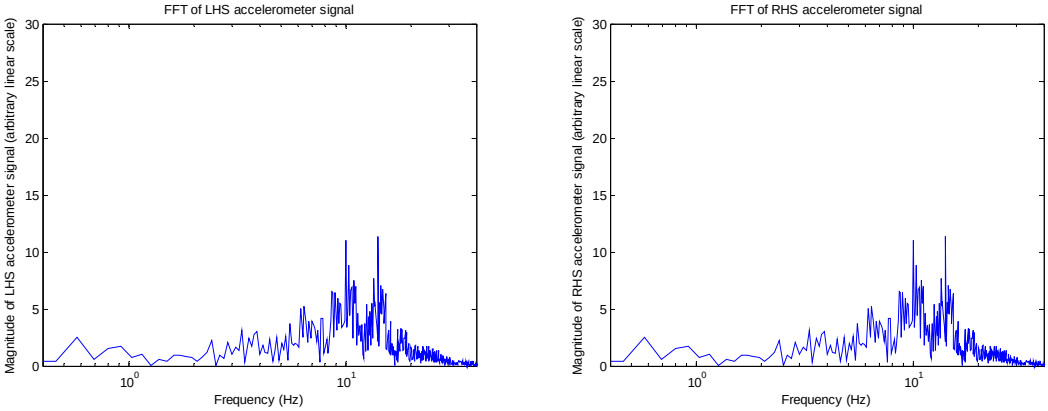

Figure 96. FFT of accelerometers - std suspension, coach loaded, 40km/h, test 54

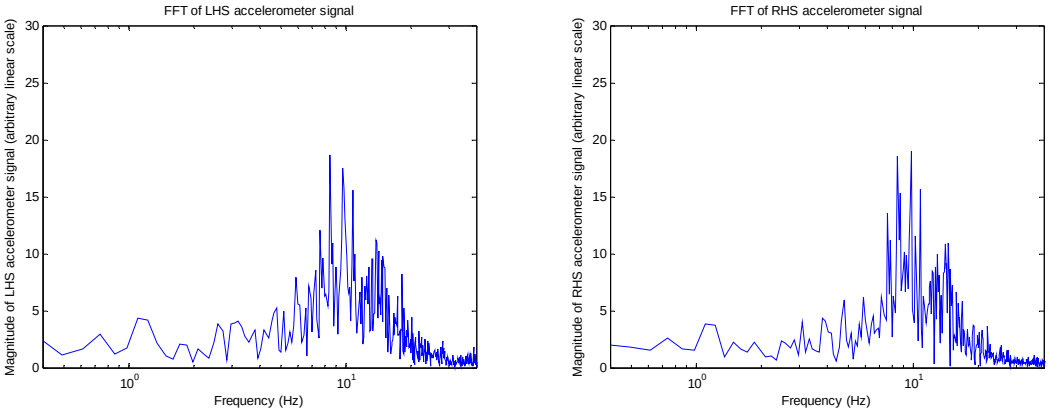

Figure 97. FFT of accelerometers - std suspension, coach loaded, 60km/h, test 56

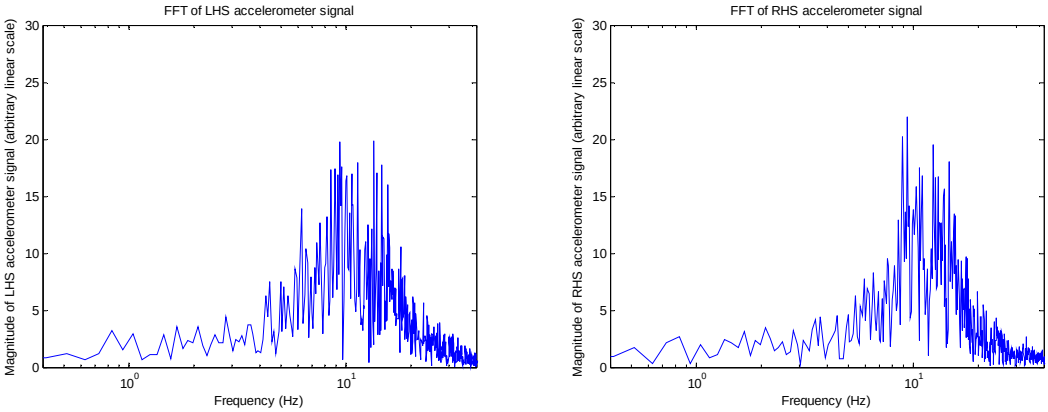

Figure 98. FFT of accelerometers - std suspension, coach loaded, 70km/h, test 61

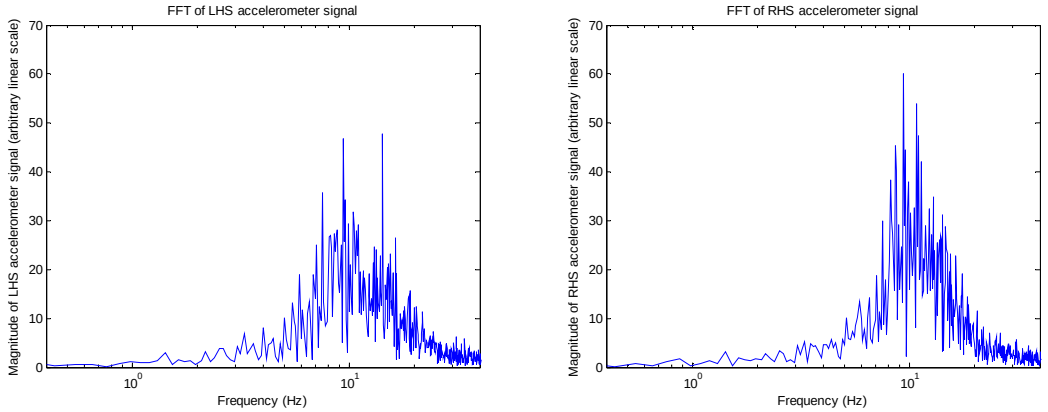

Figure 99. FFT of accelerometers - std suspension, coach loaded, 80km/h, test 43

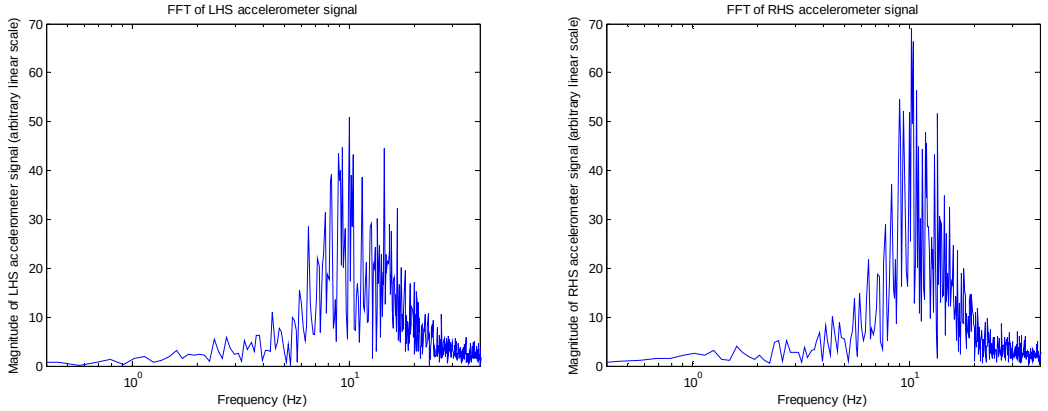

Figure 100. FFT of accelerometers - std suspension, coach loaded, 90km/h, test 46

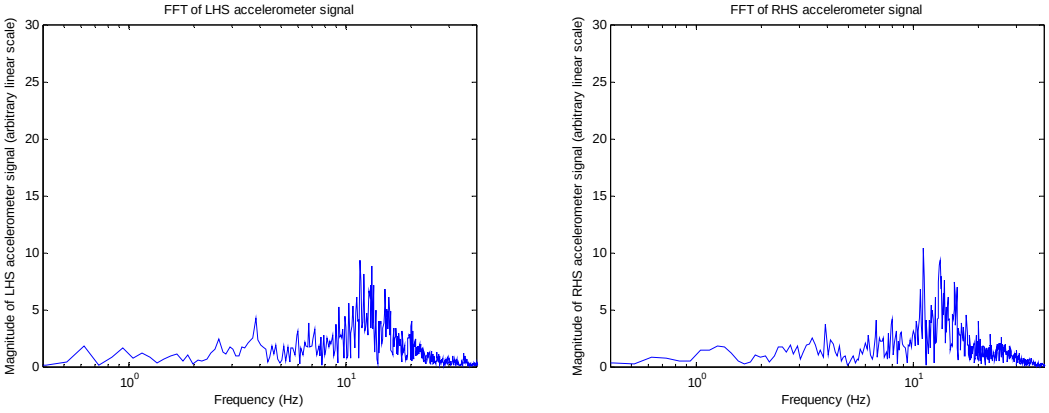

Figure 101. FFT of accelerometers - std suspension, semi-trailer loaded, 40km/h, test 132

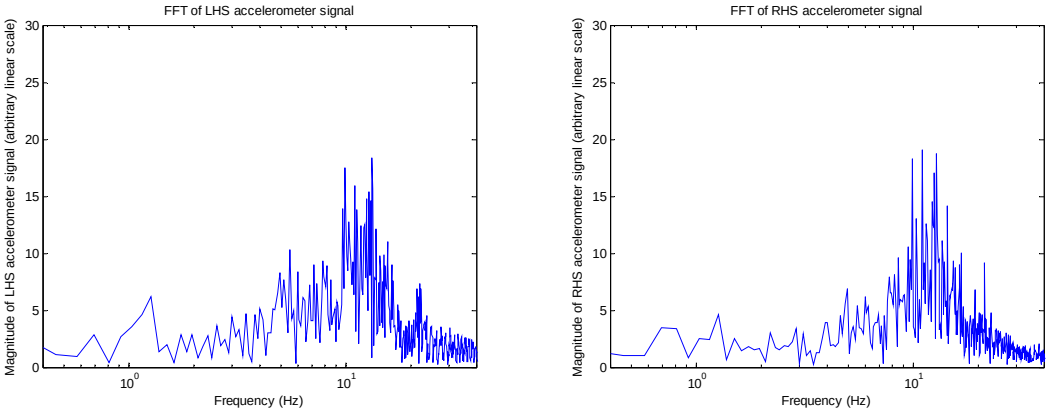

Figure 102. FFT of accelerometers - std suspension, semi-trailer loaded, 60km/h, test 134

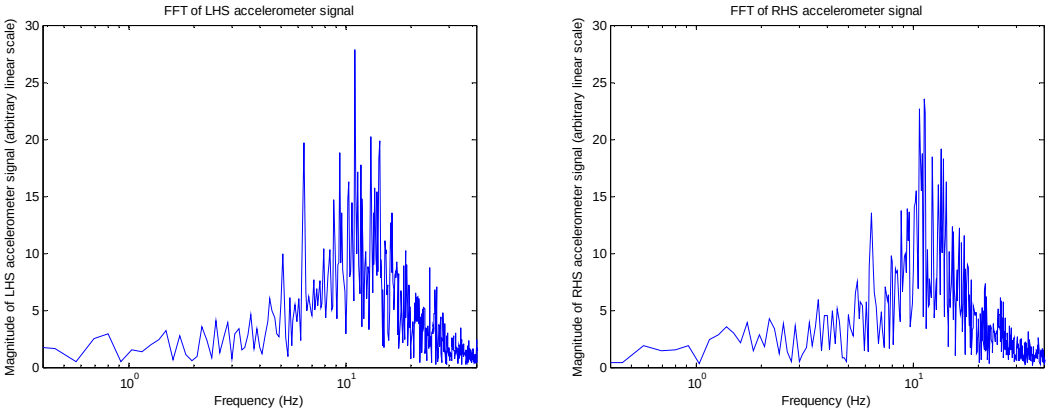

Figure 103. FFT of accelerometers - std suspension, semi-trailer loaded, 70km/h, test 143

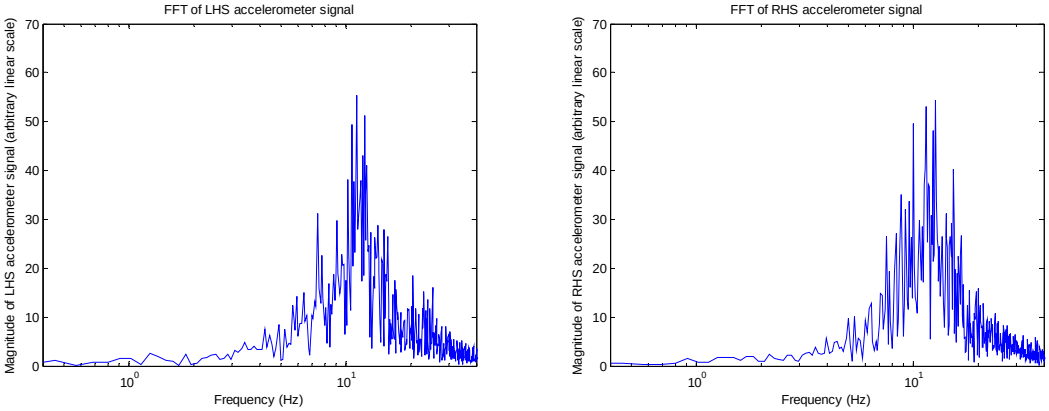

Figure 104. FFT of accelerometers - std suspension, semi-trailer loaded, 80km/h, test 136

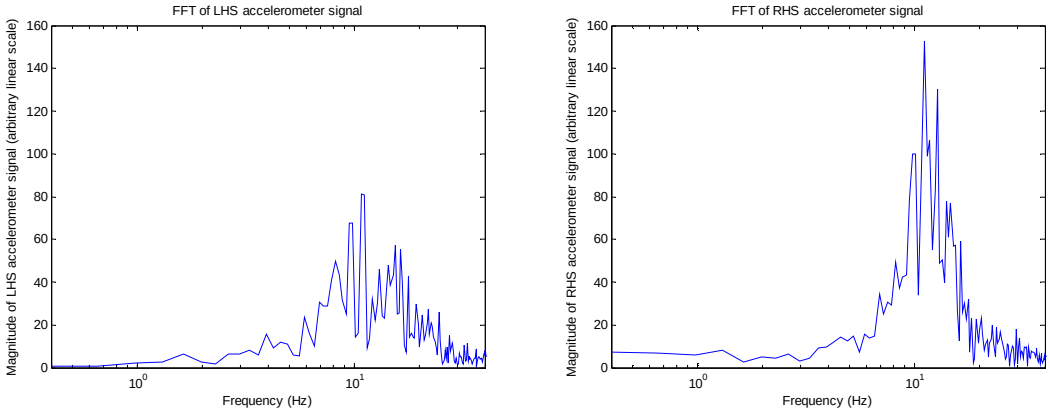

Figure 105. FFT of accelerometers - std suspension, semi-trailer loaded, 90km/h, test 138

Suspension with large longitudinal air lines

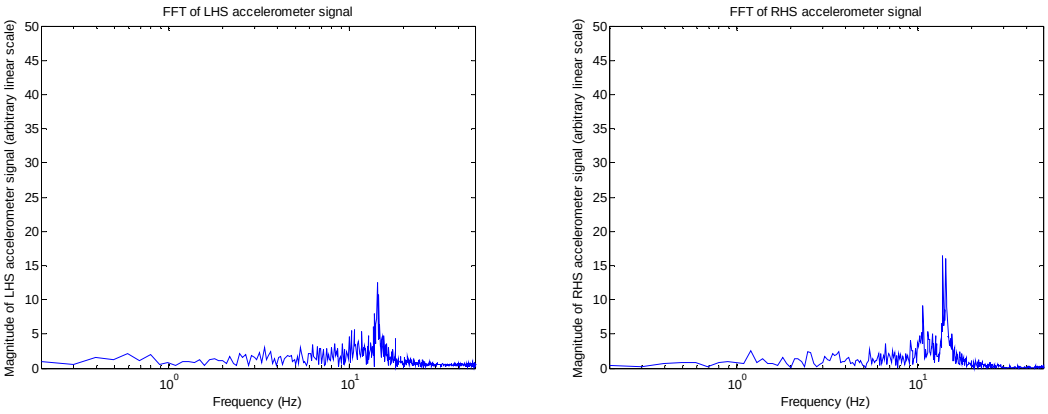

Figure 106. FFT of accelerometers - modified suspension, bus loaded, 40km/h, test 259

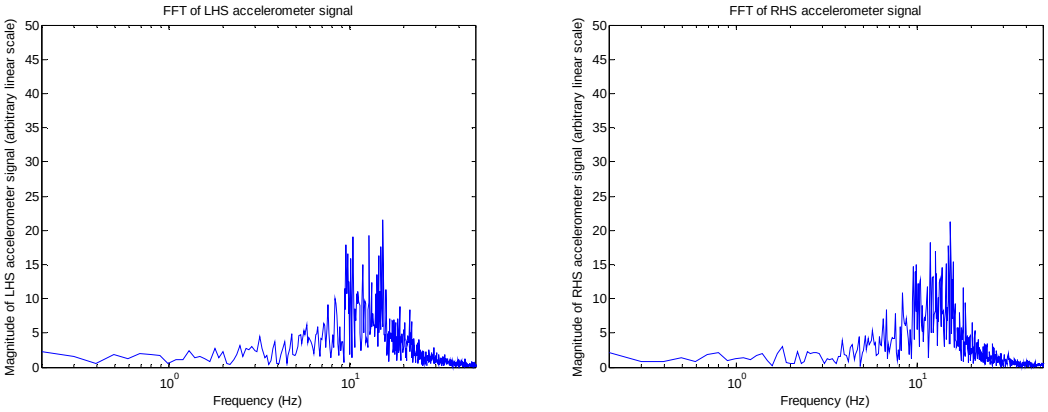

Figure 107. FFT of accelerometers - modified suspension, bus loaded, 60km/h, test 273

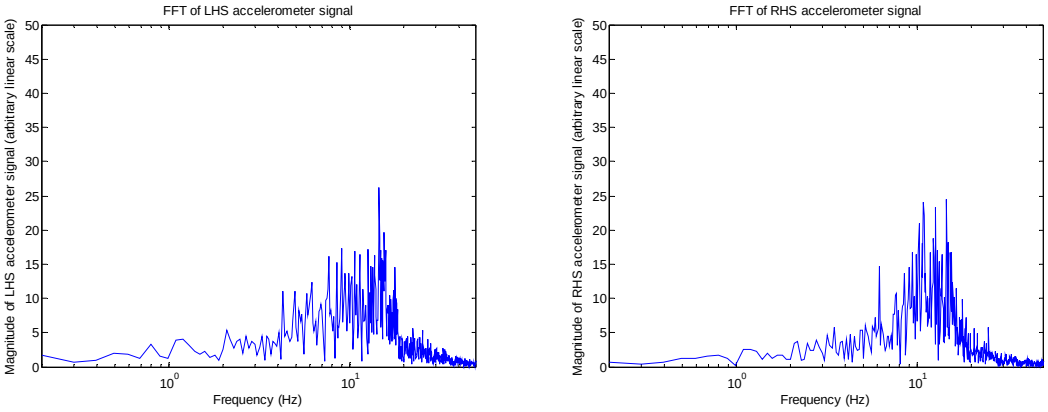

Figure 108. FFT of accelerometers - modified suspension, bus loaded, 70km/h, test 272

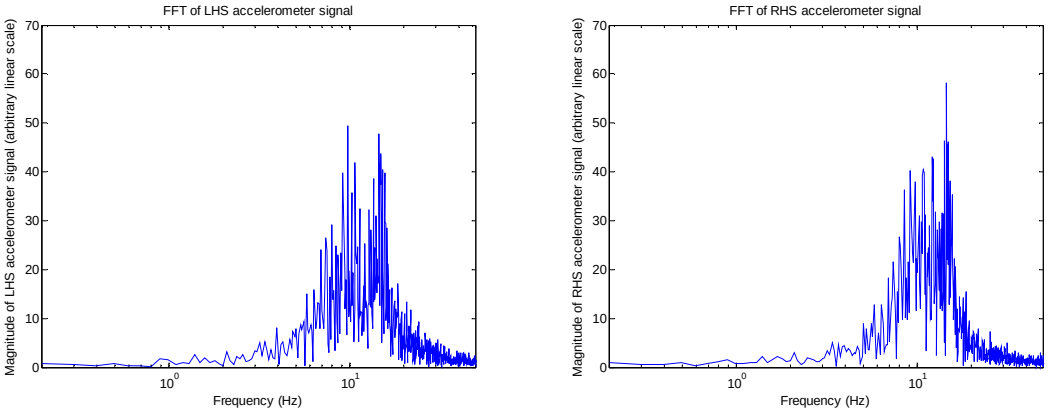

Figure 109. FFT of accelerometers - modified suspension, bus loaded, 80km/h, test 269

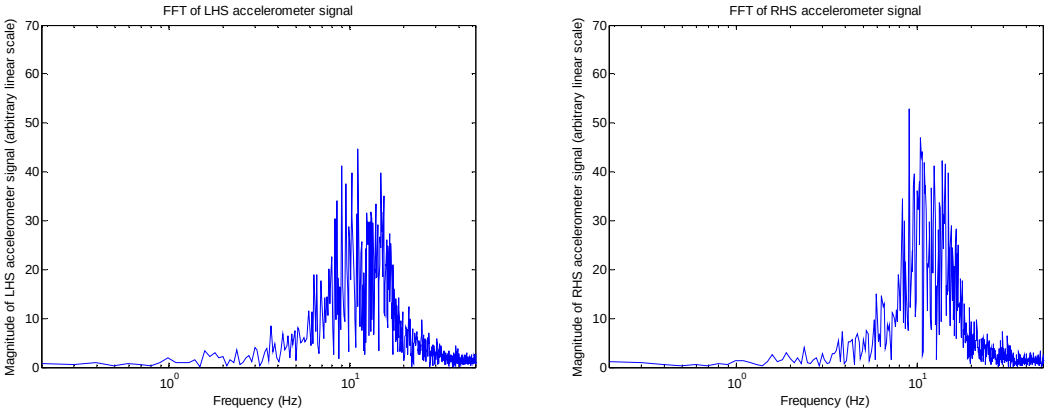

Figure 110. FFT of accelerometers - modified suspension, bus loaded, 90km/h, test 267

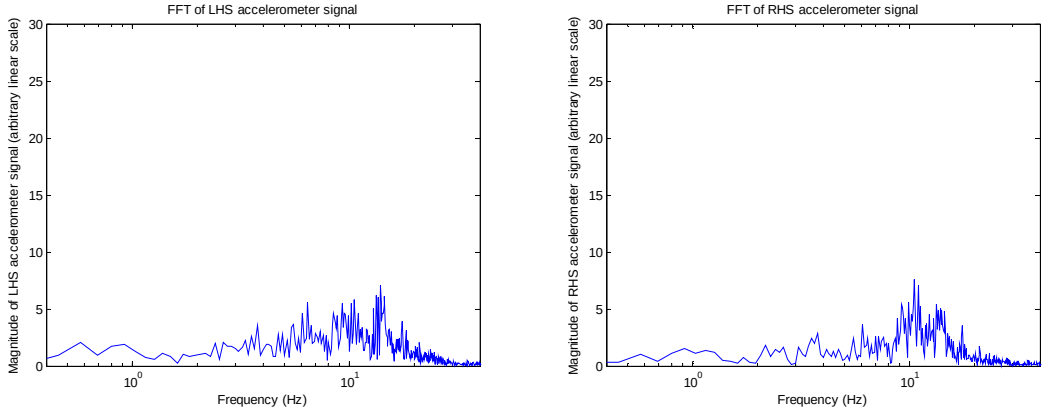

Figure 111. FFT of accelerometers - modified suspension, coach loaded, 40km/h, test 64

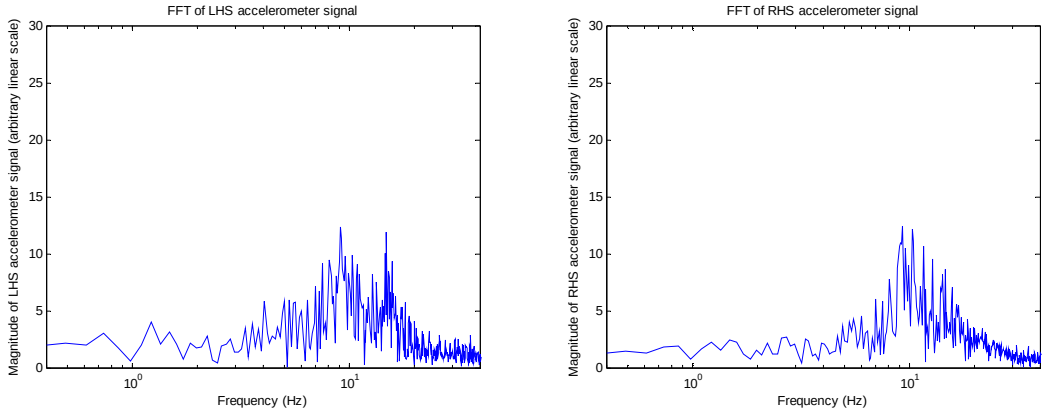

Figure 112. FFT of accelerometers - modified suspension, coach loaded, 60km/h, test 66

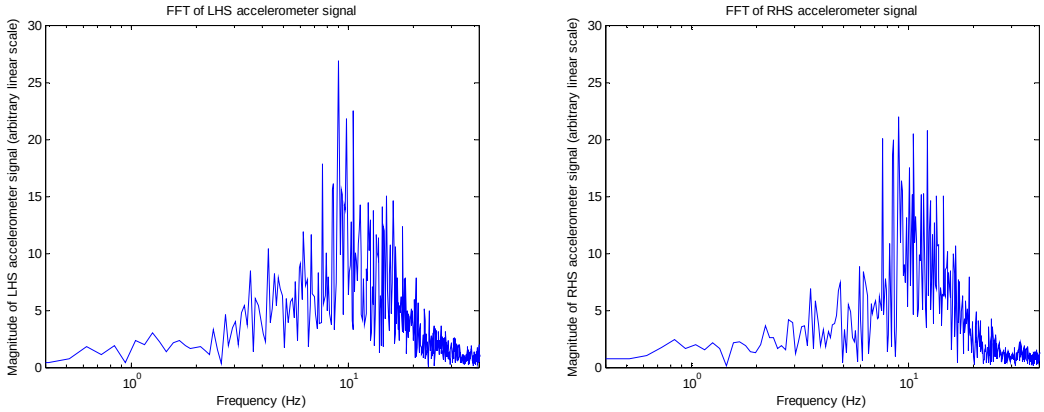

Figure 113. FFT of accelerometers - modified suspension, coach loaded, 70km/h, test 75

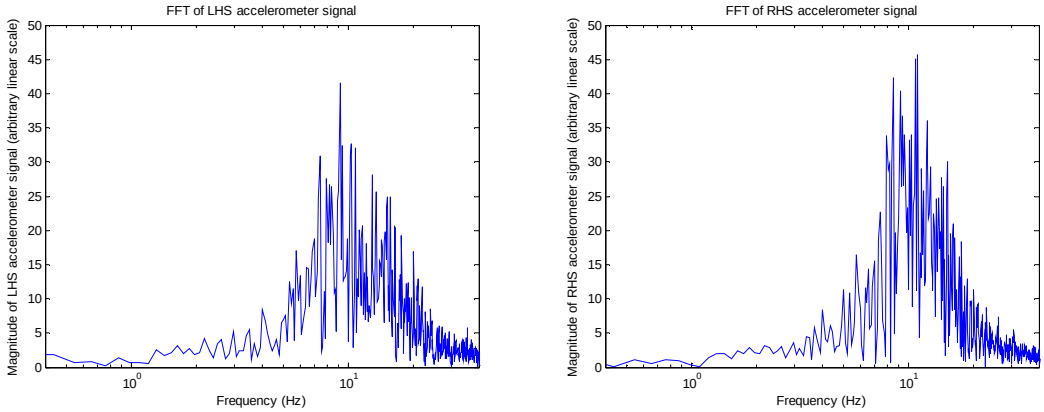

Figure 114. FFT of accelerometers - modified suspension, coach loaded, 80km/h, test 78

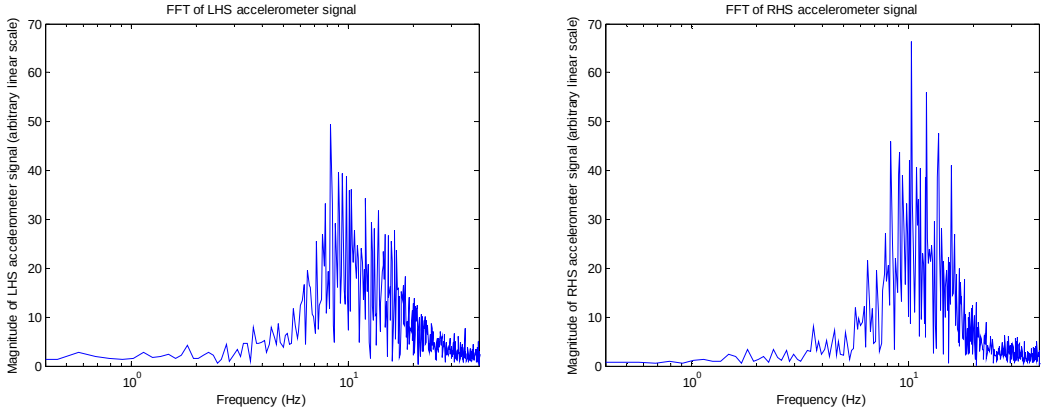

Figure 115. FFT of accelerometers - modified suspension, coach loaded, 90km/h, test 80

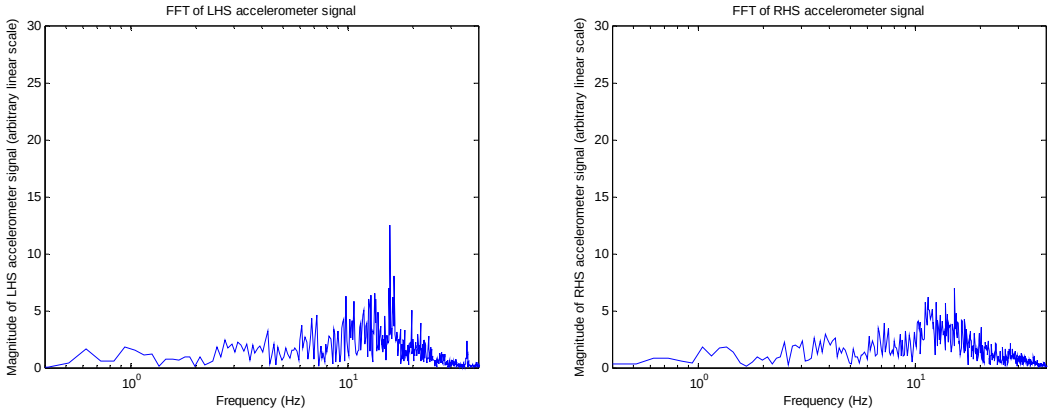

Figure 116. FFT of accelerometers - modified suspension, semi-trailer loaded, 40km/h, test 146

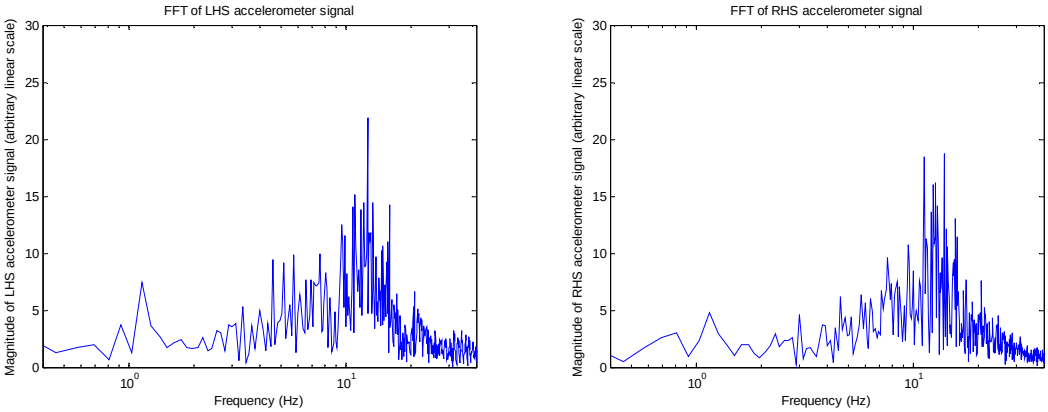

Figure 117. FFT of accelerometers - modified suspension, semi-trailer loaded, 60km/h, test 148

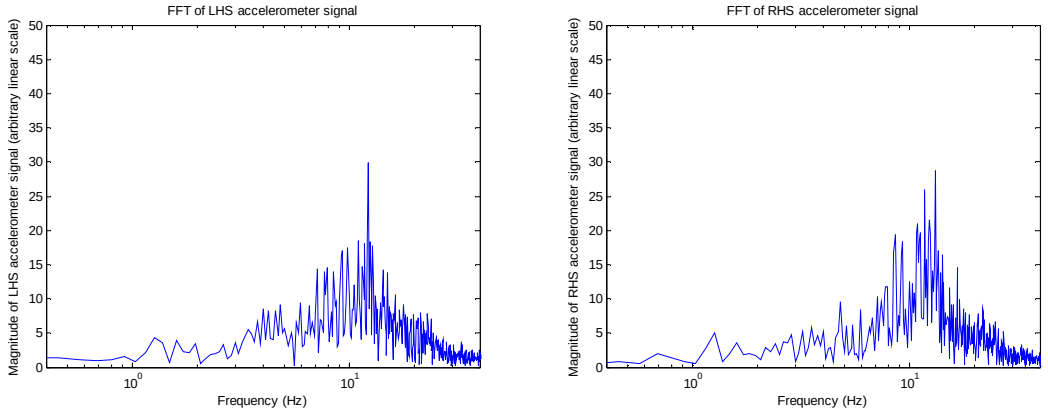

Figure 118. FFT of accelerometers - modified suspension, semi-trailer loaded, 70km/h, test 153

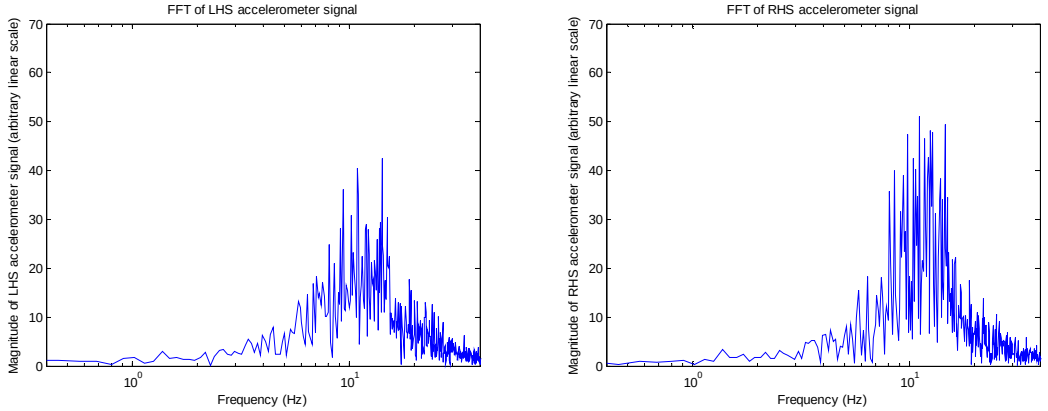

Figure 119. FFT of accelerometers - modified suspension, semi-trailer loaded, 80km/h, test 97

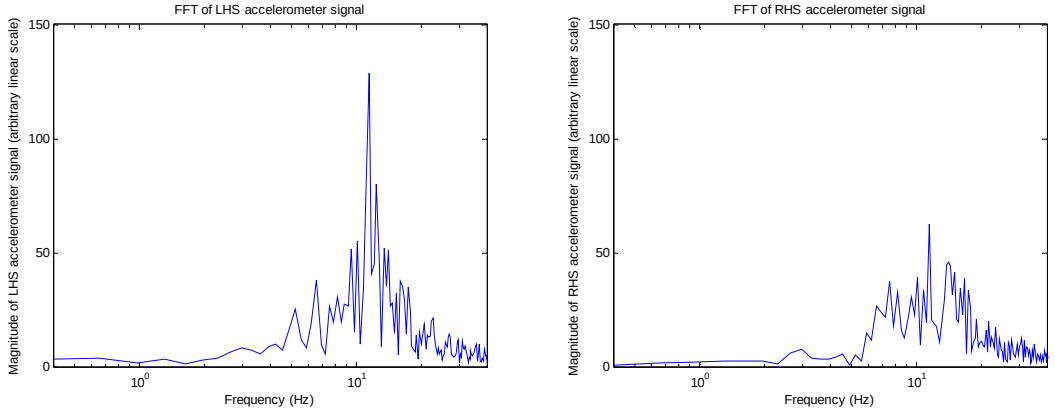

Figure 120. FFT of accelerometers - modified suspension, semi-trailer loaded, 90km/h, test 99

References

Australia Department of Transport and Regional Services. (2004a). *Certification of road-friendly suspension systems; Road-friendly suspension certification requirements*. Canberra, ACT, Australia: Australia. Department of Transport and Regional Services.

Australia Department of Transport and Regional Services. (2004b). Certified road-friendly suspensions. Retrieved 6 Sept 2007, from http://www.dotars.gov.au/roads/safety/suspension.aspx

Australia Department of Transport and Regional Services. (2004c). Vehicle Standards Bulletin No.11. Retrieved 6 Sept 2007, from http://www.dotars.gov.au/roads/safety/bulletin/vsb_11.aspx

Blanksby, C., George, R., Peters, B., Ritzinger, A., & Bruzsa, L. (2008). *Measuring dynamic wheel loads on tri and quad axle groups*. Paper presented at the International Conference on Heavy Vehicles, Paris, May 2008.

Cebon, D. (Ed.). (1999). *Handbook of vehicle-road interaction*. Lisse, South Holland, Netherlands: Swets & Zeitlinger.

Chieh, C. J. (2008). Making Sense of the Two-Sample T-Test. 2008, from http://europe.isixsigma.com/library/content/c070613a.asp

Davis, L. (2005). *Testing of heavy vehicle suspensions. Proof-of-concept: white-noisy road test and pipe test to determine suspension parameters.* Paper presented at the Conference of Australian Institutes of Transport Research (CAITR), 27th, 2005, Brisbane, Queensland, Australia.

Davis, L. (2006). *Dynamic load sharing on air-sprung heavy vehicles: can suspensions be made friendlier by fitting larger air lines?* Paper presented at the Australasian Transport Research Forum (ATRF), 29th, 2006, Gold Coast, Queensland, Australia.

Davis, L. (2007). *Further developments in dynamic testing of heavy vehicle suspensions*. Paper presented at the Australasian Transport Research Forum (ATRF), 30th, 2007.

Davis, L., & Bunker, J. (2007). *Heavy Vehicle Suspensions – Testing and Analysis. A literature review*. Brisbane, Queensland: Queensland Department of Main Roads; Queensland University of Technology.

Davis, L., & Kel, S. (2007). *Heavy vehicle suspension testing: parametric changes from larger longitudinal air lines ; Innovative systems for heavy vehicle suspension testing*. Paper presented at the Main Roads Technology Forum, 13th, 2007, Brisbane, Queensland, Australia.

Davis, L., Kel, S., & Sack, R. (2007). *Further development of in-service suspension testing for heavy vehicles.* Paper presented at the Australasian Transport Research Forum (ATRF), 30th, 2007, ATRF.

Davis, L., & Queensland Department of Main Roads. (2006a). *Heavy vehicle suspension testing, dynamic parameters of air suspensions : Haire system vs standard longitudinal air lines. Part 2, Prime-mover and semi-trailer, final report*. Brisbane, Queensland, Australia: Queensland Department of Main Roads.

Davis, L., & Queensland Department of Main Roads. (2006b). *Heavy vehicle suspension testing, dynamic parameters of air suspensions: Haire system vs standard longitudinal air lines. Part 1, Rigid truck, final report 2nd Ed*. Brisbane, Queensland, Australia: Queensland Department of Main Roads.

Davis, L., & Sack, R. (2004). *Analysis of heavy vehicle suspension dynamics using an on-board mass measurement system.* Paper presented at the Australasian Transport Research Forum (ATRF), 27th, 2004, Adelaide, South Australia, Australia.

Davis, L., & Sack, R. (2006). *Determining heavy vehicle suspension dynamics using an on-board mass measurement system*. Paper presented at the ARRB Conference, 22nd, 2006, Canberra, ACT, Australia.

de Pont, J. J. (1997). *Assessing heavy vehicle suspensions for road wear*. (Research report No. 95). Wellington, New Zealand: Transfund New Zealand.

de Pont, J. J. (1999). Suspensions or whole vehicles? Rating road-friendliness. *International Journal of vehicle design, 6*(1-4), 23.

Eisenmann, J. (1975). Dynamic wheel load fluctuations - road stress. *Strasse und Autobahn, 4*, 2.

Estill & Associates Pty Ltd. (2000). *Operational stability and performance of air suspension on various vehicle configurations.* (Report). Darwin, Northern Territory, Australia: Department of Transport and Works.

Fletcher, C., Prem, H., & Heywood, R. (2002). *Validation of dynamic load models.* (Technical documentation No. AP-T12). Sydney: Austroads.

Giacomini, I. (2007). e-mail correspondence. In L. Davis (Ed.) (mass of axle components ed.). Dandenong: York Transport Equipment Pty Ltd.

Gillespie, T. D., Karamihas, S. M., Sayers, M. W., Nasim, M. A., Hansen, W., Ehsan, N., et al. (1993). *Effects of heavy-vehicle characteristics on pavement response and performance* (Report No. 353). Washington, DC, USA: Transportation Research Board (TRB).

Gyenes L, Mitchell C G B, & Phillips S D. (1994). Dynamic pavement loads and tests of road-friendliness for heavy vehicle suspensions. *International Journal of vehicle design. Heavy vehicle systems special series, 1*(4), 14.

Gyenes, L., & Simmons, I. C. P. (1994). *The dynamic performance of suspension systems fitted to commercial vehicles.* (Project report No. 74). Crowthorne, United Kingdom: Transport Research Laboratory (TRL).

Hamburg, M. (1983). *Statistical analysis for decision making* (3rd ed.). New York, New York, USA: Harcourt, Brace Jovanovich.

Houpis, C. H., & Lamont, G. B. (1985). *Digital control systems theory, hardware, software*. New York, New York, USA: McGraw-Hill.

Jacob, B., & Dolcemascolo, V. (1998). *Dynamic interaction between instrumented vehicles and pavements*. Paper presented at the International Symposium on Heavy Vehicle Weights and Dimensions, 5th, 1998, Maroochydore, Queensland, Australia.

Karamihas, S. M., & Gillespie, T. D. (2004). *Advancement of Smoothness Criteria for WIM Scale Approaches* (Final report No. UMTRI-2004- 12). Ann Arbor, Michigan, USA: The University of Michigan Transportation Research Institute.

Kariya, T., & Kurata, H. (2004). *Generalized Least Squares*. Chichester, UK: John Wiley & Sons, Ltd.

LeBlanc, P. A., Woodroofe, J. H. F., & Papagiannakis, A. T. (1992). A comparison of the accuracy of two types of instrumentation for measuring vertical wheel load. In Cebon & Mitchell (Eds.), *Heavy vehicles and roads: technology, safety and policy* (pp. 86-94). London: Thomas Telford.

Mack-Volvo. (2007). private correspondence. In L. Davis (Ed.) (mass of axle and wheel components ed.). Albury: Volvo Australia.

Mitchell, C. G. B., & Gyenes, L. (1989). *Dynamic pavement loads measured for a variety of truck suspensions*. Paper presented at the International Symposium on Heavy Vehicles Weights and Dimensions, 2nd, Kelowna, British Columbia, Canada.

OECD. (1992). *Dynamic loading of pavements ; road transport research.* (Report No. 9264137629). Paris, France: Organisation for Economic Co-Operation and Development (OECD).

OECD. (1998). *Dynamic interaction between vehicles and infrastructure experiment (DIVINE).* (Technical report No. DSTI/DOT/RTR/IR6(98)1/FINAL). Paris, France: Organisation for Economic Co-operation and Development (OECD).

Peters, I. (2003). *In-service testing of road friendly suspensions.* University of Western Australia. School of Mechanical, Materials and Mechatronics Engineering, Crawley, Western Australia, Australia.

Potter, T. E. C., Cebon, D., & Cole, D. (1997). Assessing “road friendliness”: a review. *Journal Automobile Engineering I Mech E, 211 C*(6), 20.

Potter, T. E. C., Cebon, D., Cole, D. J., & Collop, A. C. (1996). Road damage due to dynamic tyre forces, measured on a public road. Retrieved 1 Dec 2005, from http://www-mech.eng.cam.ac.uk/trg/publications/downloads/veh_road/veh_road13.pdf

Prem, H., Mai, L., & Brusza, L. (2006). *Tilt testing of two heavy vehicles and related performance issues.* Paper presented at the International Symposium on Heavy Vehicle Weights and Dimensions, 9th, 2006, State College, Pennsylvania, USA, Pennsylvania, USA.

Roaduser Systems Pty Ltd. (2002). *Stability and on-road performance of multi-combination vehicles with air suspension systems* (Report). Melbourne, Victoria, Australia: National Road Transport Commission.

Simmons, I. C. P. (2005). e-mail correspondence. In L. Davis (Ed.). Wokingham, United Kingdom: Transport Research Laboratories Ltd.

Simmons, I. C. P., & Wood, J. G. B. (1990). *The equalisation of multi-axle bogies fitted to commercial vehicles* (Research report No. 277). Crowthorne, United Kingdom: Transport and Road Research Laboratory (TRRL).

StatPac Inc. (2007). Statistical Significance. One-Tailed and Two-Tailed Significance Tests. from http://www.statpac.com/surveys/statistical-significance.htm

Sweatman, P. F. (1983). *A study of dynamic wheel forces in axle group suspensions of heavy vehicles*. (Special report No. 27). Vermont South, Victoria, Australia: Australian Road Research Board (ARRB).

Whittemore, A. P. (1969). Measurement and prediction of dynamic pavement loading by heavy highway vehicles. *SAE technical paper, No: 690524*, 15.

Woodroofe, J. H. F. (1996). Heavy truck suspension dynamics: methods for evaluating suspension road-friendliness and ride quality. In Society of Automotive Engineers (SAE) (Ed.), *Commercial vehicles and highway dynamics SP-1201* (pp. 68). Warrendale, Pennsylvania, USA: Society of Automotive Engineers (SAE).

Woodroofe, J. H. F., LeBlanc, P. A., & LePiane, K. R. (1986). *Vehicle weights and dimensions study; volume 11 - effects of suspension variations on the dynamic wheel loads of a heavy articulated highway vehicle* (Technical report). Ottawa, Ontario, Canada: Canroad Transportation; Roads and Transportation Association of Canada (RTAC).

Woodrooffe, J. H. F., & LeBlanc, P. A. (1987). *Heavy vehicle suspension variations affecting road life*. Paper presented at the Symposium on Heavy Vehicle Suspension Characteristics, 1987, Canberra, Australia.

ISBN 978 - 1 - 9207 - 1909 - 8